THE UNIVERSITY OF MICHIGAN

INDUSTRY PROGRAM OF THE COLLEGE OF ENGINEERING

MULTIPLE EMULSION FORMATION AS A HYDRODYNAMIC PHENOMENON USING CYLINDRICAL JETS

David P. Kessler

A dissertation submitted in partial fulfillment
of the requirements for the degree of
Doctor of Philosophy in the
University of Michigan
Department of Chemical and Metallurgical Engineering
1962

June, 1962

IP-568

ACKNOWLEDGEMENTS

The author owes a debt of gratitude to many people for assistance in the course of his doctoral program. Particular thanks should go to the following people:

Professor J. Louis York, the chairman of the doctoral committee, for his assistance and encouragement throughout the course of the research.

Professors A. G. Hansen, R. B. Morrison, M. R. Tek, and G. B. Williams, the other members of the doctoral committee, for assistance in many ways, particularly with respect to interpretation of certain aspects of the data obtained, and to Dr. Keith H. Coats, who served as a committee member while a staff member of the Chemical and Metallurgical Engineering Department.

Mr. Gordon Ringrose, who constructed much of the electronic equipment used in the research.

The National Science Foundation, for support for three years of study, and to Consumers Power Company for support during the first year of graduate study.

The Commercial Solvents Corporation, who were very generous in supplying surfactants for use in the course of the research.

TABLE OF CONTENTS

LIST OF TABLES

LIST OF TABLES CONT'D

LIST OF FIGURES

LIST OF FIGURES CONT'D

LIST OF FIGURES CONT'D

LIST OF FIGURES CONT'D

LIST OF APPENDICES

NOMENCLATURE

D_i	Large drop diameter
D_n	Nozzle diameter
d	Inclusion diameter
$E(z) = \int_{\infty}^{\infty} z\, f(z)dz$	
$f(z)$	Probability density function, Section VII.3
$F(z)$	Probability distribution function, Section VII.3
$\hat{f}(z)$	Probability density function estimated from sample, Section VII.4
$\hat{F}(z)$	Probability distribution function estimated from sample, Section VII.4
$G(z) = 1/[1 - F(z)]$	
ℓ_i	distance from double exposure photograph of travel of large drop of diameter D_i
M	Maximum number of large drop size classes
N	Number of drops, see VII.3; maximum number of inclusion size classes elsewhere
$Pr(\alpha)$	Probability of the event α
Re	Reynolds number, Section VII.4
T	Temperature
v_n	Nozzle velocity
V	Volume
We	Weber number, Section VII.4
x_{ij}	Number of inclusions of diameter d_j in large drops of diameter D_i
y_i	Number of large drops of diameter D_i
$\bar{z}_{pq} = [\frac{E(z^p)}{E(z^q)}]^{1/p-q}$	; see Section VII.4

Greek

γ	Interfacial tension
$\Gamma_\alpha(\ell) = \int_0^\alpha t^{\ell-1} e^{-t} dt$; see Section VII.3	
μ	Viscosity, mean of distribution
σ	Standard deviation

Subscripts

r	Refers to receiving phase
s	Refers to sprayed phase

ABSTRACT

The classical emulsion is made up of drops of one liquid dispersed in a containing liquid. Under certain circumstances, however, some of the containing phase may form drops within the drops of the dispersed liquid, giving rise to a structure known as a double-multiple emulsion. The purpose of this study was the investigation of the formation of these structures as a hydrodynamic phenomenon.

Double-multiple emulsions were produced using both transient and steady-state liquid injection, with a cylindrical jet configuration. Analysis of the spray was by means of high-speed photography.

The distribution of the large drops and that of the included drops were both found to be satisfactorily represented by a log-normal probability function. The percent of volume and interfacial area represented by the included drops were found to be most strongly dependent on inertial forces. A simplified model based on the use of nozzle parameters was found to correlate satisfactorily percent included area and volume as a function of Reynolds number and Weber number. Large size classes of the dispersed phase drops contained proportionally many more inclusions than did the smaller size classes.

The mechanism of inclusion formation was found to involve the drawing out of a ligament or sheet from the flowing jet, followed by the re-coalescence of the free end of this ligament or sheet with the

main jet body, entraining in the process a portion of the containing phase. Thus, the inclusions pre-date the formation of the drops of the dispersed phase from the jet disruption.

I. INTRODUCTION

Before attempting a detailed discussion of the work covered in this dissertation, it is necessary to devote a little time to defining just what is meant by a "double-multiple" emulsion. Multiple emulsions are encountered seldom enough in the literature that it is well to clear up at the outset some possible sources of confusion in terminology.

The classical emulsion is made up of a number of minute drops of one liquid within a containing phase of another liquid. The two liquids are commonly referred to as the dispersed phase and the continuous phase respectively. In the simplest case we have the situation depicted in Figure 1, where there is a single dispersed phase and the containing phase is truly continuous in the sense that any two points in the containing phase can be joined by a line lying entirely within that phase.

Under some circumstances, however, it is possible to get some of the containing phase within the drops of the other phase, as shown in Figure 2, making the containing phase no longer continuous. Here the terms "continuous phase" and "dispersed phase" lose any meaning as applied to the resultant emulsion. (They will, of course, have some relevance in the sense that one normally <u>creates</u> an emulsion by adding what can be termed the "dispersed" phase to the "continuous" phase.) Emulsion structures which lack a continuous phase are normally referred to as <u>multiple emulsions</u>.

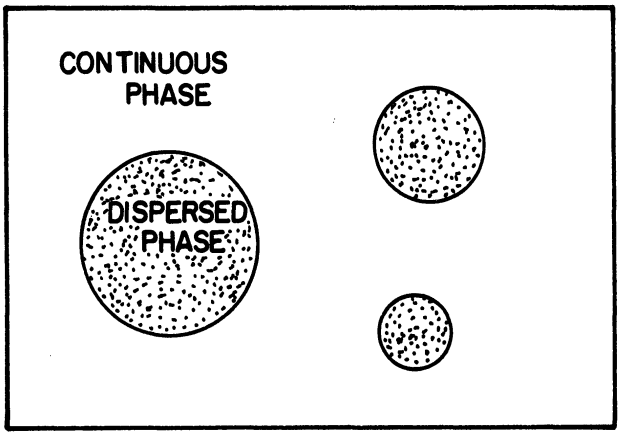

FIG. 1 SIMPLE EMULSION

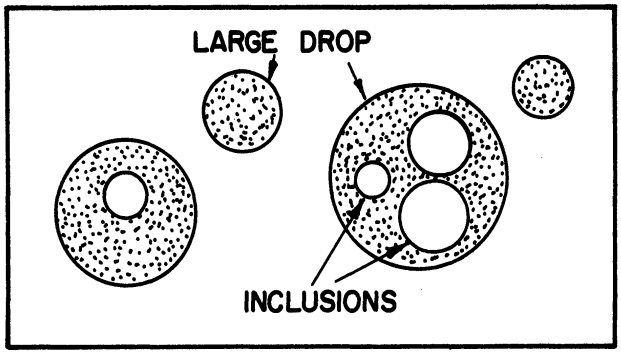

FIG. 2 DOUBLE - MULTIPLE EMULSION

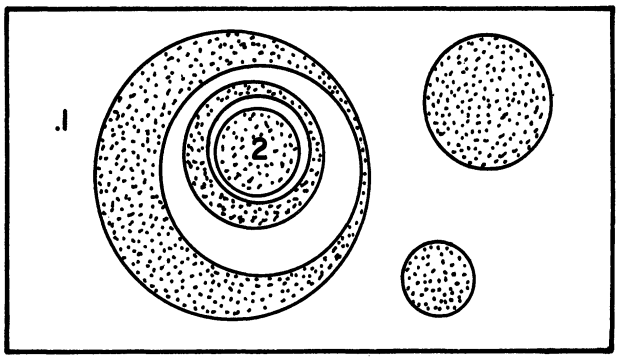

FIG. 3 QUINQUE - MULTIPLE EMULSION

Multiple emulsions structures can be created in surprising complexity - for example, Clayton[19] cites an example of a quinque-multiple emulsion, shown schematically in Figure 3. The level of the multiple emulsion might be defined as the maximum of the minimum number of phase boundaries it is necessary to cross in going from any point (x_1,y_1,z_1) in the outermost phase to any other point (x_2,y_2,z_2) of the system. Thus in Figure 3 we can see that it is necessary to cross five phase boundaries in going from point 1 to point 2. In the present study we are concerned with multiple emulsions of the "double-multiple" type shown in Figure 2.

To avoid confusion, it should be pointed out that there is often reference in the literature to "dual" emulsions. This usage usually refers to pairs of liquids which, through the use of different emulsifying agents, will form emulsions of both the O/W and W/O types, and will frequently invert from one type to the other upon addition of a suitable reagent. These are conjugate systems, but not co-existing systems; that is, at any given time only a W/O or only an O/W emulsion is present. Obviously a pair of liquids must have the "dual" property in order to form stable "double-multiple" emulsions.

As is noted in the literature review, multiple emulsions as a class are not new. The early literature is primarily concerned with their production as an inversion phenomenon, i.e., through the addition of the disperse phase or a suitable reagent to a simple emulsion, causing the structure to invert from O/W to W/O or vice versa, in the process trapping some of the original structure in the inverted emulsion. Later studies noted that there seemed to be some hydrodynamic

factors involved as well - for example, the same effect could sometimes be produced by shaking or stirring. These later studies were purely observational in nature, with no quantitative work being done on mechanism or prediction of effects.

The present study was motivated by an observation by R. H. Boll during his doctoral work at the University of Michigan. Boll was concerned with determining specific surface in liquid-liquid sprays using a light transmittance method. The sprays were produced using transient high-pressure injection through a conical spray nozzle. Certain pairs of liquids were found to give dispersions which were double-multiple emulsions.

The increased surface area that is available in a multiple emulsion offers certain obvious advantages for mass transfer operations. Boll's work suggested that one might be able to produce multiple emulsions conveniently through liquid-liquid injection, as opposed to the cumbersome inversion method. If one could only define the major variables and predict their effects, it might be possible to upgrade the efficiency of many operations involving mass transfer.

At the outset there are a number of obvious questions:

1) Can this be done in pure systems? (All the reported data are for heterogeneous systems.)
2) Is this strictly a transient phenomenon? (If so, it will be considerably more unwieldy to adapt to commercial use.)
3) What is the mechanism?

4) What are the important independent variables, and, once found, what are the dependent variables which will exhibit a correlation with these independent variables?

5) What form, if any, of probability distribution function is followed by the drops? (If the probability distribution can be defined, sampling can be reduced and systematic definition of sampling error is possible.)

The consideration of these questions and several others which arose in the course of the research is the essence of the work described in this dissertation.

There is one more matter of terminology that must be raised at this point. In the double-multiple emulsion, one has essentially two classes of drops (see Figure 2). The drops contained within the large drops, i.e., the drops of the same composition as the external phase, will be referred to throughout as the inclusions; the larger drops which are of composition opposite that of the external phase will be referred to as the large drops. This is an important point, as it is necessary to make this distinction many times in the course of the work presented here.

II. LITERATURE REVIEW

One of the earlier observations with regard to multiple emulsions is made by C. V. Boys in his classic treatise Soap Bubbles - Their Colours and the Forces Which Mould Them. Boys notes that the liquid pairs "petroleum" and water, and orthotoluidine and water will produce multiple emulsions. Boys' work was one of the earliest found which makes reference to liquid-liquid multiple emulsions (circa 1900). If, however, we do not restrict the term "multiple emulsion" to liquid-liquid systems, the history of observation of multiple emulsions reaches back perhaps to the first individual who discovered the joy of blowing ordinary soap bubbles. Boys indicates that written reference to bubbles has been made as early as Ovid and Martial. Here we must restrict our attention to liquid-liquid systems.

There is seldom any mention of multiple emulsions in the published literature from 1900 to the present day. The few instances in which some note is made are usually in conjunction with another matter entirely - for example, as when Boll[8] encountered multiple emulsions in the course of his work on specific surface in liquid-liquid sprays, or Pavloshenko and Yanishevskii[63] in their work on interfacial area of mechanically stirred liquid mixtures.

Occasionally, pictures are published in the literature which show what might be multiple emulsion structures but have been given no cognizance by the authors. Ranz[67] shows a picture of a carbon tetrachloride-into-water spray (the same system as used in much of

this research) which seems to show a well defined multiple emulsion; however, no mention of the phenomenon is made in the accompanying article. Similarly, Scott, Hayes, and Holland[81] show a picture of a kerosene-water dispersion - another system which will support multiple emulsion behavior - that appears to show multiple emulsions, but with no comment made in the accompanying article. It should be noted that in the dense dispersions shown in each of these articles, camera depth of field might give a false indication of multiple emulsion structure by picturing drops behind or in front of a large drop as inclusions.

Even what is perhaps the best known reference on emulsions, Clayton's The Theory of Emulsions and Their Technical Treatment,[19] has only two paragraphs on multiple emulsions. This is a reference work which has been through five editions from 1923 to 1954, including German and Russian translations. Such a situation tends to make literature surveying in the multiple emulsion field frequently more fortuitous than systematic.

In the 1920's and 1930's, several papers were published treating the subject of dual emulsions, which, as was pointed out in the introduction, is closely related to that of multiple emulsions. A good summary of most of this work can be found in Clayton. The most useful of these articles with respect to the work considered here are probably the ones by Woodman,[91,92] and the one by Cheesman and King.[16]

Cheesman and King made an extensive study of the stability of dual emulsions using some 16-20 different emulsifying agents. For

future work on the double-multiple emulsion systems studied here it may be possible to find stabilizing surfactants from this list. Two other remarks of interest are made. A paper by Cassel (Acta Physiochemica U.R.S.S., 6, p. 289 (1937)) is cited which makes the observation that stabilization of dual emulsions is impossible on thermodynamic grounds, and also cited is a work by Sugden (J.A.C.S., p. 174 (1926)) which notes that in some dual emulsion systems the more easily formed system - that is, O/W or W/O - is less stable and vice versa.

The interesting thing with regard to Woodman's work is that he was able to preferentially create either O/W or W/O emulsions with a given pair of liquids by varying his method of shaking the container. This indicated that hydrodynamic considerations could be controlling in the dual emulsion case, and gave encouragement to a possible hydrodynamic mechanism for the double-multiple emulsion case.

Most of the work on dual emulsions is useful in only the most general sort of way for double-multiple emulsion work. Although the dual property is necessary for the stable double-multiple case, the mechanism presented here indicates that this is truly a stability relationship, and not a requisite for formation of double-multiple emulsions. Dual emulsion systems can indicate liquid pairs and surfactants which will probably have good success in the creation of double-multiple emulsions, but any more specific conclusions are hardly justified.

In recent years, there have been two articles which make some useful observations with regard to multiple emulsions, and, in particular, with regard to multiple emulsions that apparently have been produced as a hydrodynamic phenomenon. The first of these is the article by Pavloshenko and Yanishevskii[63] on interfacial area of mechanically stirred liquids. This periodical is available in English translation as the Journal of Applied Chemistry of the U.S.S.R.

Pavloshenko and Yanishevskii were concerned with the correlation of interfacial surface area created by agitation of two liquid phases in a container using a mechanical stirrer. They observed multiple emulsions in the system machine oil into water, and show a photograph similar to some of the ones taken in conjunction with this dissertation. They also note observation of multiple emulsions in the medicinal petrolatum into water system.

The conclusion reached in this article is that the multiple emulsions seemed to be favored by dispersing a high viscosity liquid in a low viscosity medium. This is somewhat at odds with the results presented here, and is also at odds with some of the data in the article, which notes that some multiple emulsion structures were produced in the machine oil into glycerol system - obviously a viscous into viscous, rather than a viscous into non-viscous system. This point will be discussed later; at the moment it will suffice to say that this appears to be a stability phenomenon.

Two other remarks are made which are of interest. First, a decrease in surface area with increase in interfacial tension was detected, a result in agreement with the results obtained here. Second,

they remark that the two interfaces (in their double-multiple emulsion) differ greatly from a hydrodynamic standpoint.

No quantitative work was done on the multiple emulsions as they were an observation incidental to the main purpose of the research. One comment that might be in order is that the observations of the multiple emulsion structures were made after the agitator was turned off rather than in the dynamic system. This, of course, tends to make stability toward coalescence of far greater effect in the results obtained.

The second publication in recent years that is worthy of more than passing discussion is the one by R. H. Boll,[8] which, as was already mentioned, furnished the impetus for the research presented here. Boll, like Pavloshenko and Yanishevskii, was studying interfacial area of liquid-liquid dispersions, but rather than creating the dispersion by mechanical agitation, was using a conical spray nozzle and transient injection. The multiple emulsion formation was an extremely undesirable factor here, since the analysis was by light transmittance methods which were hardly compatible with the abnormal drop structure obtained.

Boll observed multiple emulsions in the SAE 10 motor oil and water, and kerosene and water systems. As in the article by Pavloshenko and Yanishevskii, these systems both involved viscous liquids. Also, in both articles, the systems which exhibited multiple emulsion behavior were highly heterogeneous. Boll studied no highly viscous pure systems, but did study the carbon tetrachloride-water system, and observed no multiple emulsions. This is a system which the present research has

shown will support multiple emulsion behavior, although coalescence is rapid. Again, later discussion will show why this stability consideration rectifies the apparent contradiction.

The bibliography shown in the Appendix is not intended to be exhaustive. In general, the field of sprays is very well covered in the bibliography by De Juhasz[25] listed. Rather, the listing here is intended to bring together some of the articles with observations and techniques which suggest possible application to the study of multiple emulsion formation in a dynamic system. References are listed for the general spray considerations, the various aspects of drop mechanics, the surface chemistry considerations, the statistical and experimental design questions, and the photographic problems.

III. PRELIMINARY CONSIDERATIONS

Prior to the construction of the equipment which was used for the majority of the data obtained in this study, it was necessary to do some qualitative work to determine approximate ranges for operating variables and to define an appropriate method of analysis. It is also necessary at this point to consider some general aspects of the spray process with regard to interpretation of data presented later.

III.1 Investigations with Microscope and Well Slide

The first experimental effort was an attempt to create multiple emulsions using a simpler flow geometry than a conical spray. Toward this end a well slide was constructed of acrylic resin and a hypodermic needle and syringe used to inject the sprayed phase into the stagnant receiving phase. Examination was by means of a Bausch and Lomb binocular microscope.

First the system water into kerosene was tried to see if this system (which produced multiple emulsions for Boll[8] with a conical spray nozzle) would produce multiple emulsions with simple cylindrical jet. Multiple emulsions were produced and, as Boll remarked, the emulsions were "packed in." In other words, the included drops had the appearance of filling the parent drop, as shown in Figure 4, very much as one might fill a cellophane bag with marbles. This indicated that whatever mechanism was active with respect to producing the multiple emulsions from a conical spray nozzle was active in the breakup of the simple cylindrical jet. Since the cylindrical jet represents a much

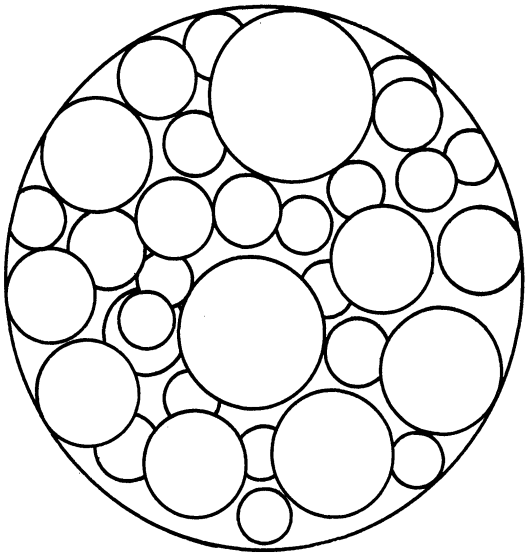

Figure 4. Schematic Drop with Inclusions "Packed In."

simpler type of flow geometry than the breakup of a conical sheet, the investigations were carried on in this simpler system for the remainder of the research.

The next effort was toward producing multiple emulsions in a homogeneous system. Two of the systems where Boll had failed to produce multiple emulsions were the benzene-water system and the carbon tetrachloride-water system. Investigation using the well slide showed no multiple emulsions formed. The resistance of mutually insoluble liquids to interpenetration across the dividing interface is strongly dependent on interfacial tension, so the next step was an attempt at reducing interfacial tension to reduce interpenetration resistance.

Both powdered and liquid commercial detergents were used for the benzene-water system. Some multiple emulsions were produced and, with this encouragement, a search was made for a system with a sufficiently low interfacial tension that it would not require the use of a surfactant to promote multiple emulsion formation. Such a system was found in the isobutanol-water system. Interfacial tension in this system at room temperatures is about 2 dynes per centimeter (as opposed to 30-60 dynes per centimeter for most common liquid pairs). The isobutanol-water system yielded multiple emulsions without surfactant addition, and represented the first verification experimentally of the possibility of multiple emulsion formation in homogeneous systems, that is, systems without some sort of third component added to promote multiple emulsion formation.

Following this discovery, further work was done on the carbon tetrachloride-water system and multiple emulsions were produced with common household detergents, and with sodium lauryl sulfate.

In all the work done under the microscope, there were several common factors with regard to coalescence of the emulsions produced. First, the more highly heterogeneous the system, the more slowly coalescence proceeded. Very pure phases yielded emulsions with coalescence times of the order of seconds or fractions of a second. Second, the order of stability of the inclusions was higher than that of the large drops - for example, it was possible to observe large drops containing inclusions migrate to an interface and coalesce, with no effect on the inclusions. This is shown schematically in Figure 5. As the large drop coalesces with the essentially infinite body of fluid, the surface forces snap the interface back to a straight line, and impart a not inconsiderable acceleration to the inclusions, but without causing them to coalesce with one another. Third, it was observed that the order of stability of a small drop with respect to another small drop is higher than with respect to an interface of larger curvature; all inclusions produced seemed to coalesce out through the phase boundary of the parent drop rather than coalescing with other inclusions in the same drop.

It was also found that it was possible to produce multiple emulsions in pure systems through the use of Dow Chemical Company "Methocel." This is a water soluble cellulose gum which does not have an extremely pronounced effect on the interfacial tension in the amounts required - this tended to indicate perhaps a stabilizing effect rather

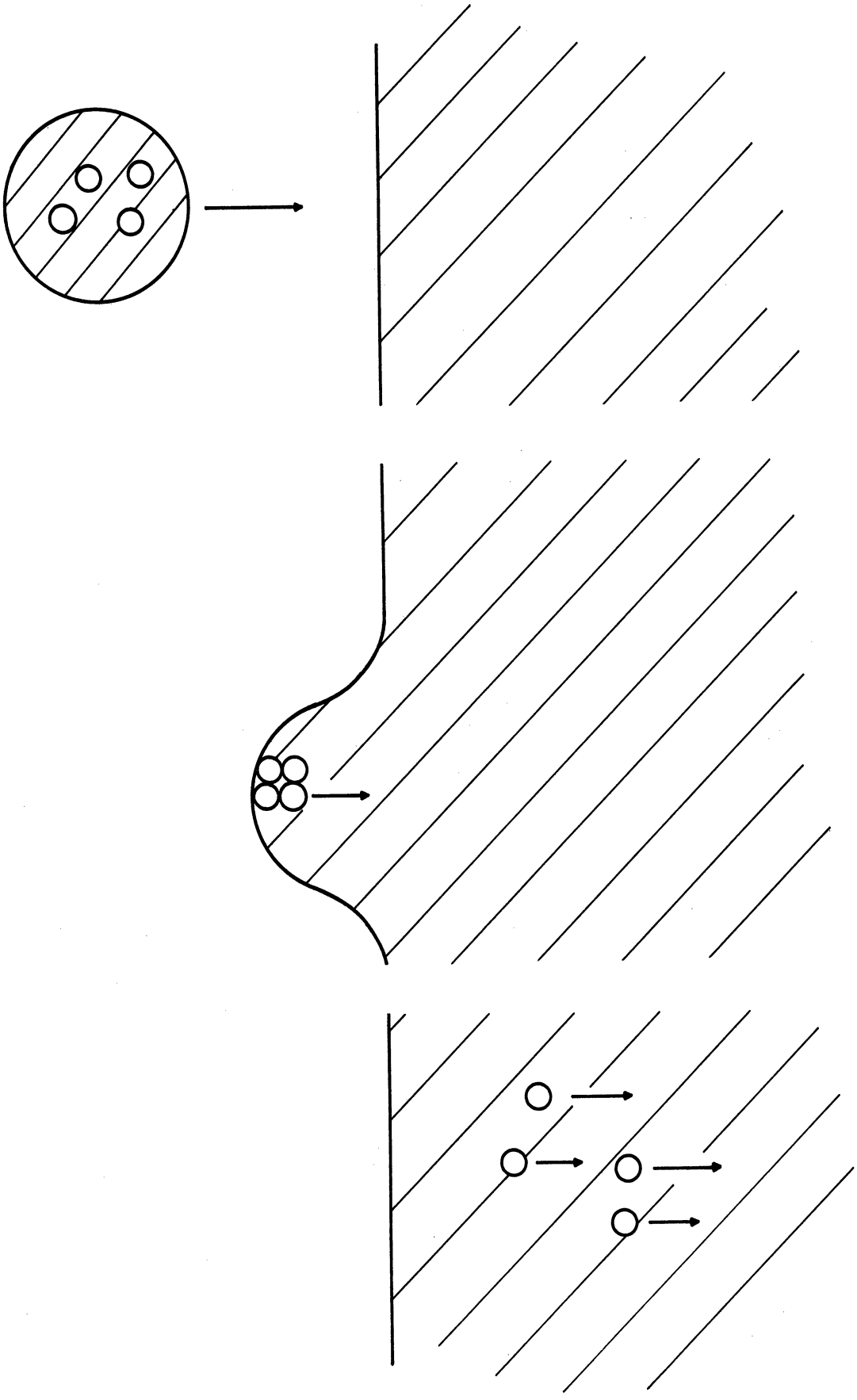

Figure 5. Coalescence of Inclusion Containing Drop with Flat Interface.

than a true effect on the promotion of multiple emulsions. If so, it was felt that study at shorter times after formation of the emulsion might reveal multiple emulsions which coalesce too rapidly to observe using the long time delays associated with a sample cell and microscope.

III.2 Investigations Using Transient Equipment

Accordingly, the next experimental investigation was carried out using the apparatus shown in Figure 6, an arrangement very similar to that used by Boll[8] in his work. The apparatus consists of a free-floating shaft which rests on a piston. The shaft can be loaded with lead weights, and is held in place with a pin. The piston fits in a stainless steel cylinder with a capacity of approximately 1 $cm.^3$, the end of which is threaded to accept various spray nozzles. The nozzle is immersed in a transparent sample cell containing the receiving fluid. To spray the liquid, the pin is pulled from the shaft and the gravity force on the weights provides pressures up to about 1500 psi. The process is essentially a transient one, since spray times are very short (maximum time of the order of one second).

The nozzle used was a conical spray nozzle with the internal components removed, so that a simple cylindrical jet was obtained. The spray was observed by means of high-speed photography using the lights and camera described in the section on experimental equipment. A trigger incorporating a microswitch was designed and built to fire the lights at any desired stage of the spray process.

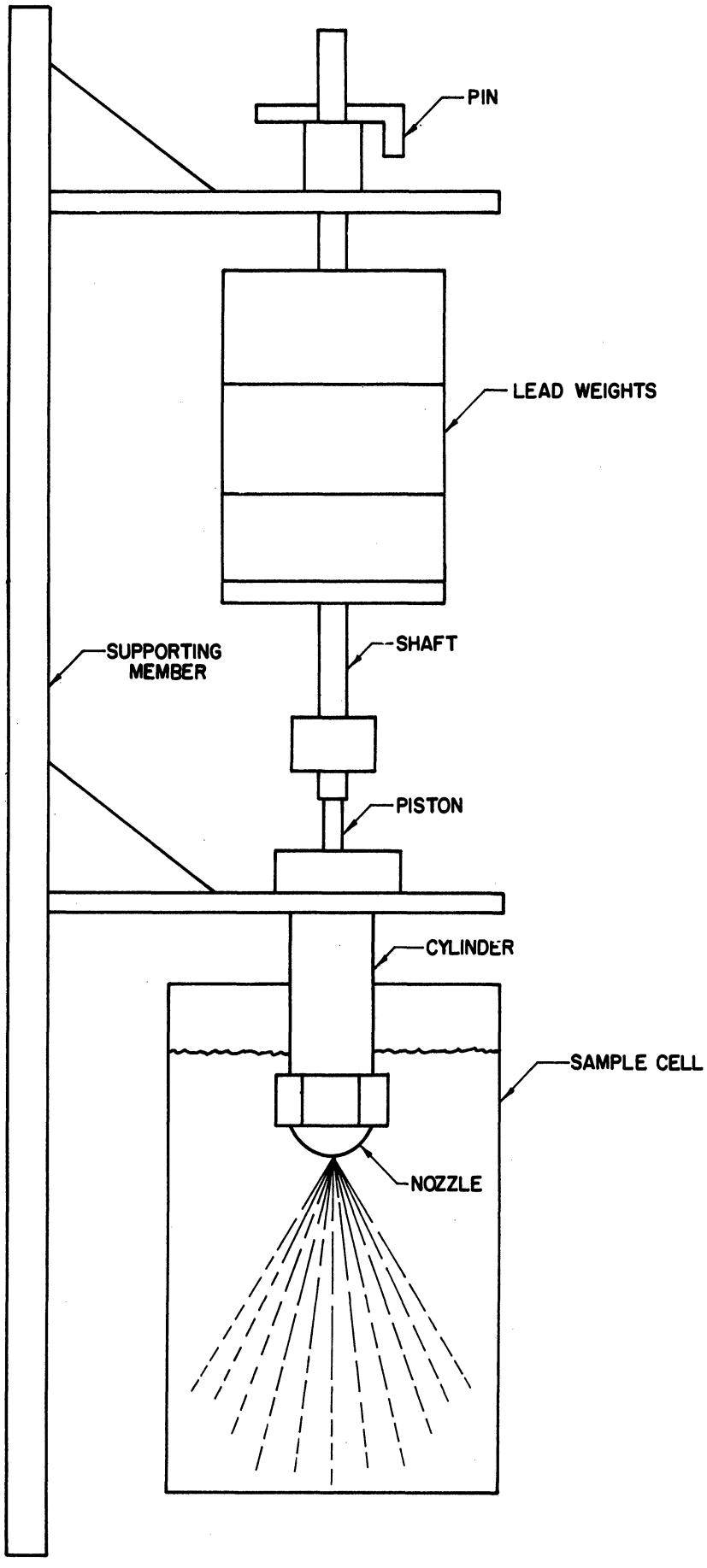

Figure 6. Apparatus for Transient Injection.

A series of photographs obtained with this equipment are shown in Figures 7 through 12. These are not photographs of a single spray, but are a series of photographs taken at successively later times on the same system but on different runs. Work with this equipment resulted in two conclusions: first, that it is possible to produce multiple emulsions from a cylindrical jet using the carbon tetrachloride-water system without surfactant addition - this conclusion was possible because multiple emulsion drops could be detected at the edges of the spray zone; and second, that it was necessary to go to lower pressures to decrease spray density to the point that more of the drops could be photographically resolved.

It was not possible to use this transient type of equipment for the lower pressures required, as the friction between the piston and cylinder became important enough that pressures could not be determined accurately. Spray times were also too low to permit more than one photograph per run. Consequently, it was necessary to build completely new equipment for the taking of quantitative data. Before discussing the experimental equipment used for the quantitative data, we will first discuss some of the general considerations involved in a suitable system of analysis.

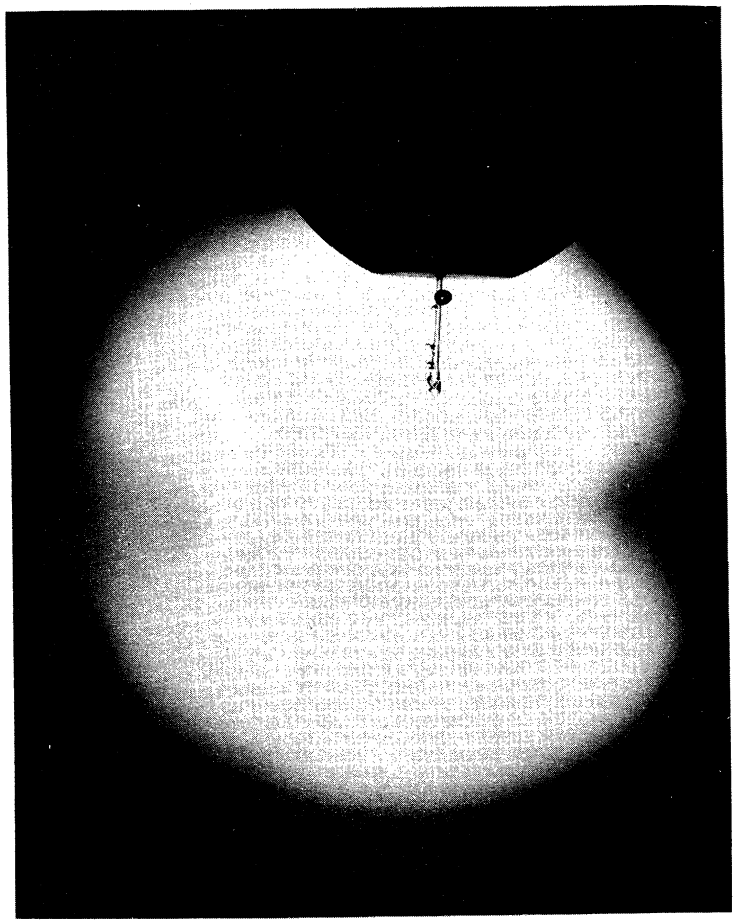

Figure 7. Photo of Transient Injection Process - 2.6X

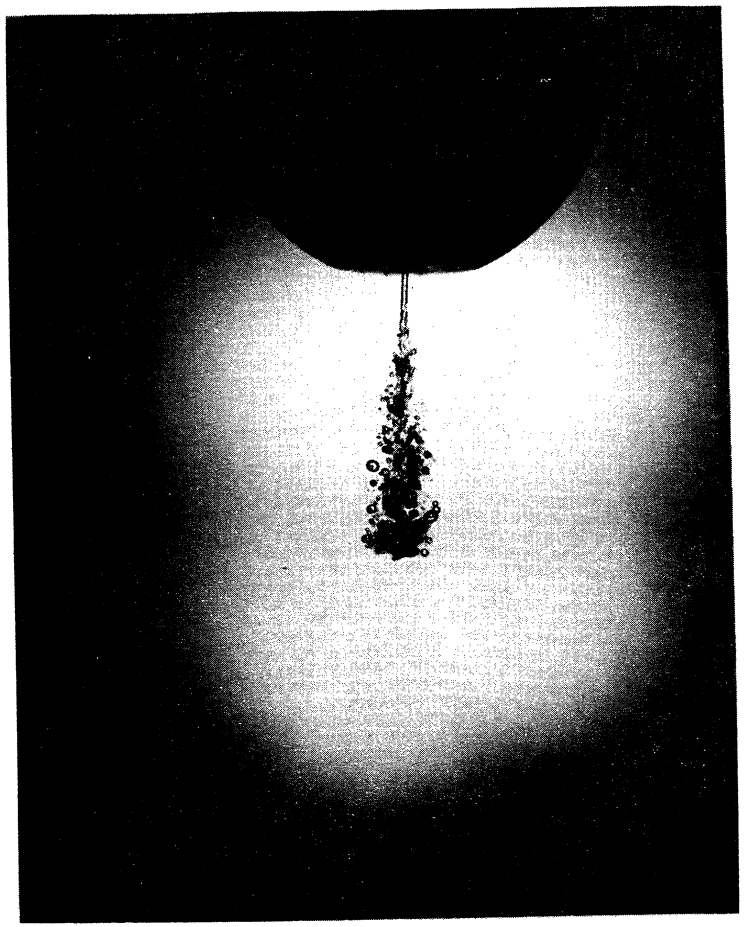

Figure 8. Photo of Transient Injection Process - 2.6X.

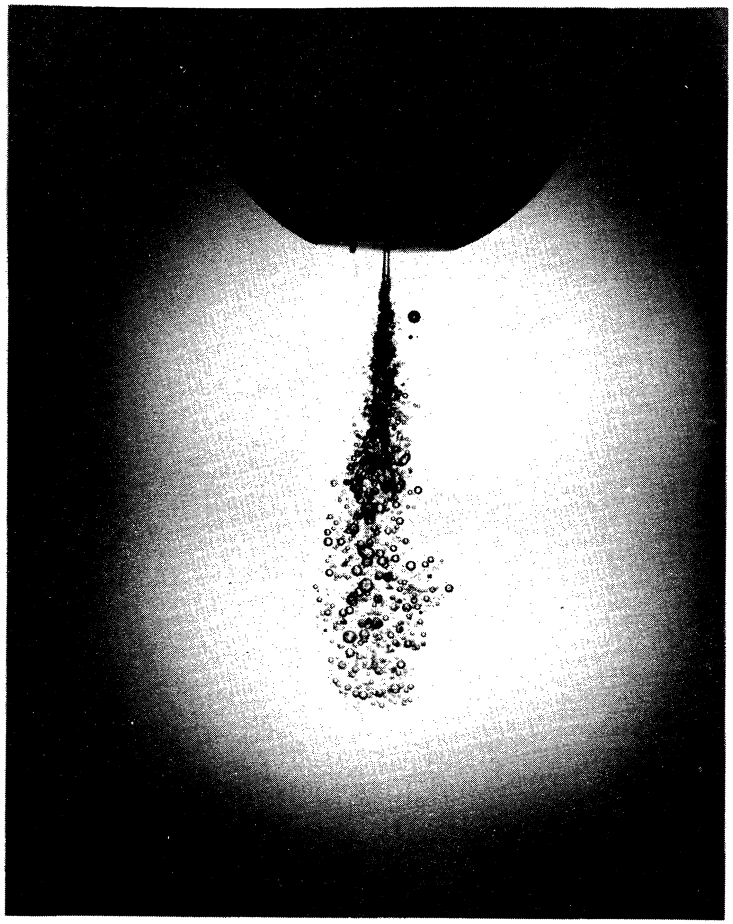

Figure 9. Photo of Transient Injection Process - 2.6X.

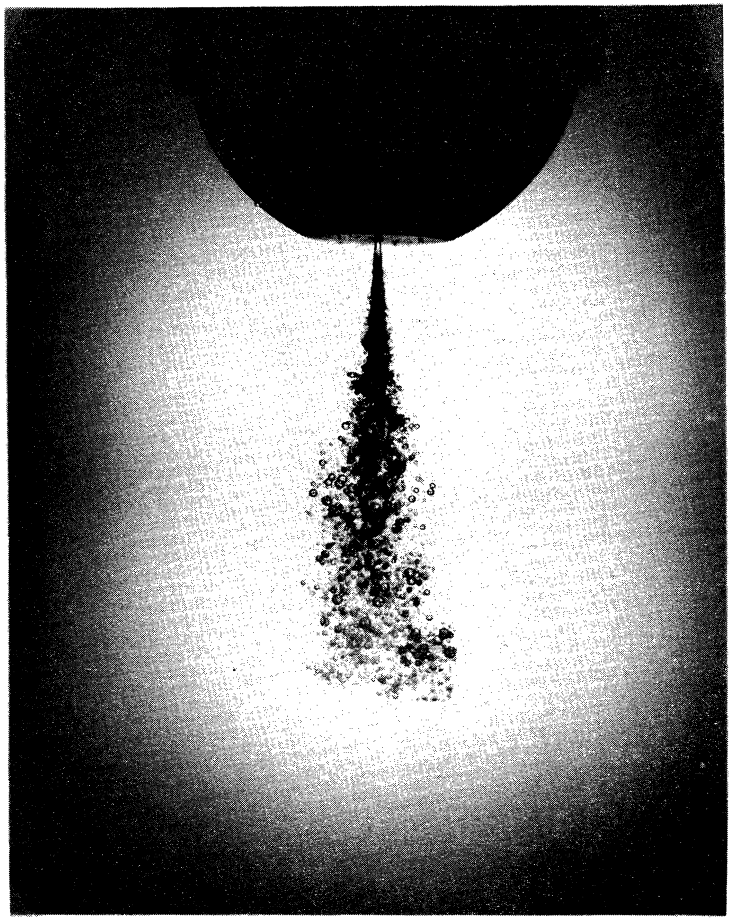

Figure 10. Photo of Transient Injection Process - 2.6X.

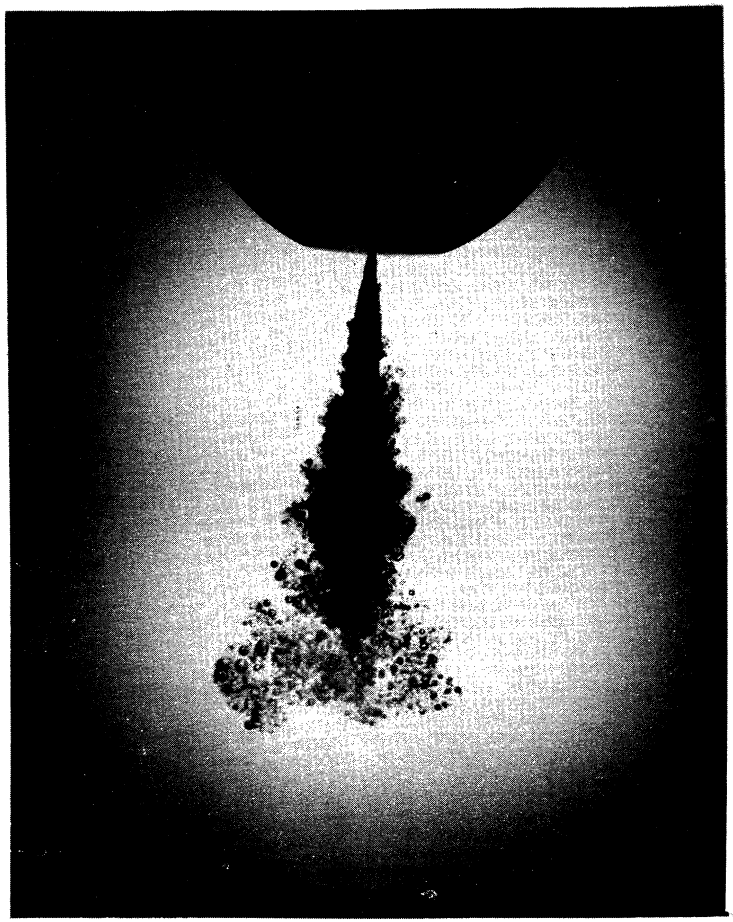

Figure 11. Photo of Transient Injection Process - 2.6X.

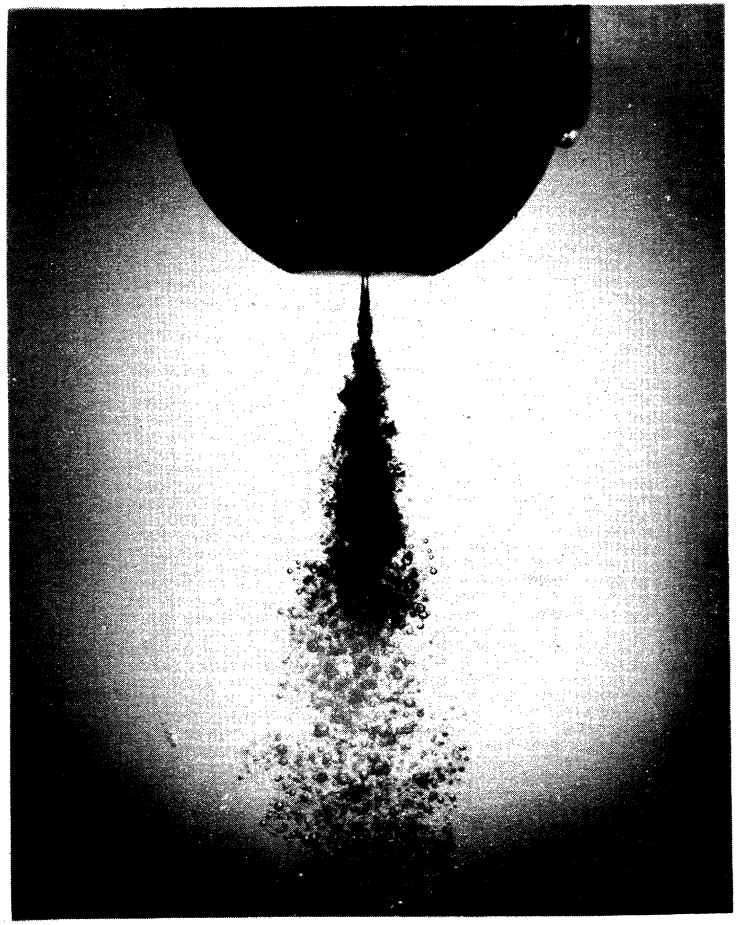

Figure 12. Photo of Transient Injection Process - 2.6X.

IV. ANALYSIS OF SPRAYS

A number of techniques have been described in the literature for general spray analysis. All have their particular advantages and disadvantages; however, not all are readily adapted to analysis of multiple emulsions, where one must not only be concerned with the main drop distribution, but with the distribution of the included drops as well.

A good summary of the various methods can be found in the report by Putnam[65], et al. Some methods depend on the physical collection of the drops, either on a specially coated slide or screen, or in a bath of a particular receiving fluid. These methods are frequently adequate for liquid-into-gas sprays, but suffer from certain disadvantages, such as distortion of the drop under its own weight and unequal evaporation rates of drops in the various size classes. Even without these disadvantages, the difficulty of introducing a collector into a liquid-liquid spray is sizeable.

Ranz[67] sampled some liquid-liquid sprays using a collector which was essentially a box with sliding, rubber-band-loaded top and bottom. With this apparatus it is possible to effectively cut a transverse slice from the spray. It does, however, introduce perturbation into the flow field, and furthermore gives a space-wise rather than the desired time-wise distribution because of varying drop velocities.

Other methods of spray analysis require the impaction of the spray upon a coated slide or suitable surface. The traces left

by the droplets are then measured to determine the spray distribution. This system obviously will not adapt to multiple emulsion study. Another technique involves the spraying of an artificial fluid - e.g., paraffin or wax - which can be solidified and the resultant particles screened or counted. Again, this method is not adaptable to multiple emulsions because of the opacity of the fluids and the difficulty in controlling the physical properties of the sprayed fluid over the desired range. Certain electronic methods use the insertion of a probe into the spray with automatic analysis based on drop impacts. This system introduces a perturbation in the flow field and, which is more serious, cannot discriminate between ordinary drops and drops with included phases.

There are in addition certain optical techniques which have been applied to spray analysis. McDonough(55) and Scott(81) have used a light transmittance method for the analysis of interfacial areas in orifice mixing of immiscible liquids. This method has the advantage of extreme rapidity, but gives only the total interfacial area and does not permit discrimination between drops and inclusions. It is also necessary to calibrate the equipment using the photographic technique which we will discuss next (and which is the method of analysis used in this research). If some way can be found to discriminate using a light transmittance technique between external drop area and area contributed by inclusions, this would be a most desirable method of analysis because of the speed and lack of expense for film, etc.

The photographic technique used in the course of this research has been known for some time, but was brought to its full application by York in 1949.[93] The method consists of taking an actual photograph of the spray droplets with high-speed still-picture photographic equipment. Double-exposure pictures are taken as well as single exposures. A known, very short time delay is used between the two exposures of the double-exposure shots. The single-exposure photographs are then counted - i.e., the number of drops in each of the selected series of size classes are determined. This gives an instantaneous, or space-wise drop distribution. The double-exposure photographs are then measured to determine the distance between successive images, and thus the velocity, of each size class of drops. By weighting the space-wise distribution with the drop velocities, one can obtain the desired time-wise spray distribution.

This process has certain disadvantages. There is a human factor of judgement involved in the counting process, and all the developing, counting, transcribing, etc., tends to grow somewhat tedious. It is, however, the only method which is applicable to multiple emulsion work at this time, since only by direct visual observation is it possible to discriminate between the large drops and the inclusions. A more detailed discussion of certain of the factors in analysis will be made in the following sections.

V. EXPERIMENTAL EQUIPMENT

The experimental equipment used for the majority of this investigation can be divided into four categories:

1) Liquid injection system.

2) Photolights and electronic time delay system.

3) Camera, film, and darkroom equipment.

4) Interfacial tension determination.

V.1 Liquid Injection System

Figure 13 shows the physical relationship of the camera, injection equipment, and photolights while taking data. Valves 2, 3, and 4 are 1/8" needle valves, while valves 1 and 5 are petcocks. The injection system consists of a charging funnel, a reservoir, a nitrogen supply to pressurize the reservoir, a metering system on the nitrogen stream, and a method for attaching a nozzle to the outlet stream from the reservoir. The injected fluid passes into the stagnant receiving fluid which is contained in the sample cell.

All lines shown in Figure 13 are 1/4" copper tubing. The reservoir is fabricated of stainless steel pipe. The funnel is a standard pyrex lab funnel about 3" in diameter, and is attached to the system by a short length of clear plastic tubing. This tubing serves as a sight glass for the liquid level in the reservoir while charging the system.

Pressure is supplied by a standard nitrogen cylinder, and is regulated with an ordinary nitrogen pressure regulator. A ballast

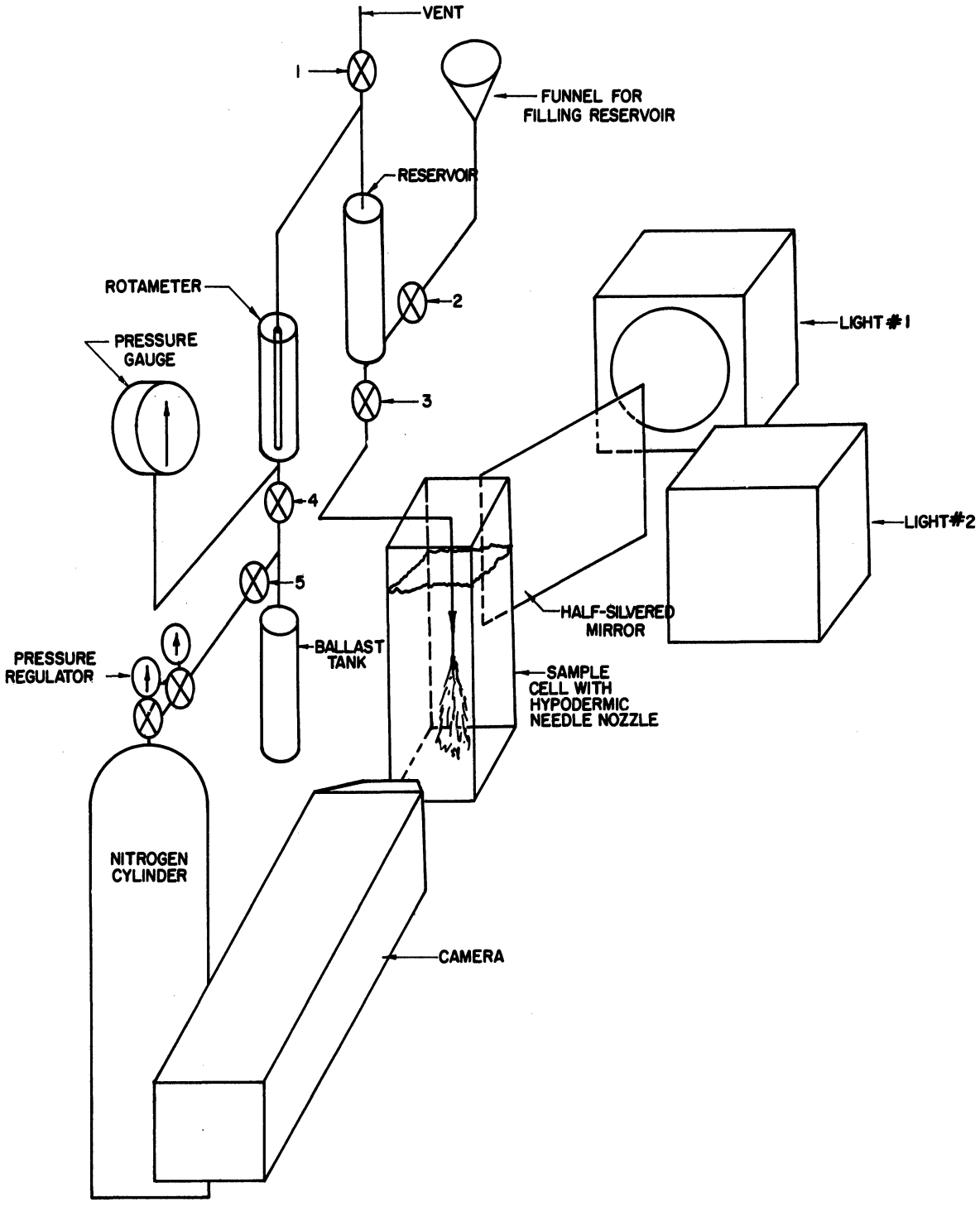

Figure 13. Schematic Diagram of Experimental Equipment.

tank fabricated of steel pipe coupled with a throttling valve (4) damps out pressure fluctuations caused by the pressure regulator. Valve 5 is a petcock used to shut off the nitrogen cylinder while charging the reservoir to avoid the slowness of using the cylinder valve.

The nitrogen stream was metered at a known pressure by a rotameter. The pressure gauge is indicated as dial-type, however, both dial-type gauges and manometers were used. Calibrations for the pressure gauges are given in the Appendix. The rotameter used was a dual-float type manufactured by the Manostat Corporation, New York, New York, catalog number FM1043T. The flowmeter had spherical floats, one of stainless steel and one of sapphire. Calibration curves for the pressures used are given in the Appendix. Room temperature was essentially constant - it was recorded, however, as a routine observation - but no temperature correction was required.

As nozzles, standard Becton, Dickinson, and Company hypodermic needles were used, except that the ends were ground flat and the exit hole reamed. These nozzles were checked under a microscope to verify smoothness and lack of eccentricity, and the inside diameters are tabulated in Table I. L/D ratios were fairly large; however, many studies have indicated[30,31,32,94] that this will not be a significant variable for the work considered here. The main effect of high L/D ratios is on discharge coefficient, and here the flow rate was measured directly.

The needles were attached to the copper tubing by fabricating a connector using a Becton, Dickinson, and Company standard adapter

TABLE I

DIAMETERS OF HYPODERMIC NEEDLES USED AS INJECTION ORIFICES

Size Designation Number	Inside Diameter, Millimeters
13	1.87
15	1.42
16	1.22
17	1.042
19	.642
20	.614
21	.532
22	.420
24	.317
25	.277
27	.229

with a female "Luer-Lok" fitting for hypodermic needle on one end and a male thread on the other. The "Luer-Lok" fitting accepts the standard male "Luer-Lok" fitting on the hypodermic needle. The male thread was of a non-standard type, and so was filed smooth. The resulting surface was silver soldered into one side of a standard 1/4" copper tubing connector, which then was attached to the copper tubing from the reservoir.

The sample cell which held the stagnant receiving phase was fabricated of 1/4" safety plate glass held in an angle iron frame. The five sheets of glass which comprised the bottom and four sides of the cell were held together with Carter epoxy resin glue. Some difficulty was experienced with leakage, and so the cell was also caulked on the outside with litharge-glycerol cement. This mitigated the problem, but no means was found to obviate it altogether - a cell fabricated of a continuous piece of glass would do this but the cost is prohibitive.

V.2 Lights and Time Delay System

Photolights that were used were General Electric catalog number 9364688G. These lights give an extremely intense flash with a time duration of 1-2 microseconds. The lights were triggered with two time delay units constructed as shown in Figures 14 and 15. These units use number 2050 thyratrons for triggering, and can be adjusted to give time delays varying from about 10 microseconds to 1500 microseconds using the internal R-C network. Longer delays can be produced by adding an external capacitor. The two delay units were used in series,

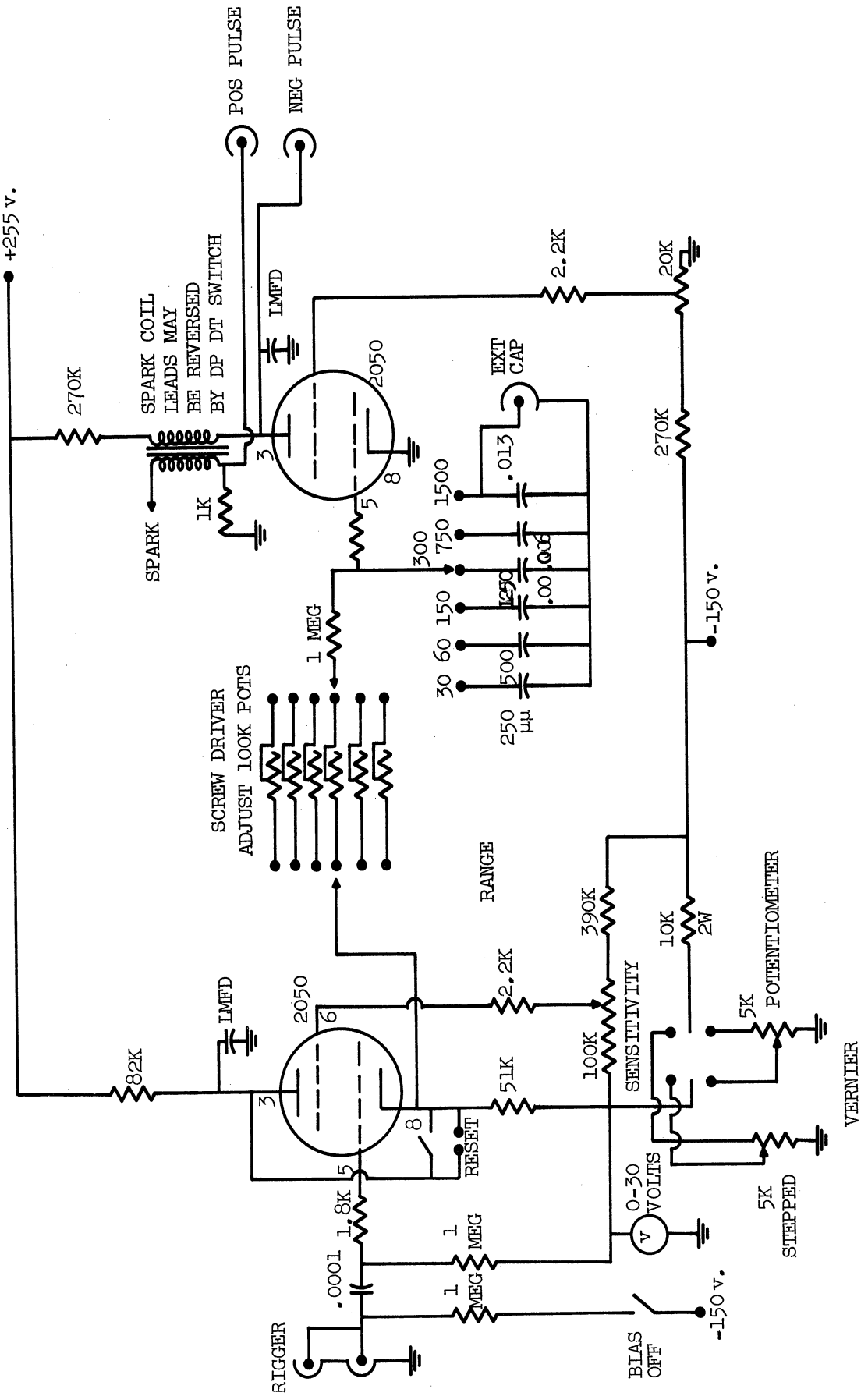

Figure 14. Time Delay Unit.

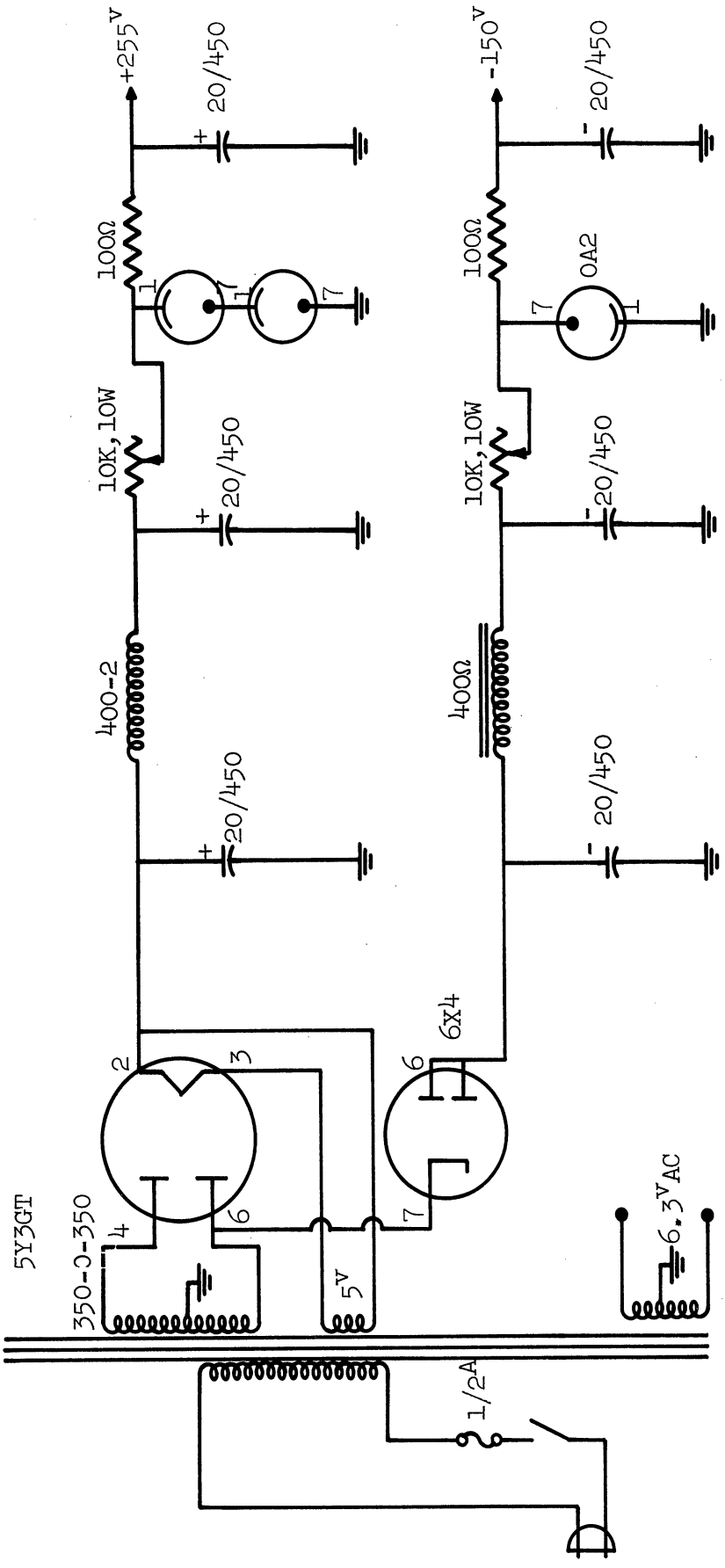

Figure 15. Power Supply for Time Delay Unit.

with the trigger pulse to the first unit being supplied with a pushbutton. The first unit fired the first light and simultaneously supplied a pulse to the second delay unit. The second delay unit was set for the desired time delay, and upon receiving the pulse from the first unit delayed the desired interval and fired the second light.

Time delays were measured each time the lights were fired by triggering a Hewlett Packard Model 524B counter (with a Model 526B time interval unit) from the pulse which triggered the lights. Prior to use of the light system in experimentation, checks were made using photocells to ensure that the response time of the lights, i.e., the time between receipt of the high voltage pulse and the flash, was negligible compared to the delays used.

V.3 Camera, Film and Darkroom Equipment

Two cameras were used - one with a magnification of 10X and the other with magnification of 2.6X. All counted data was taken using the 10X camera. Camera magnification, lenses, and depth of field calibrations are shown in the Appendix. Film used was Kodak Contrast Process Ortho 4" x 5" cut film. This is a fine-grained orthochromatic film with an ASA tungsten rating of 50. The film was developed for five minutes at 68°F. in Kodak D-11 developer, rinsed for 30 seconds, placed in Kodak Acid Fix for 10 minutes, rinsed for 30 seconds, placed in Kodak Hypo Clearing Agent for 2-3 minutes, rinsed for 10 minutes, and dried.

V.4 Interfacial Tension Determination

Interfacial tensions were determined using a Cenco (Central Scientific Co.) interfacial tensiometer type 70545. Manufacturer's serial number for this instrument was 410; the serial number of the Department of Chemical and Metallurgical Engineering was C7-8. The platinum ring used had a circumference of 5.998 cm. and was also manufactured by the Central Scientific Company (model 70542).

It is interesting to note that in using a ring type tensiometer for interfacial tension (as opposed to surface tension) work it is necessary to lower the ring rather than raise it to avoid contamination by the second phase. This was not found to be an important consideration in work of the order of accuracy required here, but in more precise determinations an appreciable error can be introduced. Even though there was not a great difference in the readings obtained by raising and lowering the ring, all determinations were made from the values obtained by the conventional lowering method. Between each reading the ring was rinsed in potassium dichromate - sulfuric acid cleaning solution and rinsed in double distilled water as it was found that residual contamination after one reading affected reproducibility. Under very strict laboratory conditions, a ring-type tensiometer can be made accurate to .05 dyne/cm., far in excess of the requirement for this work. The ring-type tensiometer has the advantage of speed over some of the other methods for interfacial tension determination such as capillary rise, drop weight, pendant drop, etc. A calibration curve for the interfacial tensiometer is given in the Appendix.

VI. EXPERIMENTAL PROCEDURE

In taking data, the camera was first focused on the spray issuing from the orifice. This was done by using a ground glass screen in place of the film, and using a General Radio Corporation Model 1531A Strobotac for illumination. By setting the Strobotac for relatively low flashing rates it was possible to effectively "stop" the spray process for focusing purposes. This was a new technique in conjunction with the photographic method of analysis, and eliminated much of the trial and error focusing necessary when using a steady source of light. Most of the spray could be included in the field, so it was not necessary to traverse the spray to remove effects of non-uniformity.

Experimental conditions during the course of a run were recorded on a standard mimeographed form, and pictures were normally taken in groups of 24. After developing and drying, each negative was stamped with an identification number and the corresponding number stamped on the data sheet. Approximately 1000 pictures were taken in the course of the investigation.

The negatives were examined using a Jones and Lamson Bench Comparator, which projected an image of the negative on a ground glass screen, and gave a magnification factor of 10, so that the 2.6X negatives were examined at a total magnification of 26 and the 10X negatives at a total magnfication of 100. In Figure 16 through 19 are shown typical single and double flash shots. Figure 17 and

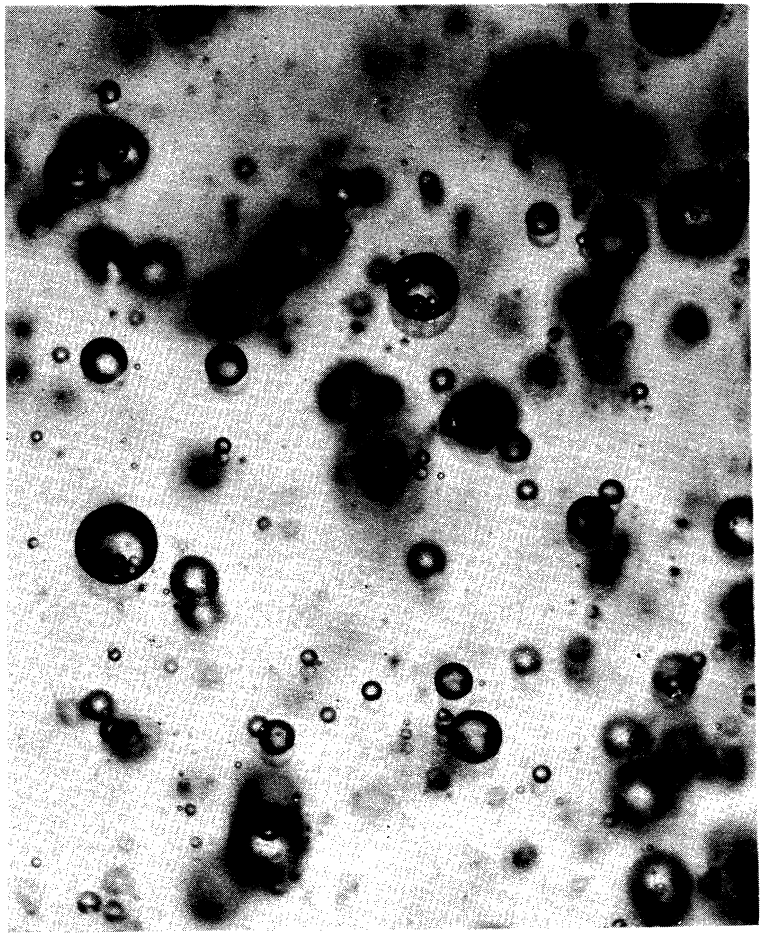

Figure 16. Print from Typical Double Flash Photo.

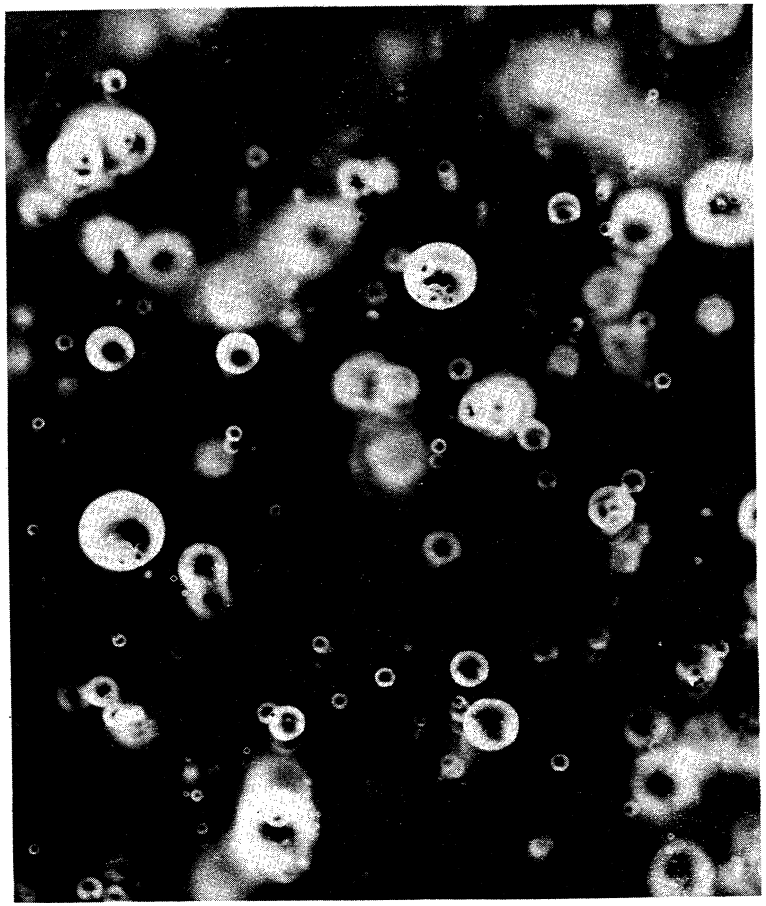

Figure 17. Typical Double Flash Negative - 10X.

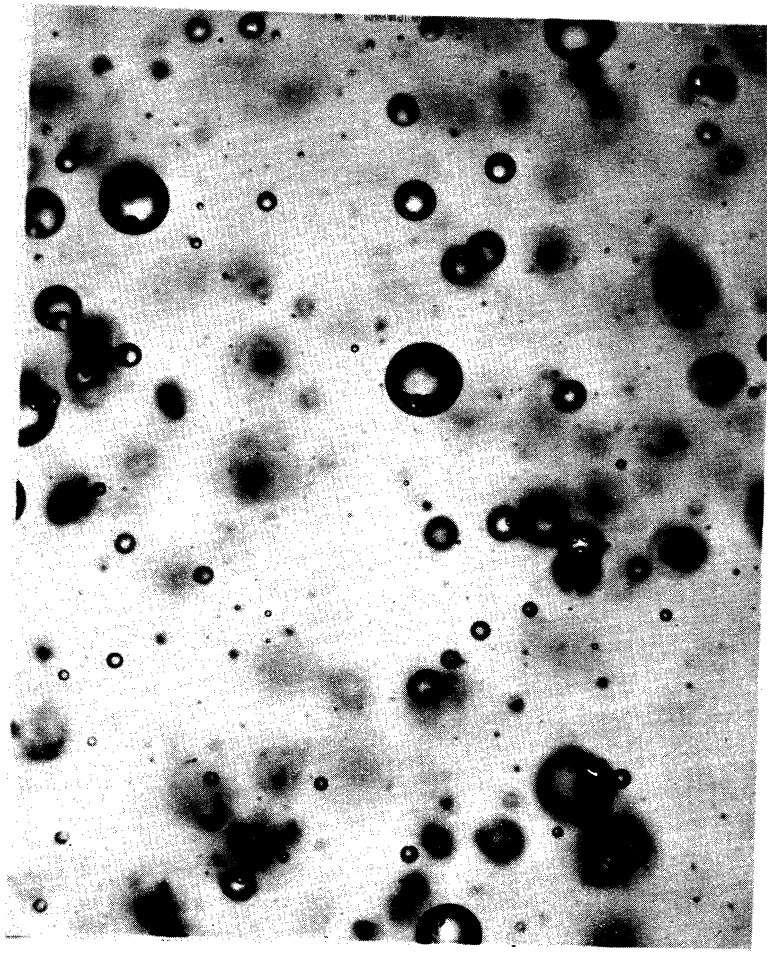

Figure 18. Print from Typical Single Flash Photo.

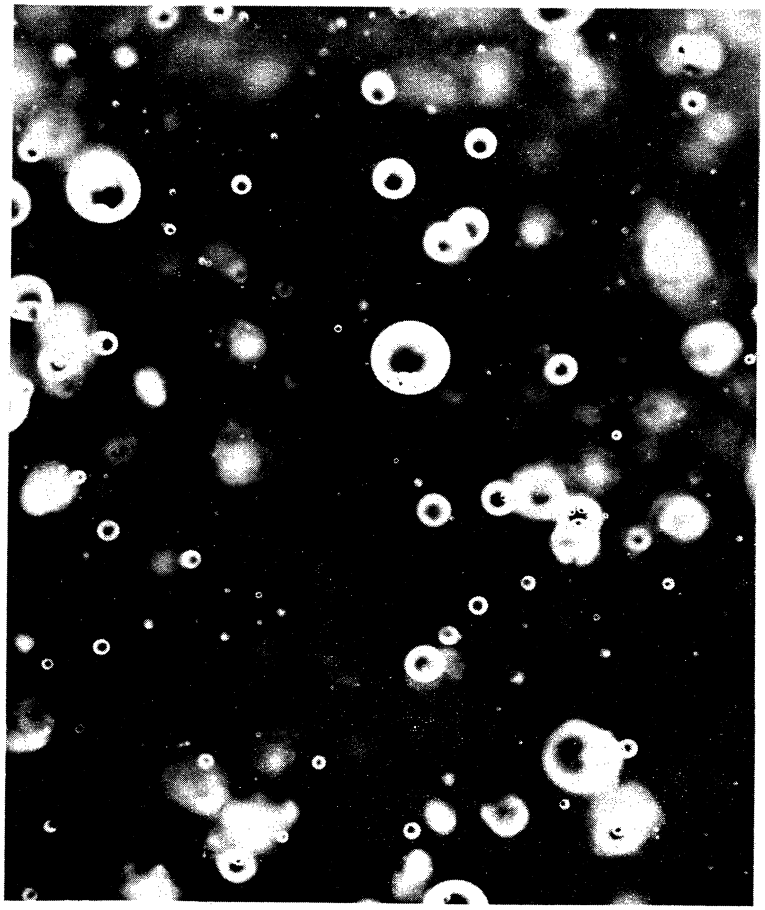

Figure 19. Typical Single Flash Negative - 10X.

19 show the appearance of the negative as it was counted; Figures 16 and 18 are conventional contact prints from the negative. Considerable detail has been lost in these prints over the original negative, but it is still possible to distinguish the inclusions nestling in some of the parent drops. The original negatives have sufficient detail to permit measurement of the diameters of the inclusions as well as of the parent drops.

The drops were counted using a transparent template made by engraving a scale on a piece of clear photographic film. The same template was also used for distance measurements for the double-exposure photographs. The appearance of the drops when magnified an additional 10 diameters over the magnifications in the photographs presented here is much as shown in Figure 20. It can be demonstrated that the inertial forces tend to control whether the inclusions rise or sink with respect to the main drop. The causes the clustering shown in Figure 20.

Two remarks should be made at this point with regard to the human error in the analysis. First, the judgement factor as to whether or not a drop is in focus is much less important than in the usual spray analysis, because primarily relative areas, volumes, etc. are being measured. This will become apparent in the discussion of the analysis of the counted data. Second, the clustering of the inclusions in either the top or bottom of the parent drop makes analysis more uncertain, since it is difficult to estimate numbers and diameters of drops that are partially, or in some cases totally

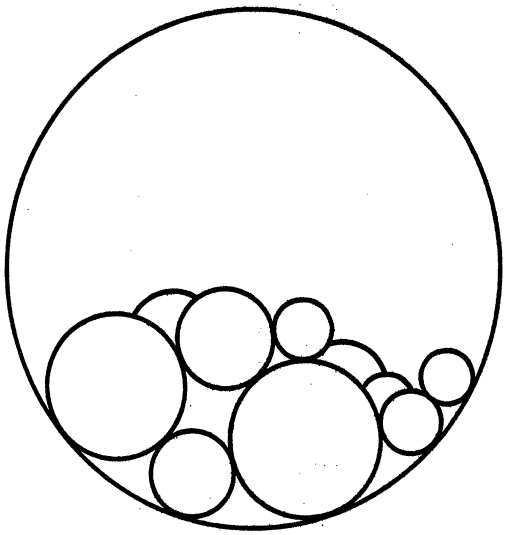

Figure 20. Schematic Diagram of Drop Appearance During Counting.

obscured. This tends to give results which may be systematically low for the included area and volume. The error should be more nearly self cancelling for diameter distribution measurements, but will still contain some bias since it is easier to obscure a small drop totally than a large one. In effect, this would tend to skew the distribution toward the large size classes. Considering the relative numbers of drops in the small and large size ranges, however, coupled with the log normal form that the distribution takes as pointed out below, the effect on distribution measurements should be negligible.

With some high rates of flow, difficulty was encountered in getting a sufficiently non-scattered light beam from the object drop to the lens, resulting in a loss of contrast. It was possible to overcome this difficulty to some degree by using the arrangement shown in Figure 21 to examine the negatives. The negative is illuminated by glancing light from an intense light source (in this case, light from a microscope illuminator). This system makes the drops in focus stand out from the background, and also helps in discrimination between in-focus and out-of-focus drops.

Typical drop travel data obtained from the double-exposure photographs is shown in Figure 22. Points shown are averages of many drop measurements; the velocity of drops of a given diameter will show a considerable range, and averaging facilitates the smoothing of the data. As can be seen from this typical run, velocity differences are more pronounced in the lower size ranges, as would be expected. Because of the shape of the parent distribution, the points plotted

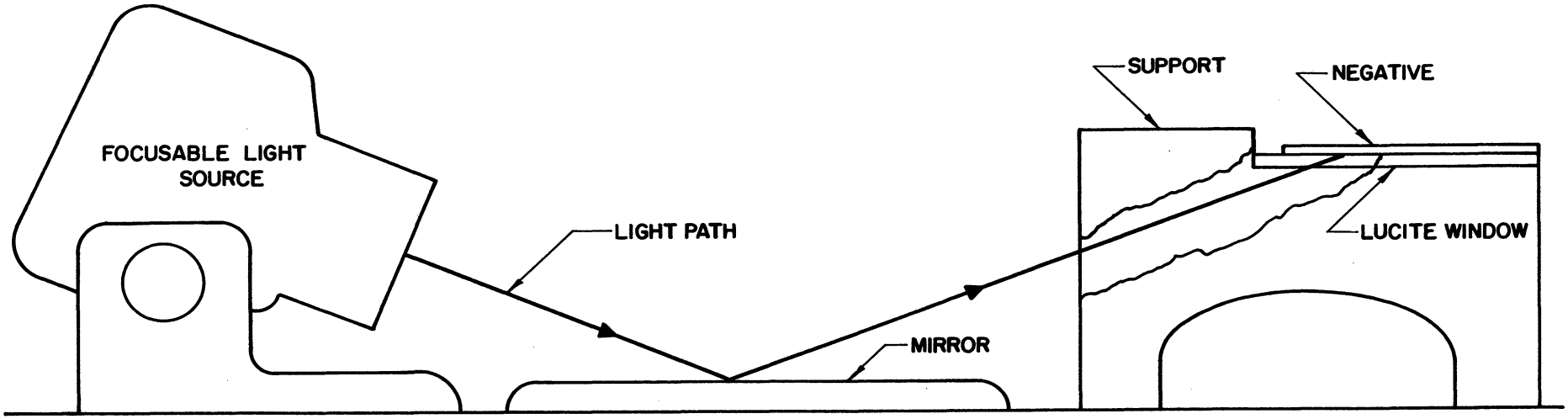

Figure 21. Reflected Light Method for Examination of Negatives.

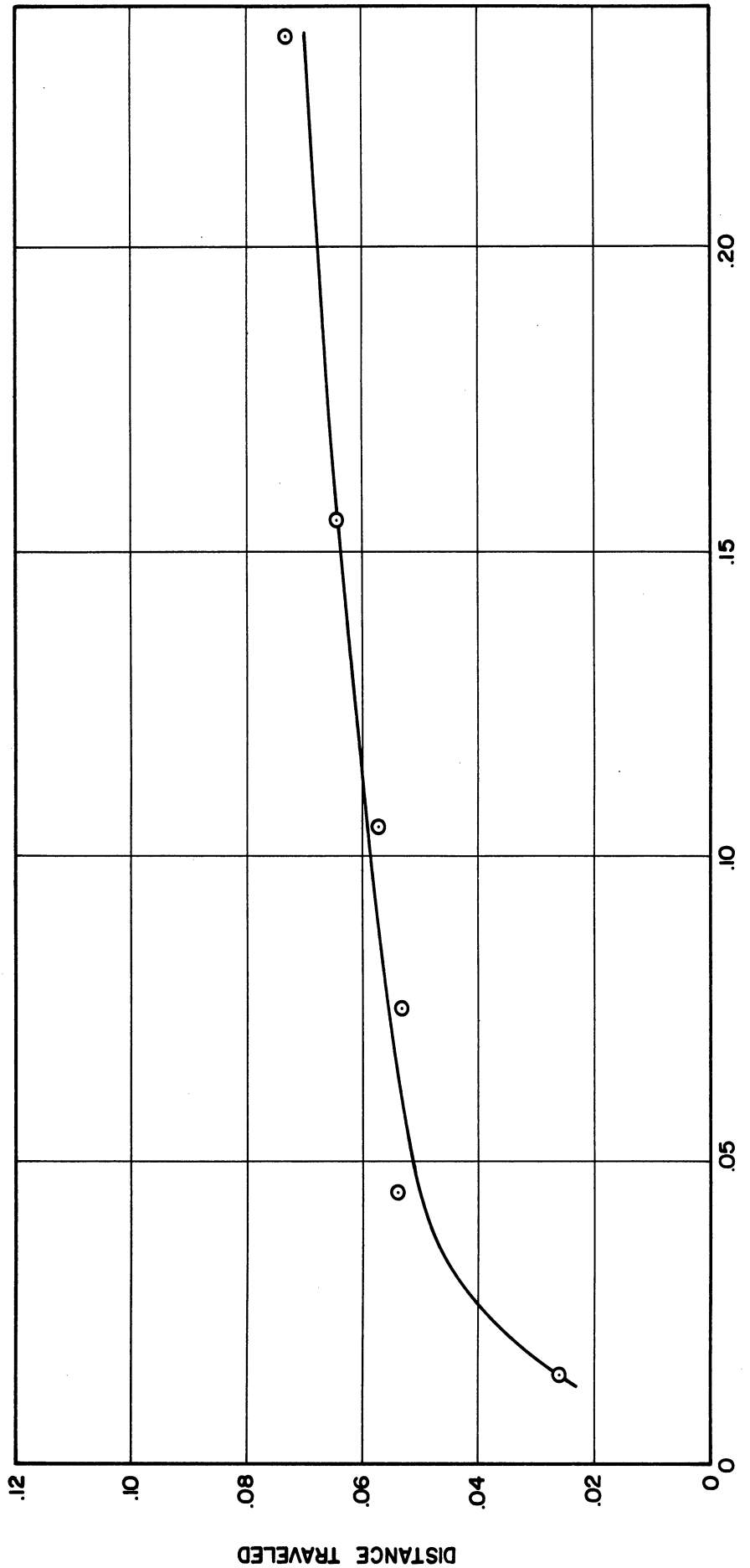

Figure 22. Typical Drop Travel Data - Run Number 4.

representing the lower size ranges represent a larger sample of drops than those at larger diameters.

From counting the single-exposure photographs, one obtains the distribution of large drops within a preselected series of size ranges, and the distribution of inclusions within another preselected series of size ranges according to the diameter of the parent drop.

The counted data obtained can be depicted as shown in Figure 23. For M preselected size ranges we can characterize the diameter of the large drops by the mean diameter of the range, denoted by $D_m (1 \leq m \leq M;\ m = \text{integer})$. Similarly we can preselect N size ranges for the inclusions and characterize them by their mean diameter $d_n (1 \leq n \leq N; n = \text{integer})$. Associated with the vector D_i $(i = 1,2,3 \ldots M)$ there will be two vectors obtained from the drop counting process. The first is the distance vector, which we denote by ℓ_i, and which represents the distance traveled by drops in the respective size range obtained from the smoothed data as shown in Figure 22. Coupled with knowledge of the time delay used, this vector will yield our velocities. The second vector represents the number of drops, y_i, of diameter D_i which we observe in counting the single-flash photographs.

We also obtain a matrix of values x_{ij} $(i = 1,2,3 \ldots M;$ $j = 1,2,3 \ldots N)$, where x_{mn} $(1 \leq m \leq M; 1 \leq n \leq N)$ denotes the number of inclusions counted of size d_n within a parent drop of size D_m. This data, coupled with the data on flow rate, interfacial tension, etc., is fed to a computer program which carries out the routine calculations.

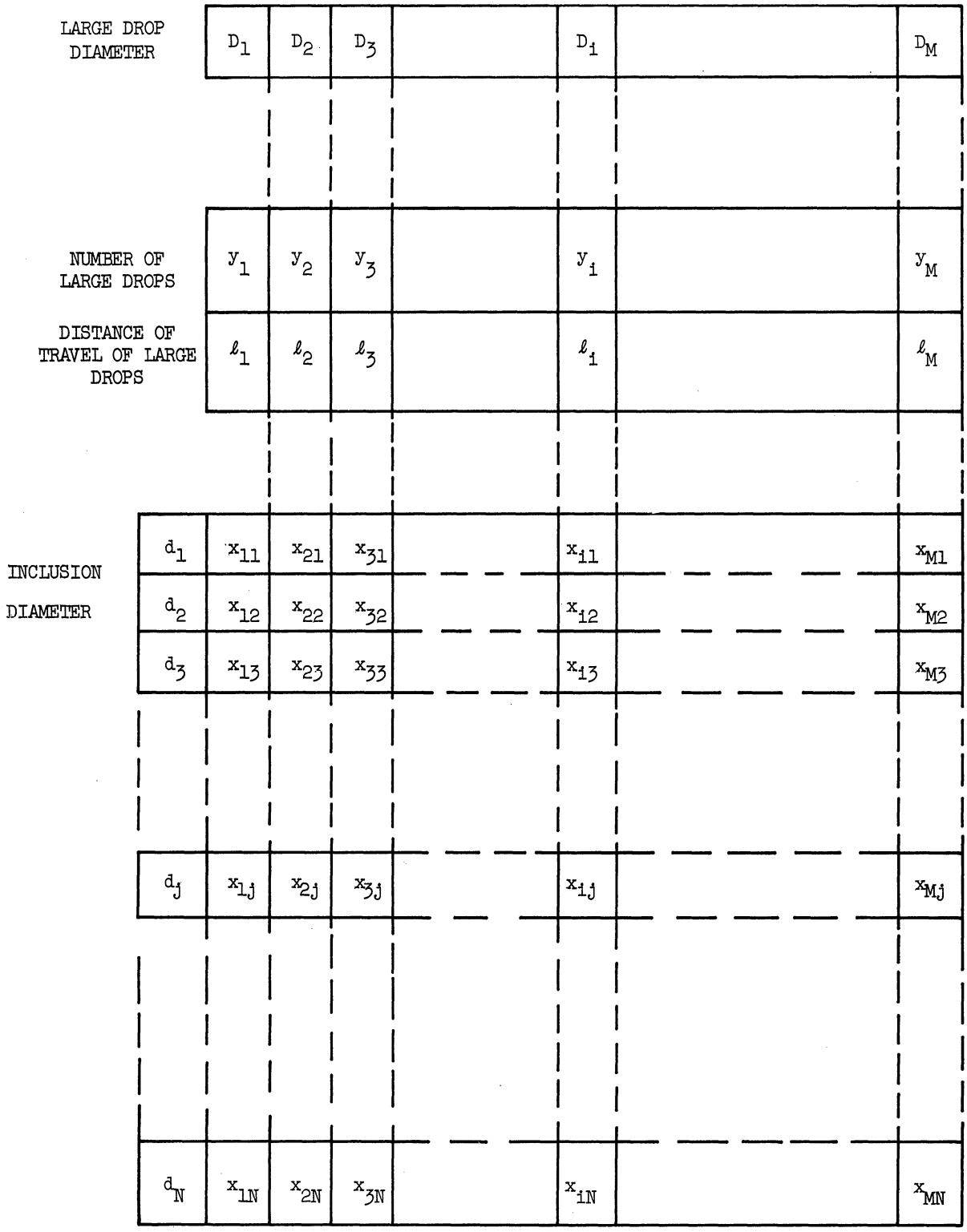

Figure 23. Schematic Diagram of Counted Data.

With regard to interfacial tension, it might be mentioned that checks were made on the fluids both before and after spraying to pick up any contamination effects from the equipment. No appreciable effects were found, and the interfacial tension of the fluids used would remain constant over extended periods of time.

VII. DISCUSSION AND RESULTS OF COUNTED DATA

The experimental system used for the counted data was the carbon tetrachloride - water system. This system offers several advantages. First, it has been used by a number of investigators working in the field of liquid-liquid sprays.[8,37,67] Second, the non-flammability of carbon tetrachloride made it a convenient liquid to use in the open sample cell. Third, the first derivative of the interfacial tension - temperature curve for the carbon tetrachloride - water system is a known constant ($\frac{d\gamma_i}{dT} = .098$)[89] permitting ready estimation of possible temperature effects. Fourth, the system offers a reasonable density difference. Finally, it was desirable to retain water as one component of the system since so much of emulsion technology utilizes water as one component.

The selection of the independent variables to be studied is a sizeable problem in itself. For the moment, we will let it suffice to say that the independent variables used were nozzle diameter, velocity through the nozzle, density ratio of the two phases, and interfacial tension.

VII.1 Ranges of Variables Studied

Three nozzle diameters were used: 0.420 mm. (No. 22 hypodermic needle), 0.642 mm. (No. 19 hypodermic needle), and 1.042 mm. (No. 17 hypodermic needle). Nozzle velocities ranged from 39 to 902 cm./sec., and interfacial tension was run at two levels, 32.0 and 11.7 dynes/cm. Density ratio was varied by interchanging sprayed and receiving fluid

with levels of .63 and 1.60 resulting. For the counted data, all runs were at a viscosity ratio of approximately 1.0; however, work done on mechanism was at a viscosity ratio of receiving fluid to sprayed fluid of about 1000, with the same mechanism operative.

For this research, limits on the operating variables were these:

1) Nozzle diameters were limited at the low range by resolution of the camera system, and at the high range by the size reservoir and sample cell required.
2) Velocities through the nozzle were limited on the low side by cessation of multiple emulsion formation and on the high side by clouding of the sample cell.
3) Density ratio was limited by the combination of cost and physical and chemical properties of available liquids.
4) Viscosity ratios are limited both above and below by the combination of nozzle diameter and pressure required. Small diameter nozzles require excessive pressures to attain the required flow velocity, while large diameters have the limitation noted above.

VII.2 Typical Raw Data Results

Shown in Table II are the results for a typical set of counted data. (Complete raw data may be found in Appendix D.) This information is fed into a computer program (see Appendix) which carries out the detailed mathematical manipulation. The diameter ranges for large drops and inclusions were the same for all runs. From the counted data it was possible to study two things. First, it was possible to determine a probability distribution function which would adequately represent the distribution of the large drops and that of the inclusions. It was then possible to correlate certain parameters of the process against the independent variables. Table III gives experimental conditions for the various runs and some of the more important derived data.

VII.3 Determination of Probability Density Functions

In order to use a given function f(z) as a probability density function there are two primary criteria that must be met:

$$f(z) \geq 0 \qquad \text{(VII.3.1)}$$

$$\int_{-\infty}^{\infty} f(z)\, dz = 1 \qquad \text{(continuous case)} \qquad \text{(VII.3.2)}$$

$$\sum_{i=-\infty}^{\infty} f(z_i)\, \Delta z_i = 1 \qquad \text{(discrete case)}$$

If these two criteria are fulfilled, and if in addition we can demonstrate that, for the random variable Z:

$$P_R(Z \leq z_1) = \int_{-\infty}^{z_1} f(z)\, dz \qquad \text{(VII.3.3)}$$

TABLE II

TYPICAL RAW DATA SET - RUN NUMBER 10

System: Saturated Carbon Tetrachloride into Saturated Water
Flow Rate: 130 cc/min.
Nozzle Diameter: .0642 cm.
Interfacial Tension: 32 dynes/cm.
Viscosity of Flowing Phase: 1 cps.
Density of Flowing Phase: 1.595 gm./cc.
Time Delay: 1.55×10^{-3} sec.

	Large Drop Size Range cm. x 10^{-2}	0.-1.	1.-2.	2.-3.	3.-4.	4.-5.	5.-6.	6.-7.	7.-8.	8.-9.	9.-10.	10.-11.	11.-12.
	No. Large Drops	193	304	140	63	36	15	11	11	7	4	3	2
	Average Distance, cm. x 10^2	1.75	2.10	2.45	2.80	3.10	3.40	3.75	4.10	4.40	4.75	5.10	5.45
Number of	0.-.5	0	11	17	5	11	15	11	14	4	5	0	0
Inclusions	.5-1.0	0	2	14	12	9	13	9	6	3	9	0	1
by Size	1.0-1.5	0	0	8	13	28	4	15	17	22	6	6	8
Range,	1.5-2.0	0	0	0	6	6	6	5	5	10	5	11	4
cm. x 10^2	2.0-2.5	0	0	0	2	7	5	1	5	12	4	0	0
	2.5-3.0	0	0	0	0	1	1	0	1	0	2	1	0
	3.0-3.5	0	0	0	0	1	2	3	2	2	1	1	2
	3.5-4.0	0	0	0	0	0	0	0	1	0	0	0	0
	4.0-4.5	0	0	0	0	0	1	0	1	0	1	1	0

TABLE III

EXPERIMENTAL CONDITIONS AND DERIVED DATA

Run No.	Nozzle Diameter, cm.	Flow Rate $cm^3/sec.$	Velocity Through Nozzle cm/sec.	Interfacial Tension Dynes/cm.	Reynolds Number	Weber Number	Reynolds No. x Weber No.	System	% Included Volume	% Included Area	Large Drops			Inclusions		
											$\bar{D}_{32}$ cm.	$\bar{D}_{10}$ cm.	Log Geom. Std.Dev'n	$\bar{d}_{32}$ cm.	$\bar{d}_{10}$ cm.	Log Geom. Std.Dev'n
1	.1042	4.58	537	32.0	89.3	1500	1.34×10^5	CCl_4 into H_2O	5.33	17.9	.0232	.0305	.309	.0138	.0164	.262
2	.1042	4.58	537	32.0	89.3	1500	1.34×10^5	CCl_4 into H_2O	5.39	17.4	.0237	.0304	.295	.0132	.0154	.250
4	.1042	1.53	180	32.0	29.8	167	4.99×10^3	CCl_4 into H_2O	0.00	0.00	.0397	.0678	.379	--	--	--
5	.1042	.333	39	32.0	6.49	7.92	5.14×10^1	CCl_4 into H_2O	0.00	0.00	.215	.220	.060	--	--	--
7	.0642	1.50	463	32.0	47.5	687	3.26×10^4	CCl_4 into H_2O	2.68	10.4	.0197	.0295	.379	.00940	.0115	.294
8	.0642	2.17	670	32.0	68.6	1440	9.87×10^4	CCl_4 into H_2O	5.05	16.2	.0146	.0186	.314	.00867	.0103	.272
9	.0642	2.17	670	32.0	68.6	1440	9.87×10^4	CCl_4 into H_2O	6.76	17.5	.0160	.0206	.314	.00843	.0106	.310
10	.0642	2.17	670	32.0	68.6	1440	9.87×10^4	CCl_4 into H_2O	6.01	16.9	.0153	.0196	.314	.00854	.0104	.292
11	.0642	.834	258	32.0	26.4	212	5.60×10^3	CCl_4 into H_2O	0.00	0.00	.0367	.0810	.404	--	--	--
13	.0642	.750	232	11.7	23.7	470	1.12×10^4	CCl_4 into H_2O	3.05	10.6	.0159	.0220	.354	.00861	.0107	.308
14	.0642	1.50	463	11.7	47.5	1880	8.93×10^4	CCl_4 into H_2O	7.50	18.9	.0159	.0194	.277	.00840	.00958	.242
15	.0642	1.33	411	32.0	26.4	339	8.94×10^3	H_2O into CCl_4	3.64	13.2	.0153	.0190	.295	.00899	.0102	.236
16	.0642	.918	284	32.0	18.2	161	2.94×10^3	H_2O into CCl_4	2.21	8.88	.0177	.0238	.334	.00894	.0103	.251
6	.0420	.367	264	32.0	17.7	17.7	2.61×10^3	CCl_4 into H_2O	1.55	5.40	.0246	.0332	.311	.00727	.00861	.279
12	.0420	1.25	902	32.0	60.4	60.4	1.03×10^5	CCl_4 into H_2O	4.28	12.1	.0133	.0157	.262	.00662	.00770	.267
17	.0420	.517	373	32.0	15.7	15.7	2.86×10^3	H_2O into CCl_4	1.13	3.67	.0220	.0274	.281	.00904	.0101	.226
18	.0420	.833	601	32.0	25.2	25.2	1.19×10^4	H_2O into CCl_4	3.27	7.01	.0136	.0162	.268	.00996	.0112	.226

we may say that f(z) is the probability density function for Z. An analogous definition holds for the discrete case. We will here restrict discussion to continuous random variables, since there is no discrete density function commonly used in particulate statistics.

In addition to the probability density function, we can define a probability distribution function as a simple integral transformation of the density function:

$$F(z) = \int_{-\infty}^{z} f(z)\, dz \qquad \text{(VII.3.4)}$$

The random variable Z can be associated with any characteristic of the spray for which a probability density or distribution function can be determined. Most small particle statistics work has associated F(z) or f(z) with either the number or weight distribution of particles ($f(z) = \frac{dV}{dz}$ or $\frac{dN}{dz}$). Since we can write:

$$\frac{N\pi z^3}{6} = V \qquad \text{(VII.3.5)}$$

$$\frac{dV}{dN}\frac{dN}{dz} = \frac{dV}{dz} \qquad \text{(VII.3.6)}$$

$$\frac{\pi z^3}{6}\frac{dN}{dz} = \frac{dV}{dz} \qquad \text{(VII.3.7)}$$

where: N = number of drops

z = diameter of drops

V = volume of drops

or, for estimates from our samples

$$\frac{\pi z^3}{6}\frac{\Delta N}{\Delta z} = \frac{\Delta V}{\Delta z} \qquad \text{(VII.3.8)}$$

we can obviously transpose a number distribution to a weight distribution, and similarly for other diameter-related functions. It should be noted that although F(z) and f(z) are associated with the weight or number distributions the functions are still written in terms of the diameter, although this is not necessary.

There have been many probability density functions proposed for use in spray research. Most of these are some specialization of a function of the type:(65)

$$f(z) = \alpha z^{\beta} e^{-\gamma z^{\delta}} \qquad \text{(VII.3.9)}$$

The decision as to which distribution to use must be made on purely pragmatic grounds - it is occasionally possible to justify a given distribution on theoretical grounds, but almost always by post hoc reasoning.

We will consider here the use of the three density functions most common in spray work:

1) The Log-Normal Distribution

$$f(\omega) = \frac{1}{\sqrt{2\pi}} e^{-\omega^2/2} \qquad \text{(VII.3.10)}$$

where

$$\omega = \frac{\log z - \log \bar{z}_g}{\log \sigma_g}$$

and $\bar{z}_g$ = geometric mean

σ_g = geometric standard deviation.

2) The Rosin-Rammler Distribution

$$f(z) = b n z^{n-1} e^{-bz^n} \qquad \text{(VII.3.11)}$$

3) The Nukiyama-Tanasawa Distribution

$$f(z) = a z^2 e^{-b z^n} \qquad \text{(VII.3.12)}$$

The log-normal distribution arises as a natural successor to the normal distribution where ratios rather than differences are important, i.e, cases where the geometric, rather than the arithmetic mean is important. The Rosin-Rammler distribution was originally developed for particulate solids, but has found some application to sprays, and the Nukiyama-Tanasawa function was developed for liquid-into-gas sprays.(65)

All three of these density functions are integrable as special cases of the incomplete gamma function:(7)

$$\Gamma_\alpha(\ell) = \int_0^\alpha t^{\ell-1} e^{-t} dt \qquad \text{(VII.3.13)}$$

This is a tabulated function available in standard references. Transformations used for the integration are shown in Table IV, along with the resultant distribution functions. The Rosin Rammler function is usually applied to the volume distribution in the form given, and the Nukiyama-Tanasawa equation to the number distribution.(65)

The main difference in the above distributions is that the log-normal distribution has two parameters, the geometric mean and variance; the Rosin-Rammler distribution has two parameters plus a pre-exponential term; and the Nukiyama-Tanasawa equation has a pre-exponential term and three parameters.

The data can be tested for fit to the various distributions in the following ways. The log-normal distribution is easily tested

TABLE IV

TRANSFORMATIONS AND INTEGRALS FOR DENSITY FUNCTIONS

	Transformation	Distribution Fct.
Log Normal	$\ell = \frac{1}{2}$ $t = \frac{z^2}{2}$	$F(z) = \frac{1}{2\sqrt{\pi}} \Gamma_{z^2/2}(\frac{1}{2})$
Rosin Rammler	$\ell = 1$ $t = bz^n$	$F(z) = \Gamma_{bz^n}(1) = (1 - e^{-bx^n}$
Nukiyama-Tanasawa	$\ell = \frac{3}{n}$ $t = bz^n$	$F(z) = \frac{a}{nb^{3/n}} \Gamma_{bz^n}(\frac{3}{n})$

TABLE V

TYPICAL LARGE DROP AND INCLUSION DISTRIBUTION DATA - RUN NO. 13

Large Drops

Size Range cm.	Cumulative Percent of Drops
0-1	21.7
1-2	42.7
2-3	63.2
3-4	74.9
4-5	83.8
5-6	89.2
6-7	91.5
7-8	93.0
8-9	95.2
9-10	96.8

Inclusions

Size Range cm.	Cumulative Percent of Inclusions
0-.5	16.6
.5-1.0	44.0
1.0-1.5	68.9
1.5-2.0	76.8
2.0-2.5	85.6
2.5-3.0	91.9
3.0-3.5	95.2

by plotting on log-probability paper the estimates of the probability distribution function F(z). These estimates may be obtained from the computer program as the cumulative percent of drops observed below the given diameter (in this case, the upper limit of the size range):

$$\hat{F}(D_m) = \frac{\sum_{i=1}^{m} y_i}{\sum_{i=1}^{M} y_i} \qquad (1 \le m \le M) \qquad \text{(VII.3.14)}$$

$$\hat{F}(d_n) = \frac{\sum_{i=1}^{M}\sum_{j=1}^{n} x_{ij}}{\sum_{i=1}^{M}\sum_{j=1}^{N} x_{ij}} \qquad (1 \le n \le N) \qquad \text{(VII.3.15)}$$

Plotting the estimates of $\hat{F}(z)$ versus D_i and d_j respectively should yield a straight line on log-probability paper if a fit to the log normal distribution is obtained. A typical run is shown in Figure 24 and Table V. (Log normal plots for all runs may be found in Appendix D.)

It should be noted that the end points have been truncated from the curves since it is impossible to fit a straight line to any finite consist using the infinite range distribution functions applied here. (Obviously there will be a maximum and minimum diameter for the particles, while the given distribution functions approach upper and lower limits asymptotically.)

Since the Rosin-Rammler function shown is applicable to volumes, we require our estimates to come from the distribution weighted by the third power of our random variable, diameter:

$$\hat{F}(D_m) = \frac{\sum_{i=1}^{m} D_i^3 y_i}{\sum_{i=1}^{M} D_i^3 y_i} \qquad (1 \le m \le M) \qquad \text{(VII.3.16)}$$

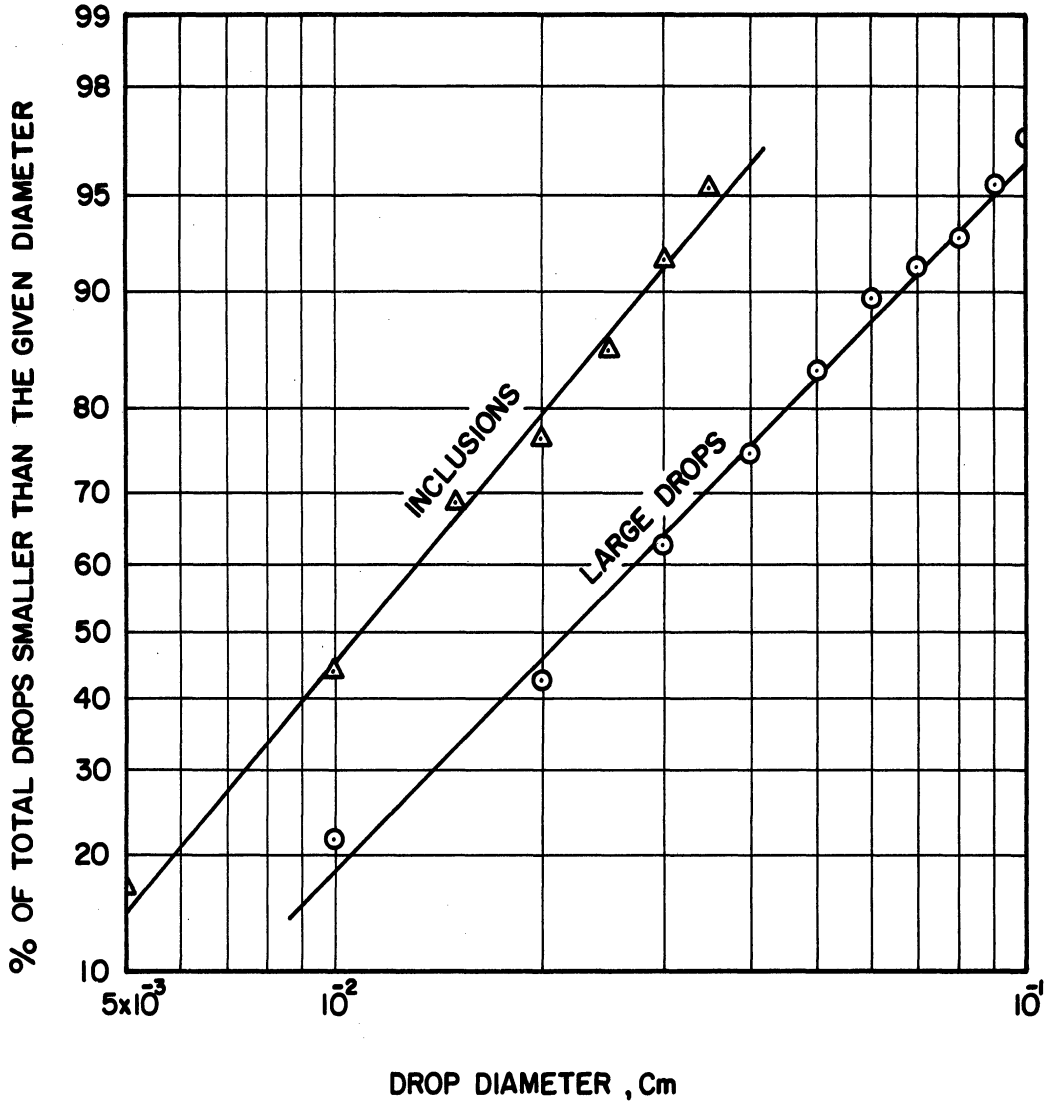

Figure 24. Typical Fit of Log-Normal Function to Large Drop and Inclusion Distributions - Run Number 13.

$$\hat{F}(d_n) = \frac{\sum_{i=1}^{M}\sum_{j=1}^{n} d_j^3 \chi_{ij}}{\sum_{i=1}^{M}\sum_{j=1}^{N} d_j^3 \chi_{ij}} \qquad (1 \le n \le N) \qquad \text{(VII.3.17)}$$

These again are readily obtained from the computer program. Now, if we replace F(z) by (1 - F(z)) in the distribution function, we have:

$$[1 - F(z)] = e^{-bz^n} = \frac{1}{G(z)} \qquad \text{(VII.3.18)}$$

where $G(z) = \dfrac{1}{1 - F(z)}$

taking logarithms twice, we have:

$$\log \log [G(z)] = -\log b - n \log z - \log \log e \qquad \text{(VII.3.19)}$$

This is a linear relationship in log log [G(z)] and log z. Hence a plot of log log [G(z)] against log z should give a straight line if the data follows the Rosin-Rammler distribution. Results are shown for the large drops of a typical run in Figure 25 and Table VI. Fits for inclusions are similar. For this particular run, values of n = 3.05 and b = 865 were obtained. It is interesting to note that associating the given distribution function with the number distribution rather than the volume distribution gives as good a fit (see Table VII and Figure 26), with n = 1.14 and b = 50.2. The variation in n reflects the skewness of the number distribution toward the smaller diameters and of the volume distribution toward the larger diameters.

With the Nukiyama-Tanasawa distribution we once again are concerned with the number distribution, with estimates of f(z) obtained as the percent (rather than cumulative percent) of drops in the given size range. Here, however, we have three parameters to fit. Dividing the

TABLE VI

TYPICAL DATA SET FITTED BY THE ROSIN-RAMMLER FUNCTION APPLIED TO THE VOLUME DISTRIBUTION

Data Set No. 13, Distribution of Large Drops

Drop Diameter cm x $10^2 = D_m$	Cumulative Number % = $\hat{F}(D_m)$ x 100	Log Log $[\hat{G}(D_m)]$	Log Diameter
1	.019	-4.097	-2.000
2	.52	-2.646	-1.699
3	2.77	-1.913	-1.523
4	6.34	-1.546	-1.398
5	12.04	-1.254	-1.301
6	18.42	-1.054	-1.222
7	22.87	- .958	-1.155
8	27.29	- .859	-1.097
9	36.64	- .703	-1.046
10	46.27	- .569	-1.000

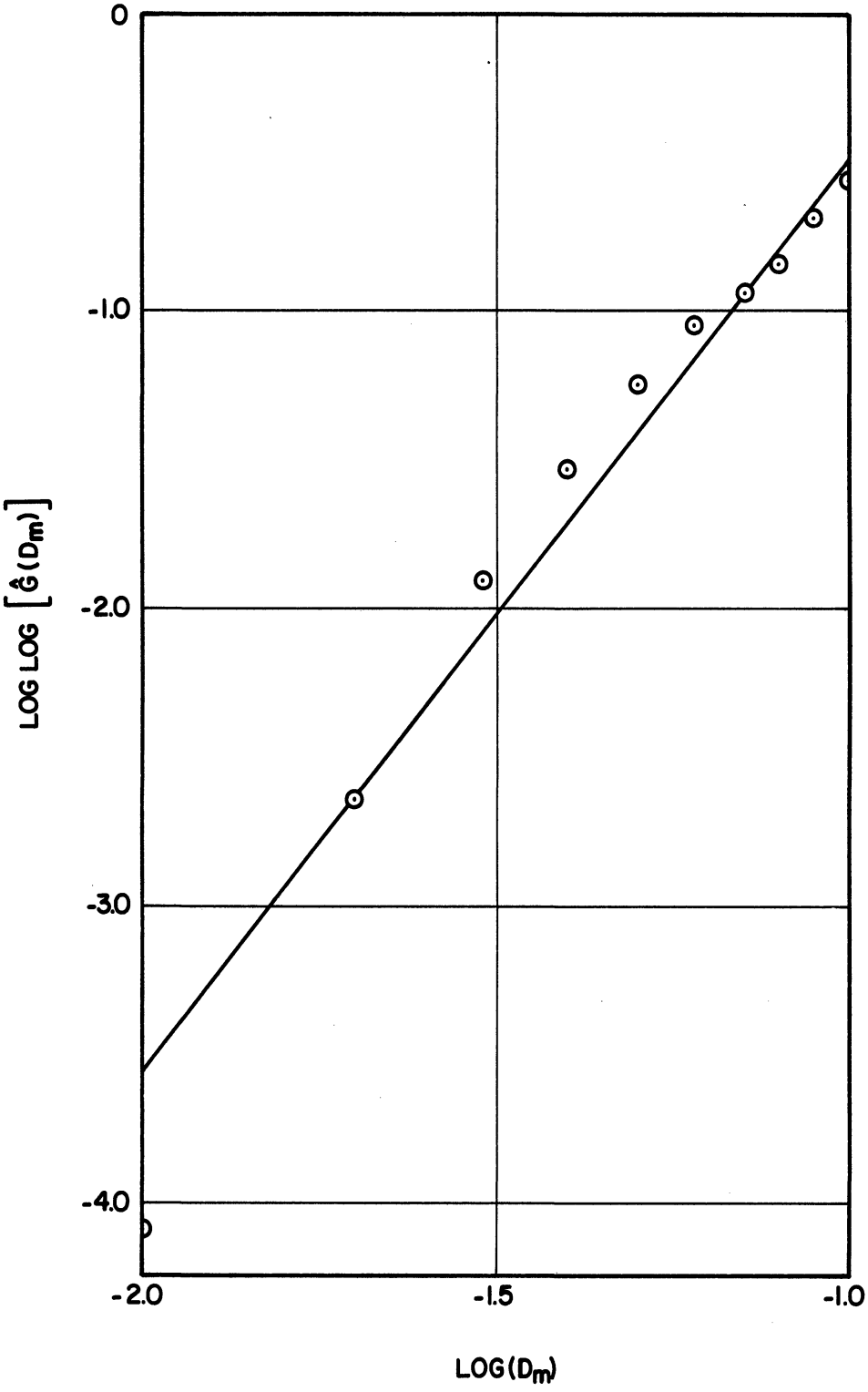

Figure 25. Fit of Rosin-Rammler Function to Run 13 Volume Distribution.

TABLE VII

TYPICAL DATA SET FITTED BY THE ROSIN-RAMMLER FUNCTION APPLIED TO THE NUMBER DISTRIBUTION

Data Set No. 13, Distribution of Large Drops

Drop Diameter cm x $10^{-2} = D_m$	Cumulative Number % = $\hat{F}(D_m)$ x 100	Log Log $[\hat{G}(D_m)]$	Log Diameter
1	21.70	-.9737	-2.000
2	42.74	-.6160	-1.699
3	63.16	-.3628	-1.523
4	74.93	-.2212	-1.398
5	83.80	-.1021	-1.301
6	89.23	-.0143	-1.222
7	91.52	.0301	-1.155
8	93.01	.0628	-1.097
9	95.16	.1191	-1.046
10	96.76	.1728	-1.000

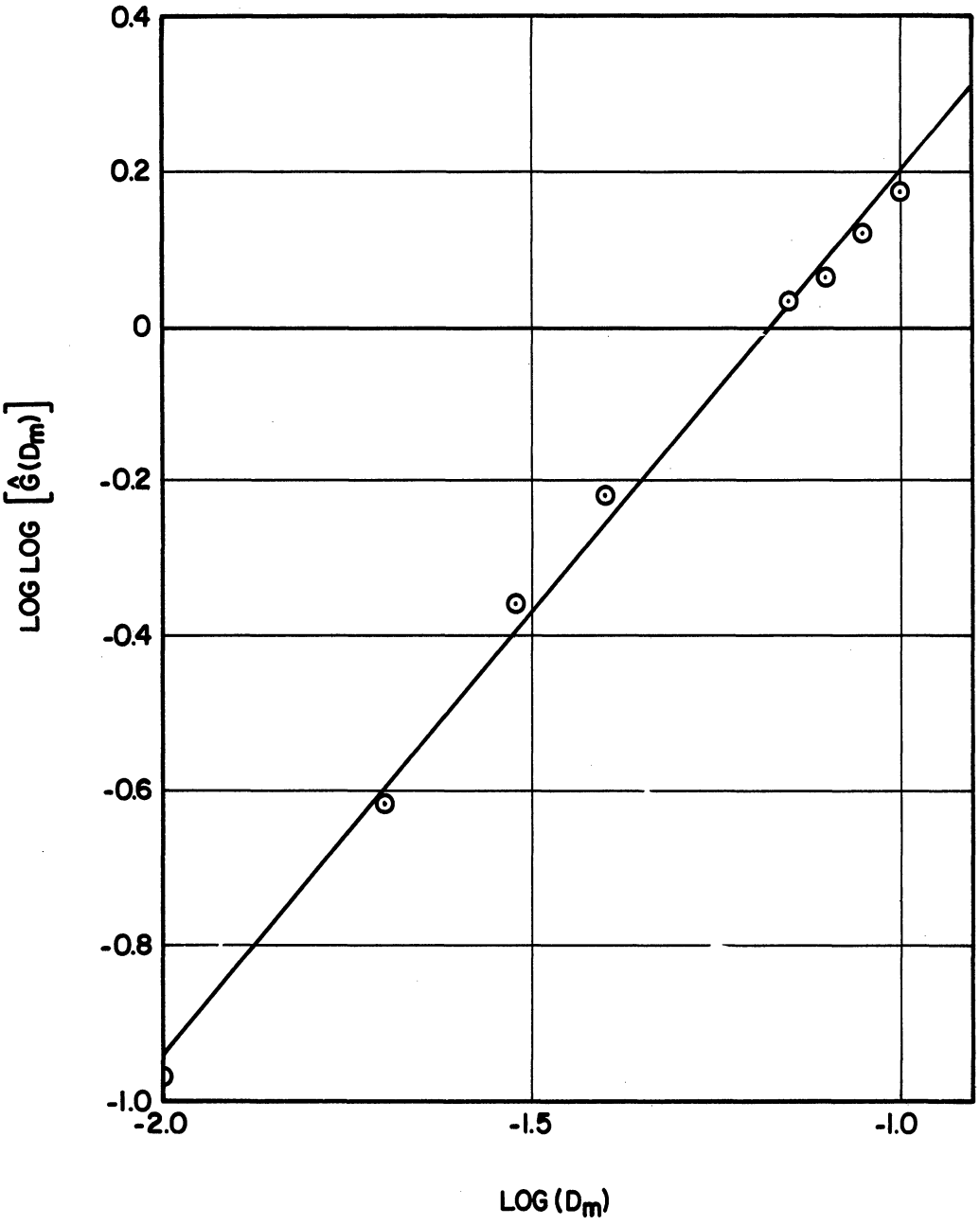

Figure 26. Fit of Rosin-Rammler Function to Run 13 Number Distribution.

density function by z^2 and taking logarithms we have:

$$\log\left[\frac{1}{z^2} f(z)\right] = \log a - b z^n \log e \qquad \text{(VII.3.20)}$$

Our estimates have the form:

$$\hat{f}(D_m) = \frac{y_m}{\sum_{i=1}^{M} y_i} \qquad (1 \leq m \leq M) \qquad \text{(VII.3.21)}$$

$$\hat{f}(d_n) = \frac{\sum_{i=1}^{M} x_{in}}{\sum_{i=1}^{M}\sum_{j=1}^{N} x_{ij}} \qquad (1 \leq n \leq N) \qquad \text{(VII.3.22)}$$

Here we have a linear function in b and a given a valve of n. Nukiyama and Tanaswa found n = 1/4 to give the best fit. Shown in Figure 27 and Table VIII is the result using n = 1/4. Values obtained are a = 5.75×10^9 and b = 31.08. These are of the same order of magnitude as those values obtained by Nukiyama and Tanasawa in their liquid-into-gas sprays. In Table VIII and Figure 28 is shown the result of using n = 1/2. No appreciably better fit was obtained.

Since the two more sophisticated functions show no better fit to the experimental data than the log-normal function, there is no justification for using the more complicated models on the basis of this work. It has often been said that the normal distribution is to statistics what the straight line is to geometry, and so it would be extremely unwise to abandon the log-normal form of distribution without well based justification.

It is interesting to observe that the log-normal form of distribution will hold even down into the varicose breakup (see Section VIII) regime for the large drops (see Figure 29). The change

TABLE VIII

TYPICAL DATA SET FITTED BY THE NUKIYAMA TANASAWA FUNCTION,
$n = 1/4$ and $n = 1/2$

Run Number 13, Large Drops

D_m cm x 10^2	$D_m^{1/2}$	$D_m^{1/4}$	$f(D_m)$ x 100 %	Log $[\frac{1}{D_m^2} \hat{f}(D_m)]$
1.0	.1000	.316	21.7	5.336
2.0	.1414	.375	21.0	4.720
3.0	.1732	.416	20.4	4.356
4.0	.2000	.447	11.8	3.868
5.0	.2236	.473	8.87	3.550
6.0	.2449	.495	5.43	3.179
7.0	.2646	.514	2.30	2.671
8.0	.2828	.532	1.49	2.367
9.0	.3000	.548	2.15	2.423
10.0	.3162	.561	1.59	2.201

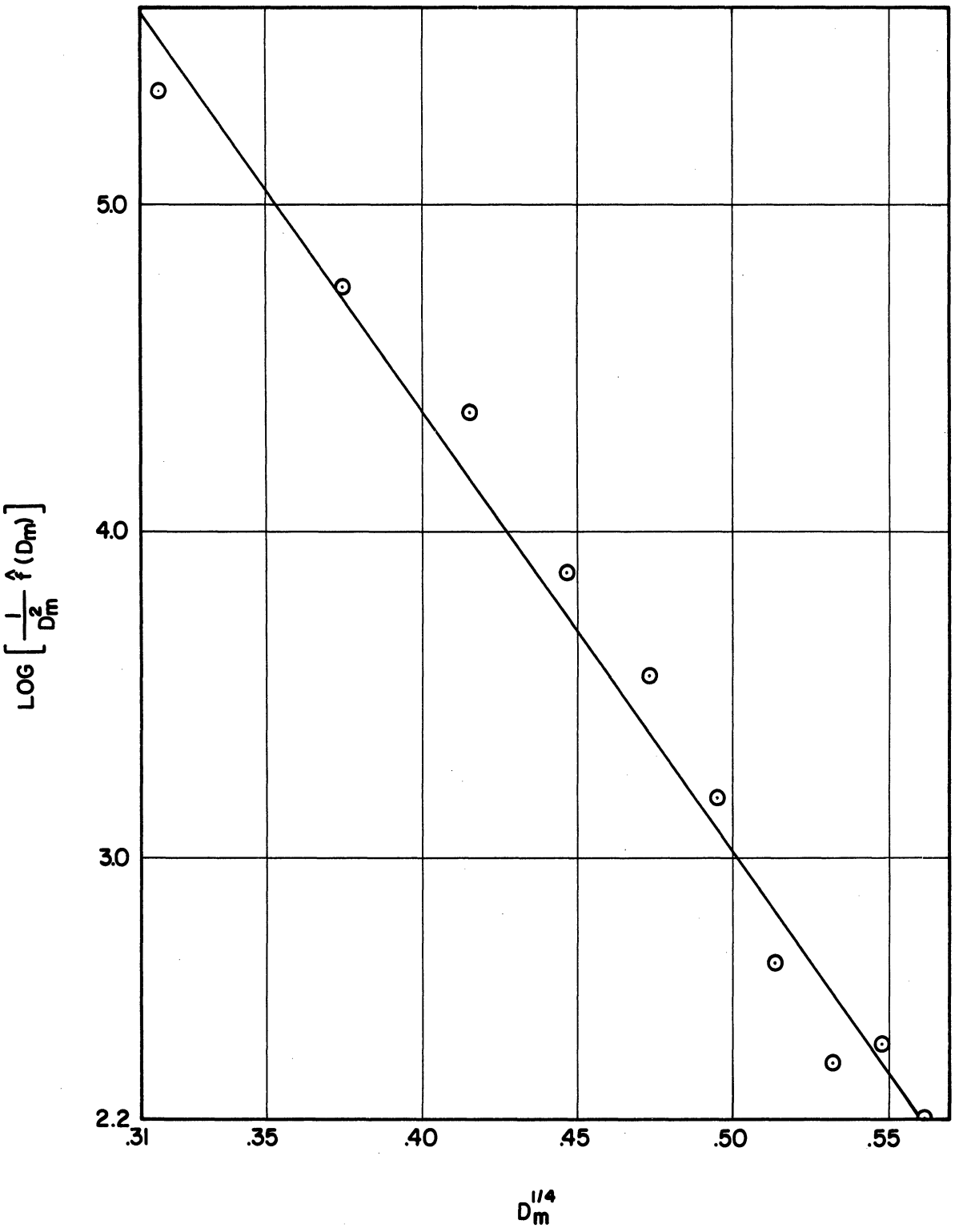

Figure 27. Fit of Nukiyama-Tanasawa Function to Run 13 Data, n = 1/4.

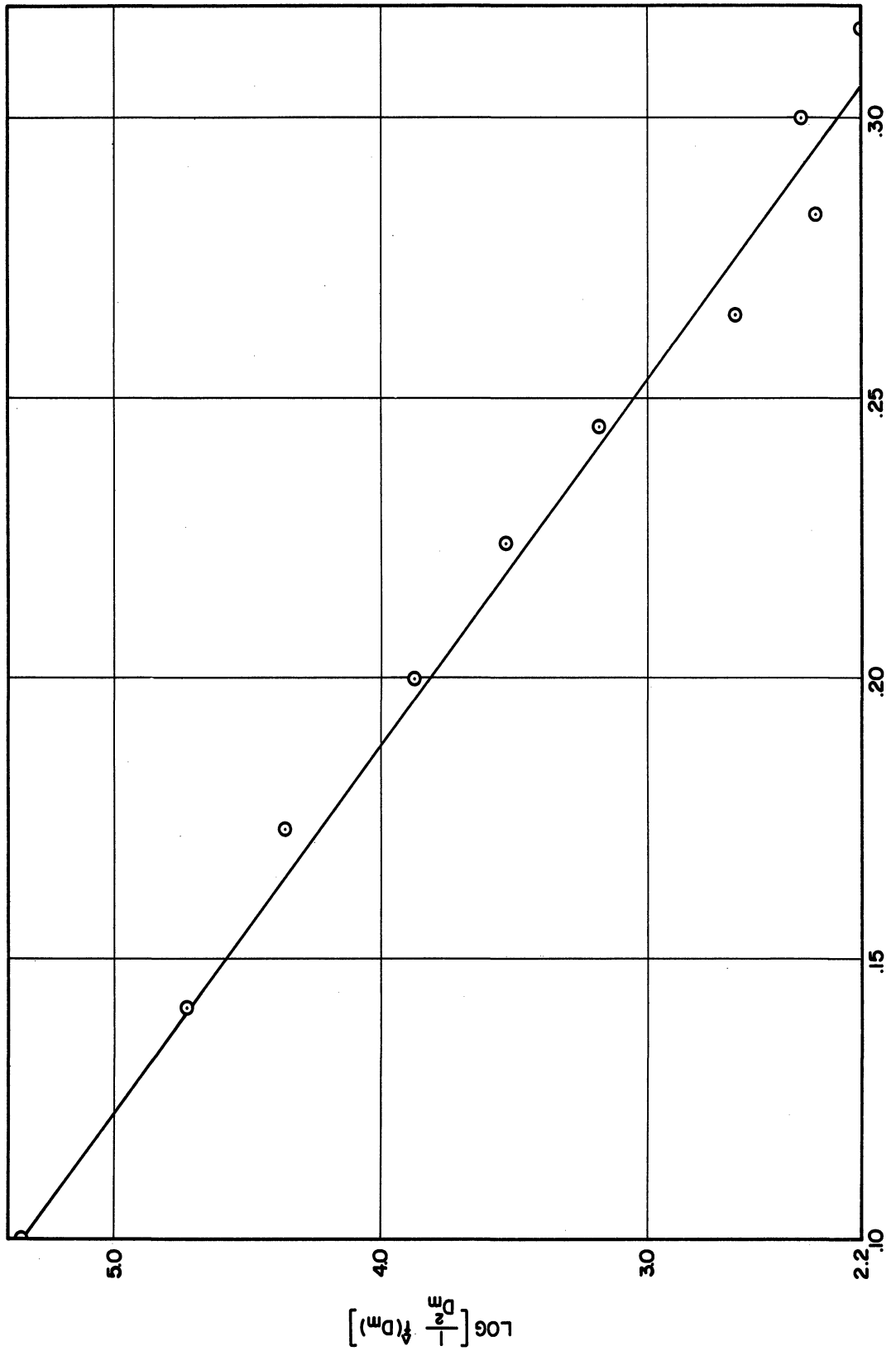

Figure 28. Fit of Nukiyama-Tanasawa Function to Run 13 Data, n = 1/2.

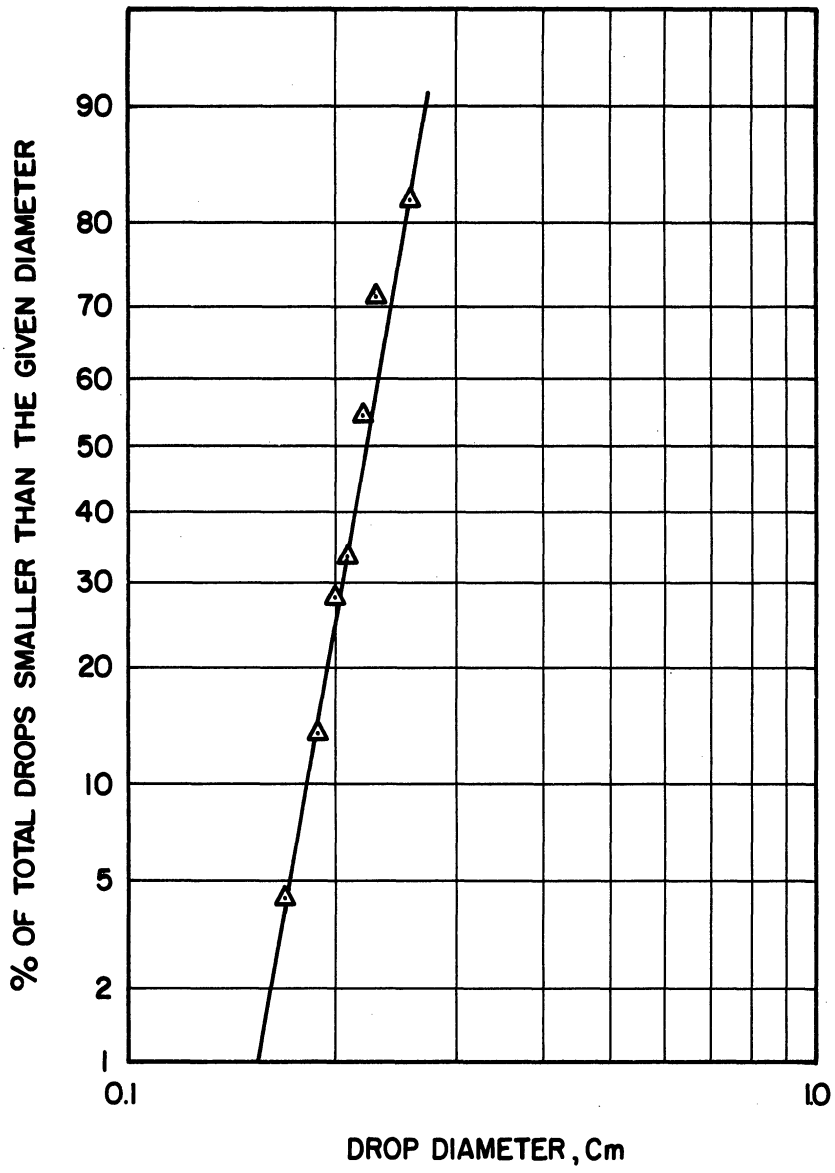

Figure 29. Log Normal Function Fitted to Distribution Data from Varicose Breakup.

from one type of breakup to the other is reflected merely in changes in the mean and variance of the distribution.

We have determined above the probability density functions for the large drops and for the inclusions. We must note, however, that the distribution for the inclusions has been treated independently of that of the large drops. Our data for the inclusions, though, implies that there may be an additional consideration. The number of inclusions, x_{ij}, is classified not only with respect to the inclusion diameter, but also with respect to the diameter of the large drop within which the inclusion is found. The next question one might ask is whether the same form of distribution function holds for inclusions within large drops of a specified diameter as holds for inclusions irrespective of the large drops; in statistical language, are the marginal and conditional distributions identical? Based on the data obtained in this study, there is no adequate reason to reject the hypothesis that the marginal distribution function of the inclusions is identical with the conditional inclusion distribution, given a range of large drop diameters. Shown in Table IX and Figure 30 is a typical set of data. Note that all the mean diameters for the inclusions obtained from the conditional distribution lie within one standard deviation of all others in Table IX. Figure 30 is a plot of data for one conditional distribution as noted.

VII.4 Correlation of Multiple Emulsion Parameters

The most immediate observation from considering the relationship of the distribution of inclusions to that of the large drops is that the large drops contain a much higher number of inclusions than

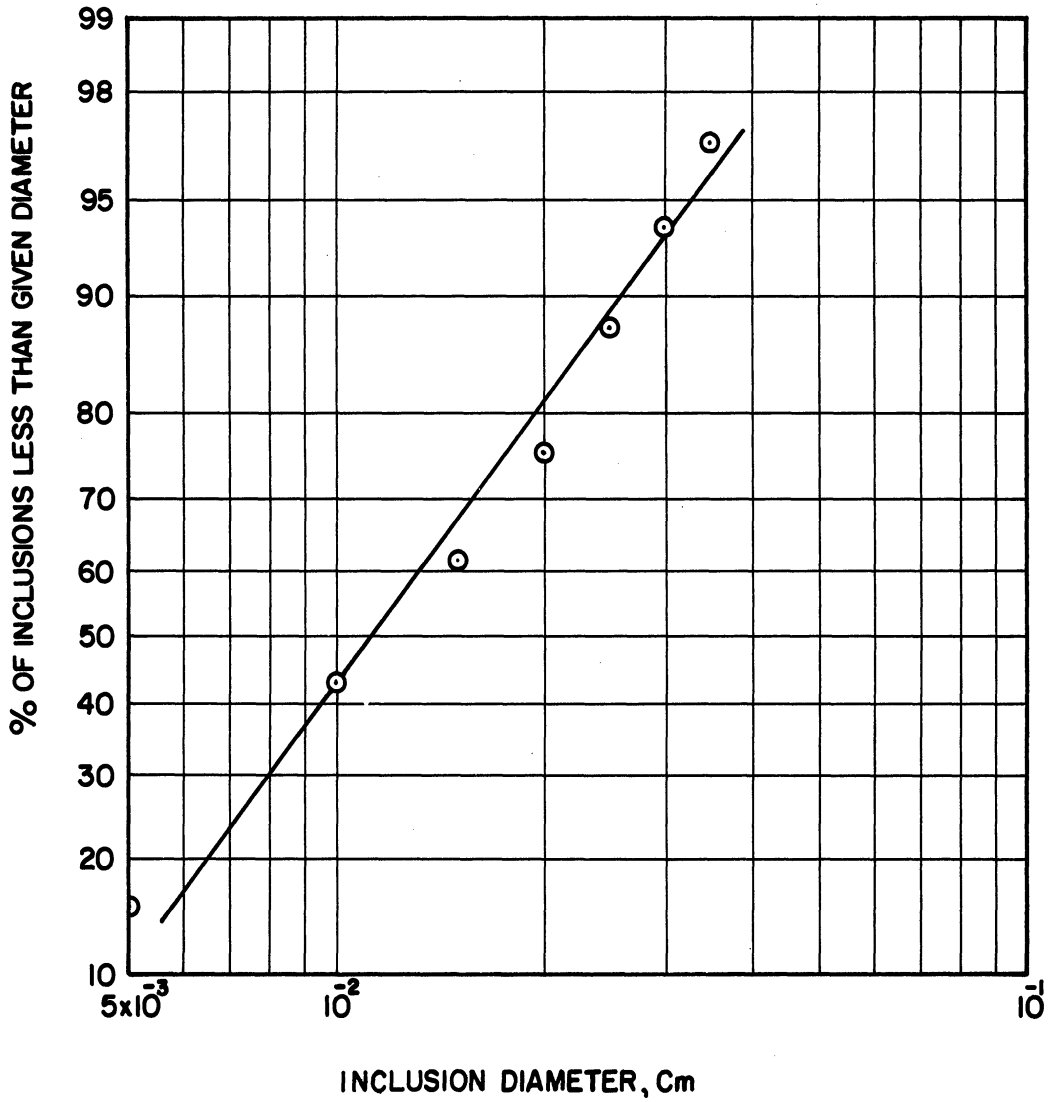

Figure 30. Typical Data for Conditional Distribution of Inclusions.

TABLE IX

CONDITIONAL DISTRIBUTION PARAMETERS
OF INCLUSIONS FOR A TYPICAL RUN

Run Number 10

Large Drop Size Range cm x 10^2	Number Inclusions	Inclusion Log Geometric Mean d_m	Inclusion Geometric Mean d_m cm x 10^{-2}	Inclusion Log Geometric Standard Deviation
4-5	63	-1.9846	.1036	.2633
5-6	47	-2.0662	.0859	.3374
6-7	44	-2.0438	.0904	.2920
7-8	52	-2.0025	.0994	.3270
8-9	53	-1.8626	.1372	.2241
9-10	33	-1.9539	.1112	.3067

the smaller drops. This can be seen graphically in Figure 31 and Table X. Stating the matter in a slightly different way, we can say that here the smallest four size classes contained 83.96% of the large drops and only 15.09% of the inclusions, a ratio of 5.6 while the largest four size classes contained only .665% of the large drops but 12.89% of the inclusions, a ratio of 5.2 x 10^{-2}. The number of inclusions per drop is of the order of 10-20 in the largest diameter drops, but less than 1 in the smallest diameter drops. This observation fits well with the proposed mechanism discussed below.

A second matter of interest arises with regard to what mean drop diameter should be used to characterize the distribution of large

TABLE X

NUMBER OF INCLUSIONS PER LARGE DROP
AS A FUNCTION OF LARGE DROP DIAMETER

Pooled Data From Runs 7, 10, 13, 14, 15, 16

Nozzle Diameter = .0642 cm.

Large Drop Diameter cm x 10^2	Number Large Drops	Number Inclusions	Inclusions Per Large Drop
0-1	519	0	0.000
1-2	817	26	.0318
2-3	471	104	.221
3-4	232	97	.418
4-5	148	194	1.311
5-6	65	151	2.323
6-7	42	130	3.095
7-8	35	131	3.743
8-9	32	149	4.656
9-10	22	128	5.818
10-11	11	71	6.455
11-12	12	86	7.167
12-13	6	44	7.333
13-14	5	34	6.800
14-15	4	35	8.750
15-16	3	44	14.67
16-17	4	81	20.25

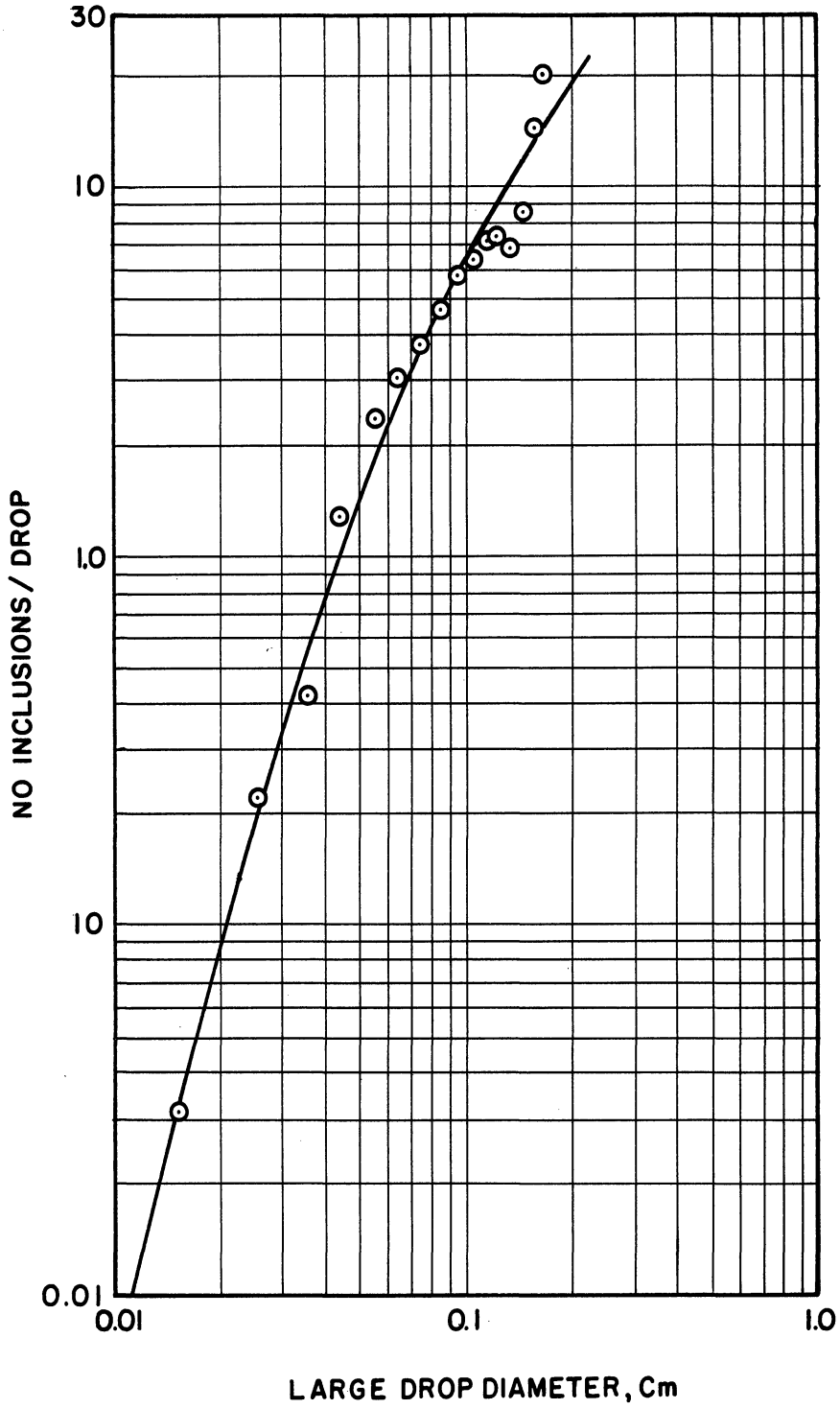

Figure 31. Number of Inclusions per Drop as a Function of Large Drop Diameter.

drops and that of the inclusions. We can define the expectation, E(z) of a random variable Z as:

$$E(z) = \int_{-\infty}^{\infty} z f(z)\, dz \qquad \text{(VII.4.1)}$$

Similarly, we can from the expectation write a generalized mean diameter as:

$$\bar{Z}_{pq} = \left[\frac{E(z^p)}{E(z^q)} \right]^{\frac{1}{p-q}} \qquad \text{(VII.4.2)}$$

Using this defintion, we can write immediately the mean diameters most commonly used in spray work:

$\bar{Z}_{10} = E(z)$ = "Length" (here diameter) Mean (VII.4.3)

$\bar{Z}_{20} = E(z^2)$ = Surface Mean (VII.4.4)

$\bar{Z}_{30} = E(z^3)$ = Volume Mean (VII.4.5)

$\bar{Z}_{32} = \frac{E(z^3)}{E(z^2)}$ = Sauter or Volume-Surface Mean (VII.4.6)

The Sauter mean diameter can be thought of as that diameter which, if the spray were made up only of drops of that diameter, would yield the same surface and volume as that possessed by the original spray. The Sauter mean can be related to specific surface by writing:

$$V_{SPRAY} = \frac{n\pi \left[\bar{Z}_{32}\right]^3}{6} \qquad \text{(VII.4.7)}$$

$$A_{SPRAY} = n\pi \left[\bar{Z}_{32}\right]^2 \qquad \text{(VII.4.8)}$$

where n = number of drops.

Then:

$$\text{Specific Surface} = \frac{A_{spray}}{V_{spray}} = \frac{6}{\bar{z}_{32}} \qquad \text{(VII.4.9)}$$

As can be seen from the above definitions, $\bar{z}_{20}$ and $\bar{z}_{30}$ are merely the second and third moments of the density function f(z). Now the log-normal distribution is uniquely defined by the geometric mean and variance, and further, the estimated mean and variance are sufficient statistics for this distribution. In other words, based on a sample $y_1, y_2, \ldots y_M$ or $x_{11}, x_{12}, \ldots x_{MN}$ we can estimate the mean and variance but no more information can be obtained from the data. This is a well known statistical result.

What implication does this have for our analysis? It means that once we have determined the log-normal distribution to be the best fitting for the data, it does not matter in any essential detail what mean diameter we choose to correlate against, so long as we estimate variance along with our selected mean diameter. Certainly some means may give more convenient graphical representations, etc., but scatter of data will not be affected. This can be seen graphically in Figure 32, where the first six weighted distributions of typical data are plotted, with the only change being in 50% intercept (mean) and slope (variance).

It is instructive to plot the points for $\bar{z}_{10}$ versus $\bar{z}_{32}$ obtained using the experimental results. Estimating $\bar{z}_{pq}$ from the sample, we can write (for the inclusions):

$$\left[\frac{\bar{d}_{21}}{\bar{d}_{10}}\right]\left[\frac{\bar{d}_{32}}{\bar{d}_{21}}\right] = \left[\left(\frac{\sum\sum x_{ij}}{\sum\sum d_j x_{ij}}\right)\left(\frac{\sum\sum d_j^2 x_{ij}}{\sum\sum d_j x_{ij}}\right)\right]\left[\left(\frac{\sum\sum d_j x_{ij}}{\sum\sum d_j^2 x_{ij}}\right)\left(\frac{\sum\sum d_j^3 x_{ij}}{\sum\sum d_j^2 x_{ij}}\right)\right] \qquad \text{(VII.4.10)}$$

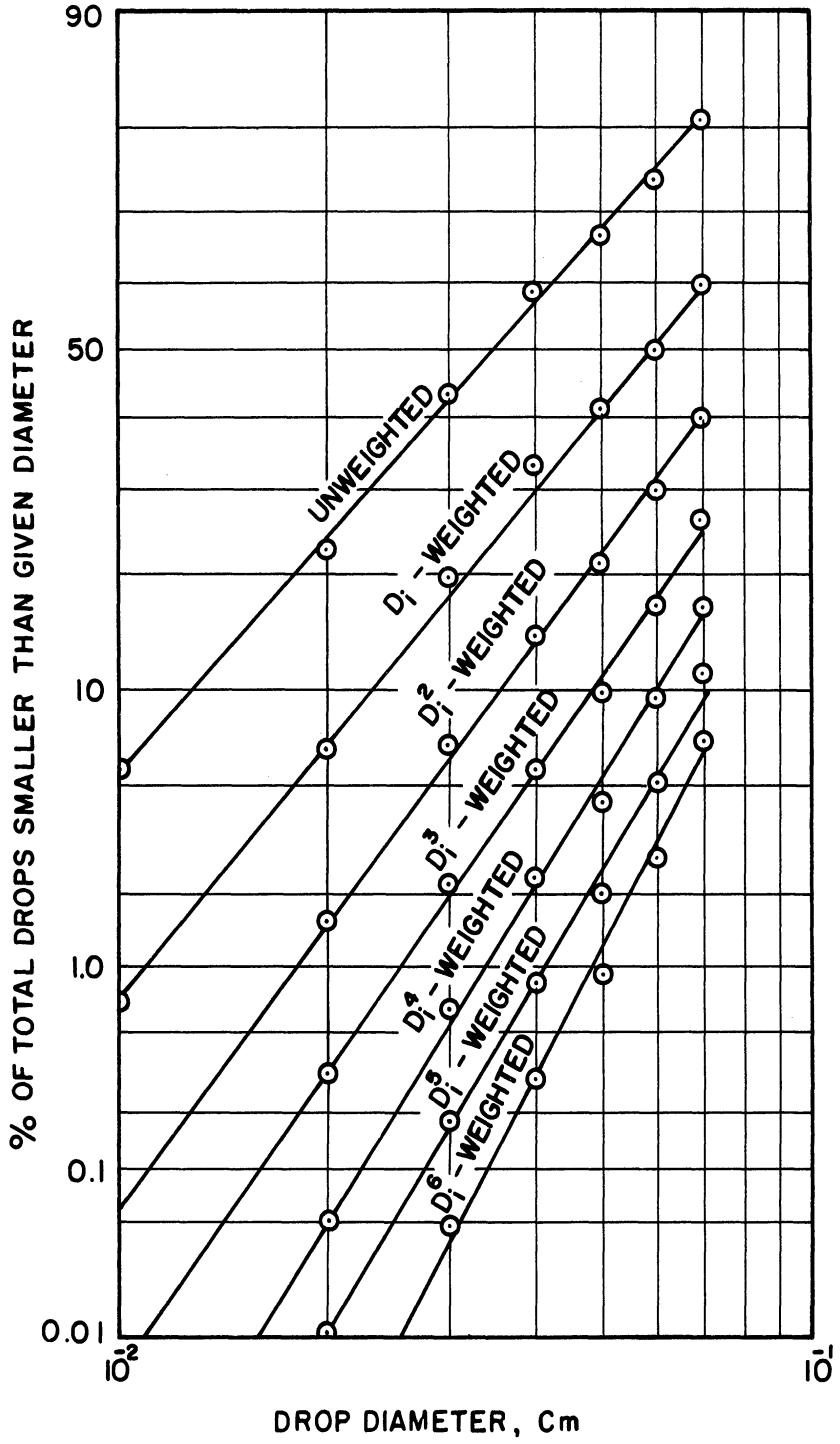

Figure 32. Typical Data for Weighted Drop Distribution.

and applying the Cauchy inequality:

$$\sum (a_i^2 b_i^2) \leq \left(\sum a_i^2\right)\left(\sum b_i^2\right) \qquad \text{(VII.4.11)}$$

to each bracketed term on the right hand side, using

$$a_i = d_j \chi_{ij}^{1/2} \qquad b_i = \chi_{ij}^{1/2} \qquad \text{(VII.4.12)}$$

and

$$a_i = d_j^{3/2} \chi_{ij}^{1/2} \qquad b_i = d_j^{1/2} \chi_{ij}^{1/2} \qquad \text{(VII.4.13)}$$

we can see that:

$$\bar{d}_{10} \leq \bar{d}_{32} \qquad \text{(VII.4.14)}$$

The equality holds only for a point distribution, and the difference between $\bar{z}_{10}$ and $\bar{z}_{32}$ is a measure of the spread of the distribution. Figure 33 is the plot of the data obtained here. The 45° line represents the equality:

$$\bar{d}_{10} = \bar{d}_{32} \qquad \text{(VII.4.15)}$$

There is insufficient data to make estimates using Figures 33 and 34; however, the apparent relationship of $\overline{D_{32}}$ and $\overline{D_{10}}$, and $\overline{d_{32}}$ and $\overline{d_{10}}$ suggests that the mean and the variance of the distributions may be related. If this relationship can be elucidated with more data, we may be able eventually to reduce our distribution functions to <u>one</u> parameter functions. That is, we can calculate some estimated mean diameter, and then use a relation of the form:

$$\sigma = \varphi(\text{mean diameter}) \qquad \text{(VII.4.16)}$$

(σ = std. deviation)

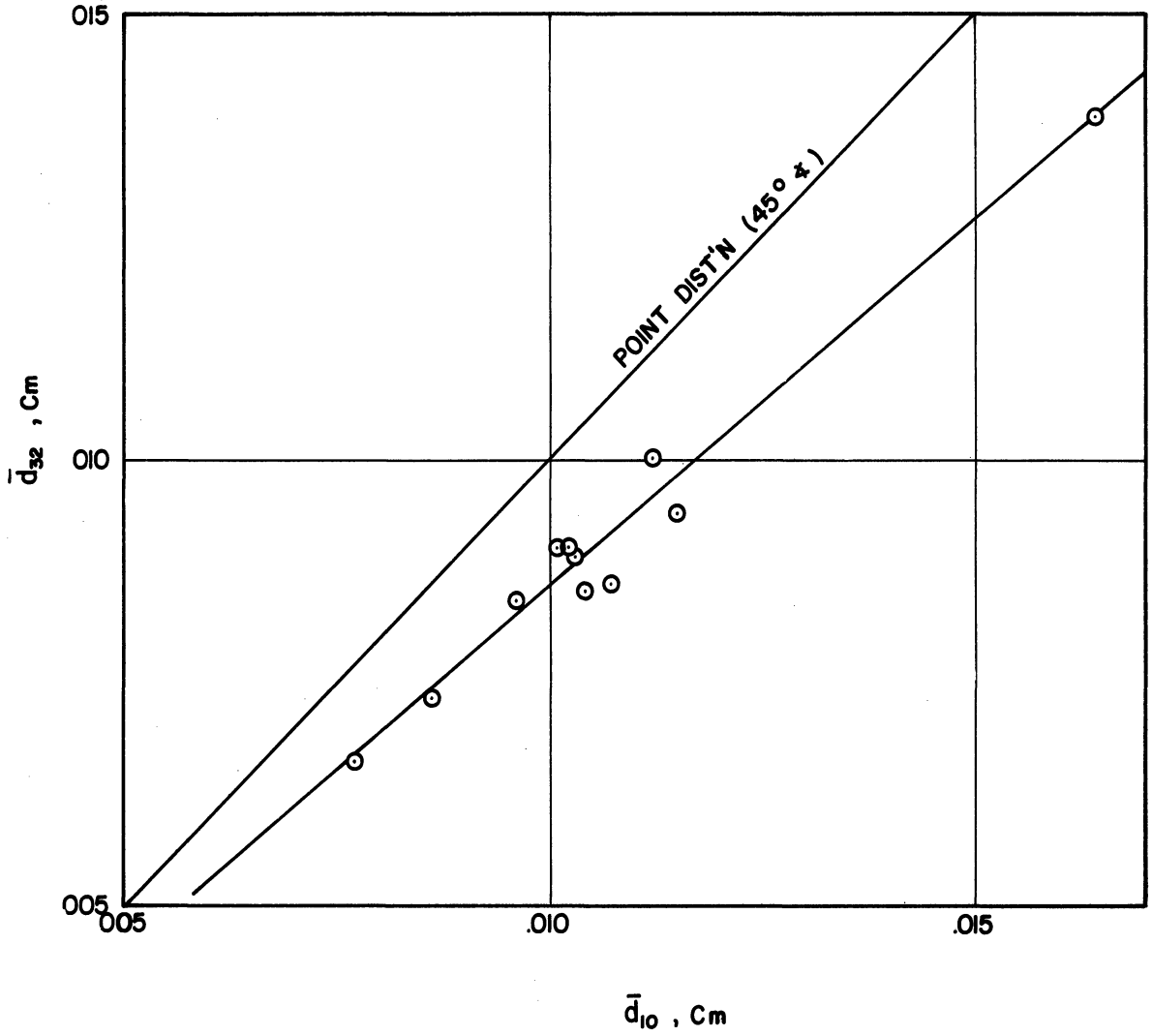

Figure 33. $\overline{d_{32}}$ versus $\overline{d_{10}}$.

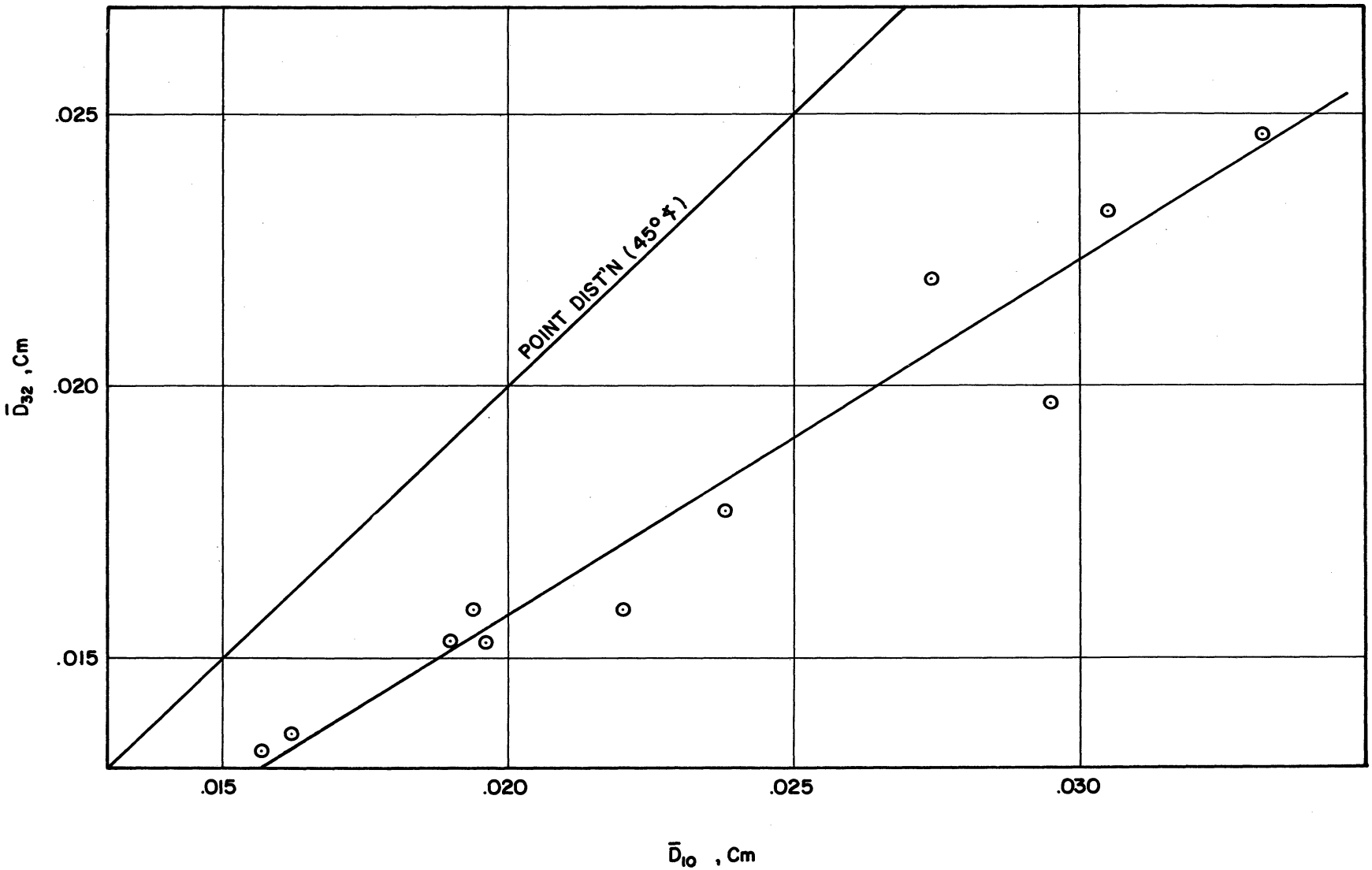

Figure 34. $\overline{D_{32}}$ versus $\overline{D_{10}}$

to calculate standard deviation directly. If such an approach is possible, it would be possible to characterize the spray completely by simply giving a mean diameter. Figures 33 and 34 suggest that standard deviation varies directly with mean.

The parameters of most immediate commercial interest are, of course, the percent included surface area and percent included volume, defined here as:

$$\% \text{ Included Area} = \frac{\text{Total Surface Area of Inclusions}}{\text{Total External Surface of Large Drops}} \times 100 \qquad \text{(VII.4.17)}$$

$$\% \text{ Included Volume} = \frac{\text{Total Volume of Inclusions}}{\text{Total Volume Enclosed by External Surface of Large Drops}} \times 100 \qquad \text{(VII.4.18)}$$

Definition was made in this manner so ready estimates of effects on existing data could be made.

The question of what independent variables to correlate against becomes somewhat involved here. It is probable that there are at least seven important independent variables in the process:

1) nozzle diameter
2) velocity through the nozzle
3) density of sprayed phase
4) density of receiving phase
5) interfacial tension
6) viscosity of sprayed phase
7) viscosity of receiving phase

To vary these seven factors at only three levels, using a complete factorial design with no replication (using higher order interactions to estimate error) would require $3^7 = 2187$ experiments.[21]

Two of the above variables were (in effect) eliminated by working with liquid pairs of essentially the same viscosity. This procedure will still give widely applicable results as many liquids used in dispersion processes have viscosities close to 1 cps, the value used. This will still leave $3^5 = 243$ experiments necessary to test the variables separately.

The obvious solution to the problem is to place further restraints on the system by dimensionless groupings of the variables. Two of the most widely used dimensionless groups in spray processes are the Reynolds number, representing the ratio of inertial to viscous forces, and the Weber number, representing the ratio of inertial to interfacial forces, here defined as:

$$R_e = \frac{D_n v_n \rho_s}{\mu_s} \qquad \text{(VII.4.19)}$$

$$W_e = \frac{D_n v_n^2 \rho_s}{\gamma} \qquad \text{(VII.4.20)}$$

where D_n = nozzle diameter

v_n = velocity through nozzle

ρ_s = density of sprayed phase

μ_s = viscosity of sprayed phase

γ = interfacial tension .

An extremely naive model, but one which permits a reasonable correlation of the data is a linear model for the relationship of the logarithms:

$$\log(\%\ \text{INCLUDED VOLUME}) = m_1 \log[(R_e)(\quad)] + b_1 \qquad \text{(VII.4.21)}$$

$$\log(\%\ \text{INCLUDED AREA}) = m_2 \log[(R_e)(\quad)] + b_2 \qquad \text{(VII.4.22)}$$

A least squares fit was run on this model and the results are shown in Figures 35 and 36. These are the best fitting straight lines using maximum likelihood estimation. The 95% confidence limits are shown for each case.

Correlation coefficients for these two models were .88 and .83 respectively. A check on experimental error was made in runs 8 and 9 of the experimental work. We can estimate error variance using standard tables of the relative range.(7) The 95% limits for % included area were plus or minus 2.25% at about the 17% level. Observed unexplained variation can be seen from Figure 36 to be of this order of magnitude. This means the residual variation (scatter) can probably be explained by experimental error. A similar argument holds for the % included volume plot.

The scatter is somewhat worse in the % included area case than for the % included volume correlation. This can be explained to a large extent by Figure 37, which shows a curvature when % included area is plotted versus % included volume on log-log paper, demonstrating that the proposed linear model cannot fit both cases. It is straightforward to fit a higher order model to % included area, but such models are notoriously untrustworthy for extrapolation. It would perhaps be preferable to estimate % included volume by the given function and

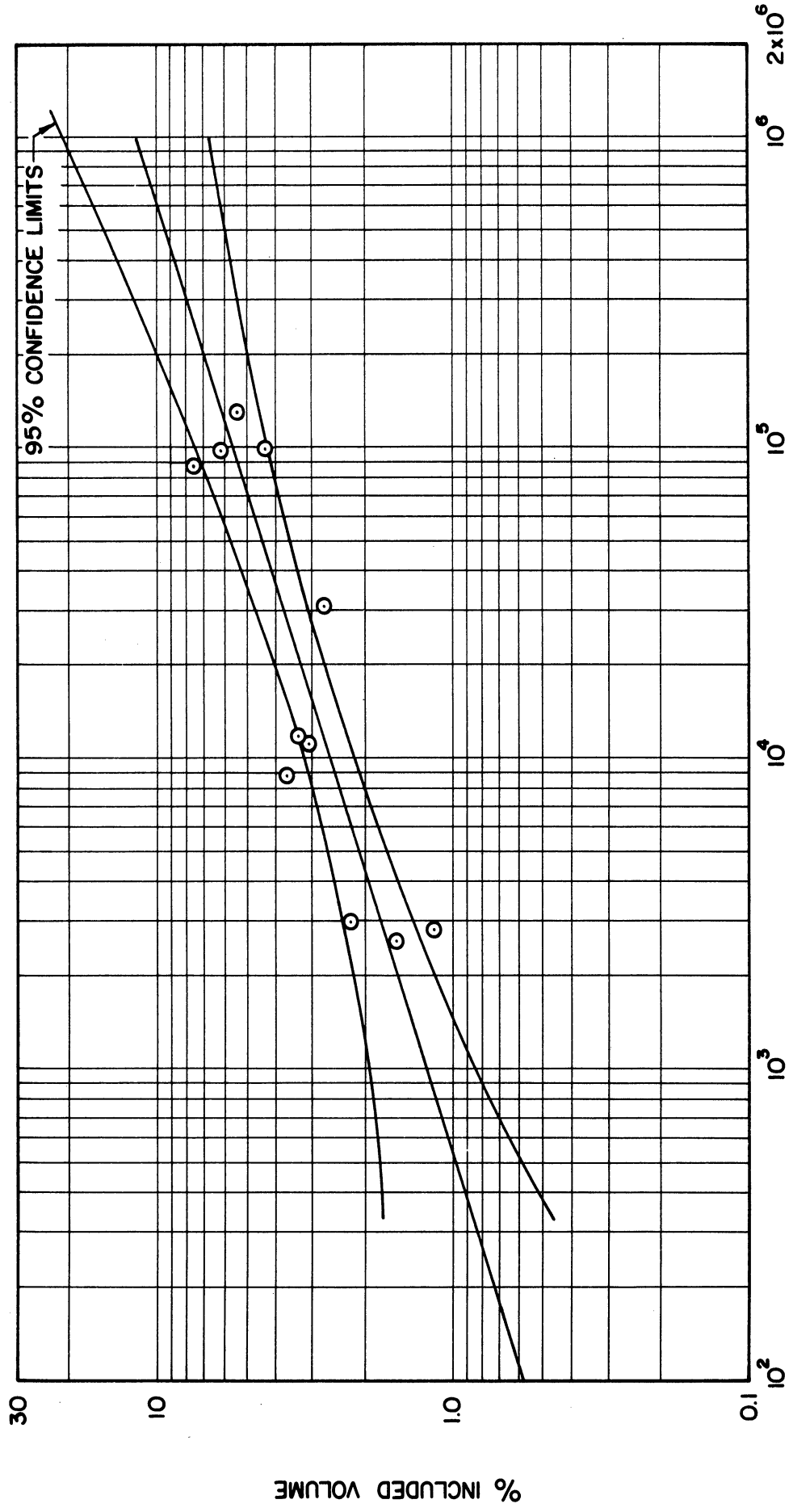

Figure 35. Percent Included Volume as a Function of Re x We.

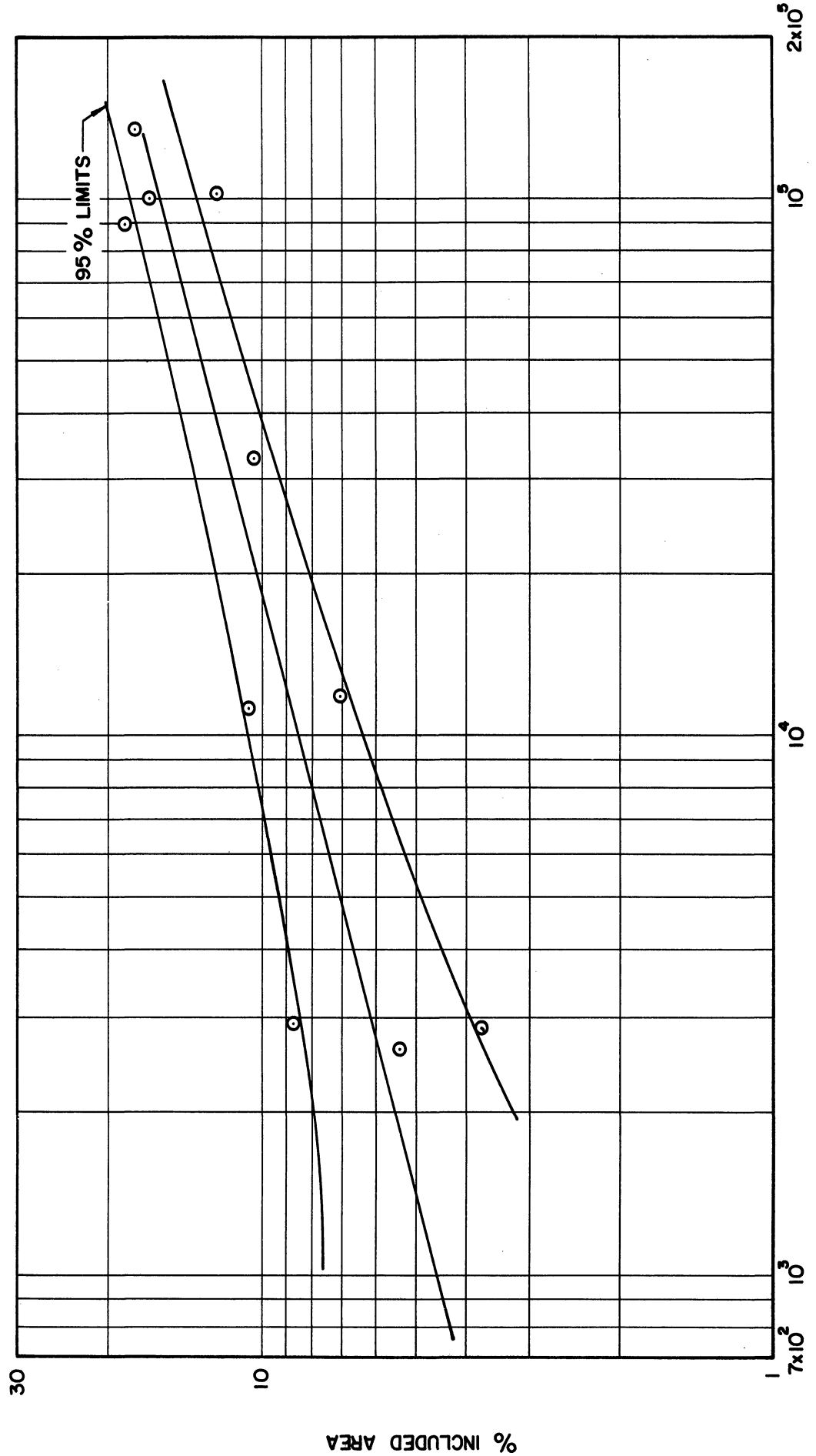

Figure 36. Percent Included Area as a Function of Re x We.

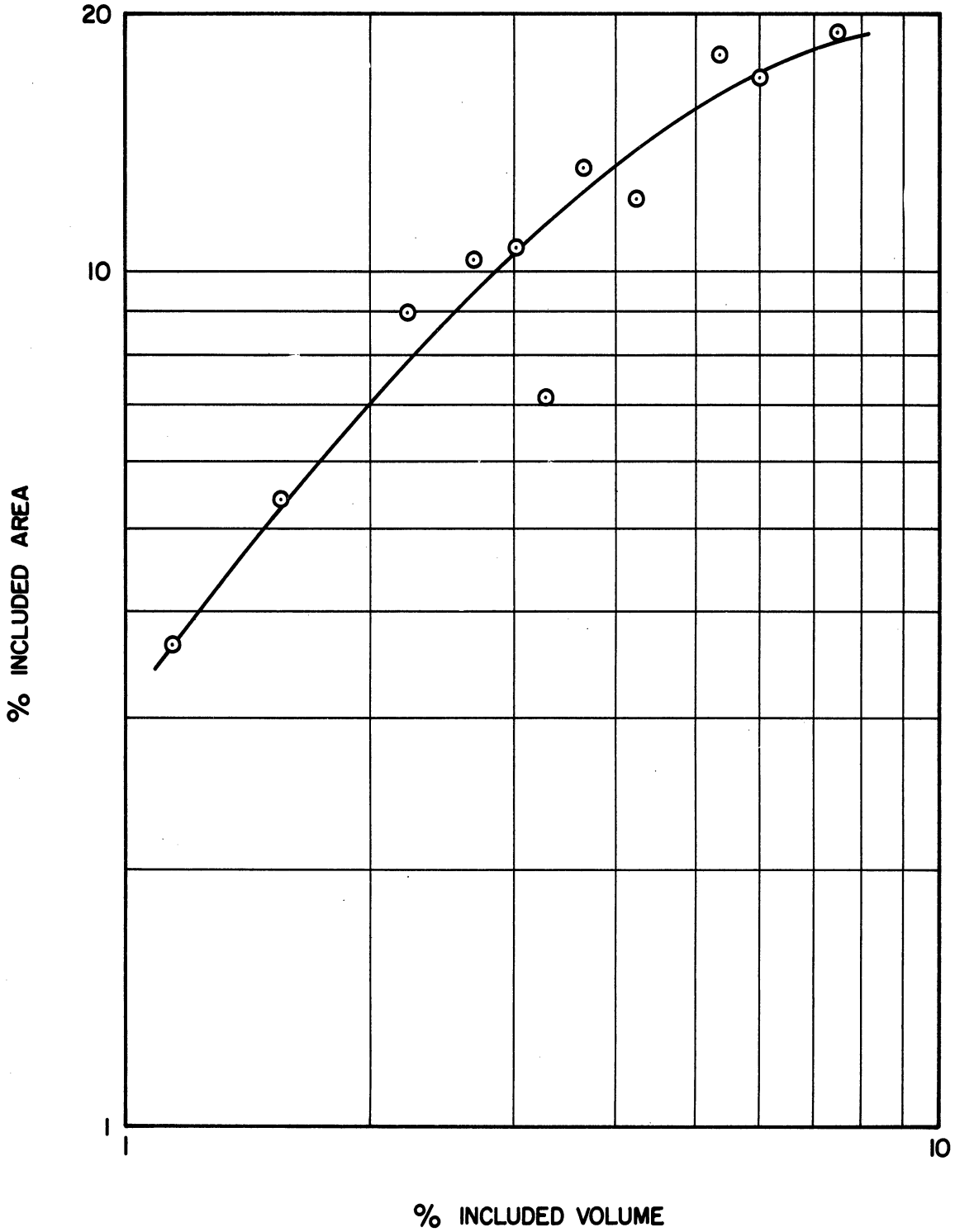

Figure 37. Percent Included Area as a Function of Percent Included Volume.

then use an estimate of mean diameter and variance to derive % included area using the log-normal distribution, since the mean and variance of the inclusion diameters appear to be quite insensitive functions.

The linear model of the type:

$$\text{Log}(\%\ \text{included} \begin{cases} \text{Area} \\ \text{Volume} \end{cases}) = m_1 \log [R\epsilon] + m_2 \log [We] + b \qquad \text{(VII.4.23)}$$

was also fitted using multiple regression techniques, with no significant improvement in correlation. Consequently, the additional parameter was not introduced. With sufficient experimental results, a test of the model:

$$\text{Log}(\%\ \text{included} \begin{cases} \text{Area} \\ \text{Volume} \end{cases}) = m_1 \log D_n + m_2 \log v_n + m_3 \log \rho_s + m_4 \log \rho_n + m_5 \log \mu_s + m_6 \log \mu_n + m_7 \log r + b \qquad \text{(VII.4.24)}$$

would probably suggest relationships applicable to a general liquid pair. Based on the correlations shown here, it is merely possible to conclude that the linear relationship used can be utilized to correlate data for a liquid pair with viscosities about 1 cps. This model indicates that inertial forces play a much more dominant role in the inclusion forming process than do interfacial forces. Before discovery of the mechanism involved, it was surprising that a correlation based on nozzle parameters would prove adequate; however, in light of the mechanism discussed below, it is not surprising that such an approach yields a good first approximation.

VIII. DETERMINATION OF MECHANISM

In most of the published literature on sprays, it is customary to distinguish about four stages in the breakup process of a jet exhibiting surface or interfacial tension:

1) Varicose breakup, where the jet is "pinched off" through the growth of symmetrical disturbances. (Figure 38).
2) Sinuous breakup, where the jet is broken into columns through a "flag waving" action, the columns then disintegrating by varicose breakup. (Figure 39).
3) Ligament formation, where initial disturbances are drawn out in the form of ligaments which detach and collapse into drops. (Figure 40).
4) Disruptive breakup, where the jet disintegrates immediately upon leaving the confinement of the nozzle.

There are, of course, secondary breakup processes which involve the splitting of the larger drops after the jet has disintegrated.

In the carbon tetrrachloride - water system used for the counted data, breakup was exterior to the nozzle, with a varying length of undisturbed jet, as shown in Figure 41. In low viscosity systems such as this, breakup of the liquid jet always took place over such a short distance that it was not possible to distinguish mechanism of

Figure 38. Varicose Breakup.

Figure 39. Sinuous Breakup.

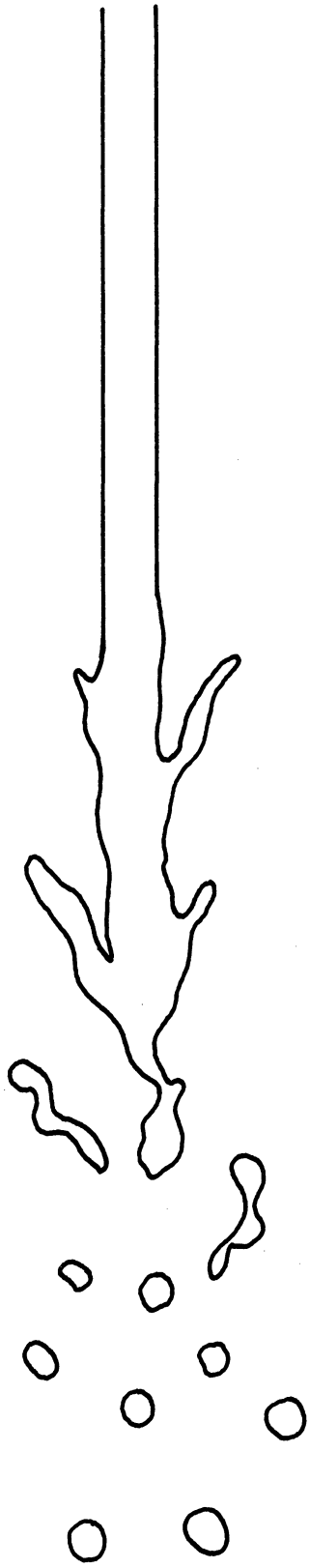

Figure 40. Ligament-Type Breakup.

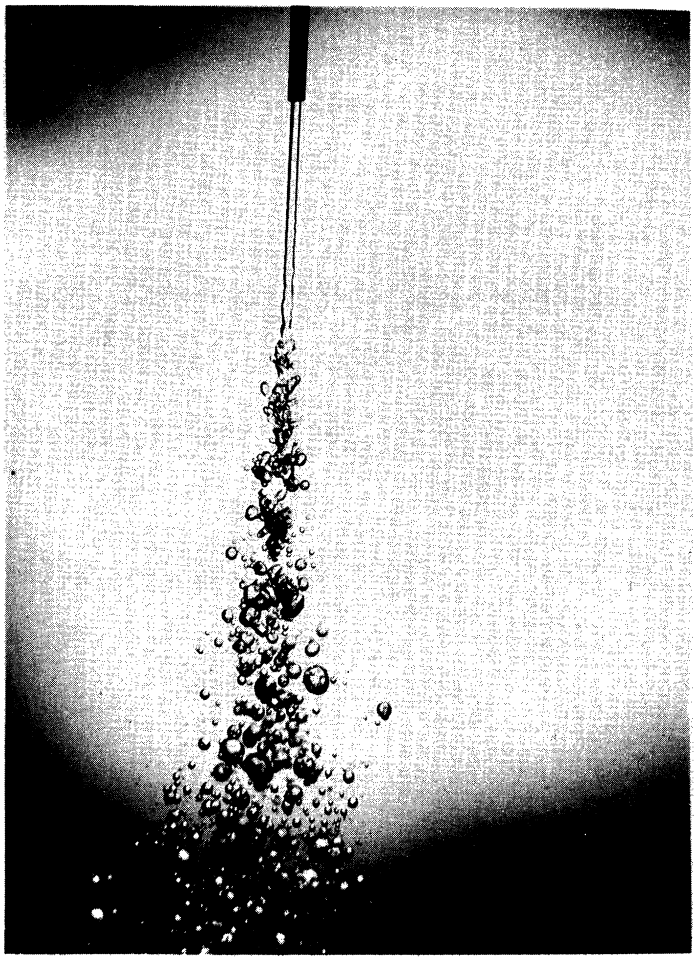

Figure 41. Typical Photograph of Jet Breakup in Low Viscosity System - 2.6X.

inclusion formation. Accordingly, runs were made using a low viscosity sprayed phase (carbon tetrachloride) and a highly viscous receiving fluid (glycerine).

Results were immediate and gratifying. Shown in Figure 42 to Figure 45 is a series of pictures taken with this liquid pair at progressively increasing nozzle velocities. As shown in the photographs, the high viscosity of the glycerine receiving phase kept breakup of the jet in the varicose regime. A most embarrassing point in the analysis of the data to this time had been the question of how the inclusions could penetrate the relatively stable large drop configuration in order to get inside. The answer yielded by this set of photographs was that the inclusions were present in the jet before it disintegrated - the inclusions literally pre-date the large drops.

Next, pictures were taken closer to the nozzle, to attempt to catch the inclusions forming. Results are shown in Figures 46 and 47. The mechanism can be seen to be the sequence of events shown in Figure 48. A ligament or sheet is drawn out from the jet, but instead of breaking off, it recoalesces with the jet, pinching off some of the external phase in the process. This elongated form then collapses to yield a drop or drops within the jet. The same mechanism is operative at various nozzle diameters, as can be seen in Figures 49 through 55. Figure 52 shows an inclusion just beginning to form, while Figures 53, 54, and 55 show to what lengths the penetration of the jet can reach, as well as the teardrop shape exhibited by the inclusions after detaching from the external phase and before being forced into a spherical configuration by the surface forces. It is interesting to note that a similar appearance can be distinguished in Figures 7 through 12, the transient case.

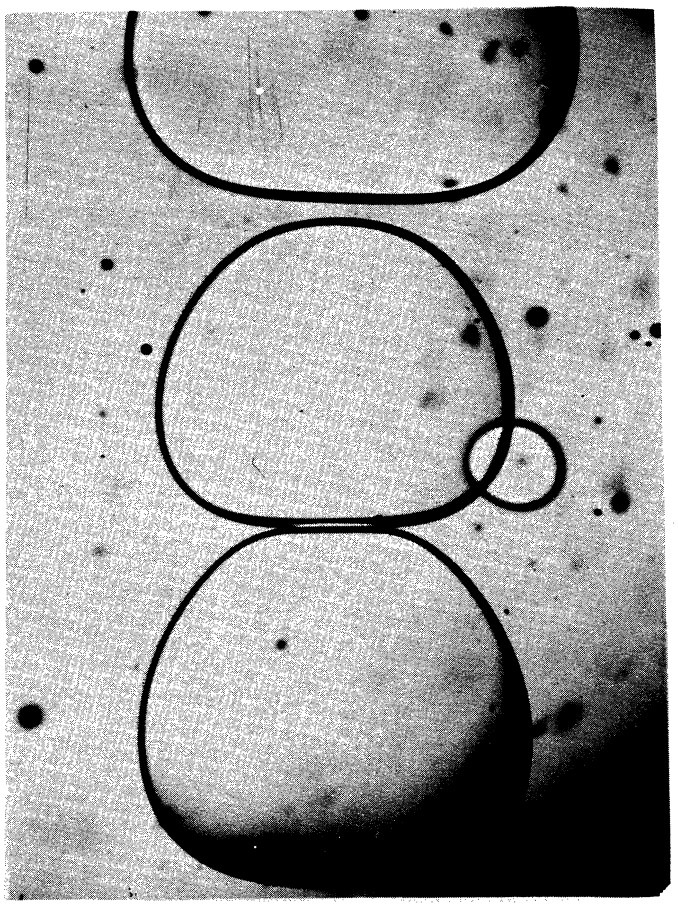

Figure 42. Carbon Tetrachloride into Glycerine - No. 19 Hypodermic Needle, 5-1/2 cm. From Orifice - 10X - Re = 7.4.

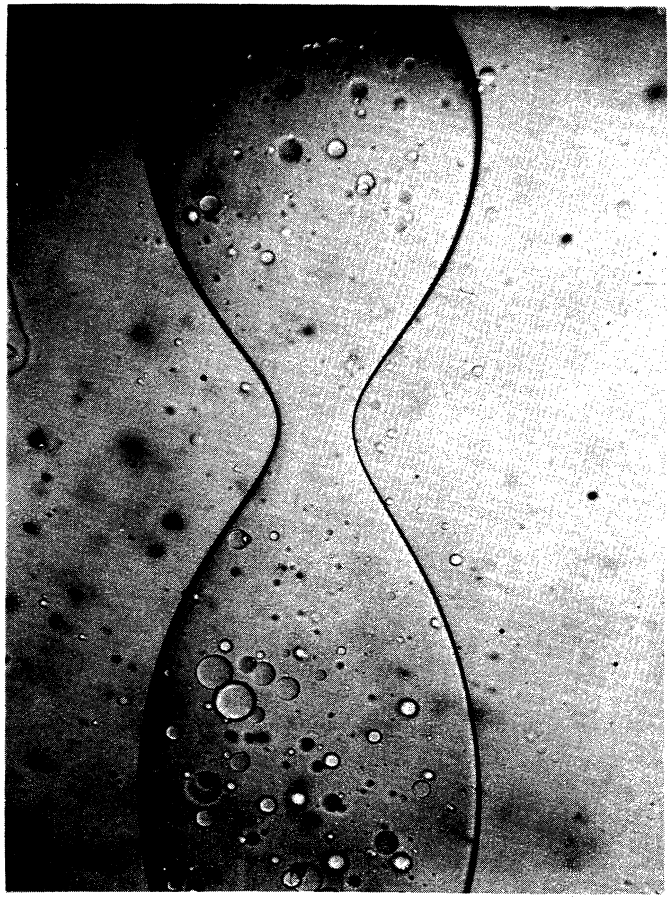

Figure 43. Carbon Tetrachloride into Glycerine - No. 19 Hypodermic Needle, 5-1/2 cm. From Orifice - 10X - Re = 35.9.

Figure 44. Carbon Tetrachloride into Glycerine - No. 19 Hypodermic Needle, 5-1/2 cm. From Orifice - 10X - Re = 48.6.

Figure 45. Carbon Tetrachloride into Glycerine - No. 19 Hypodermic Needle, 5-1/2 cm. From Orifice - 10X - Re = 63.4.

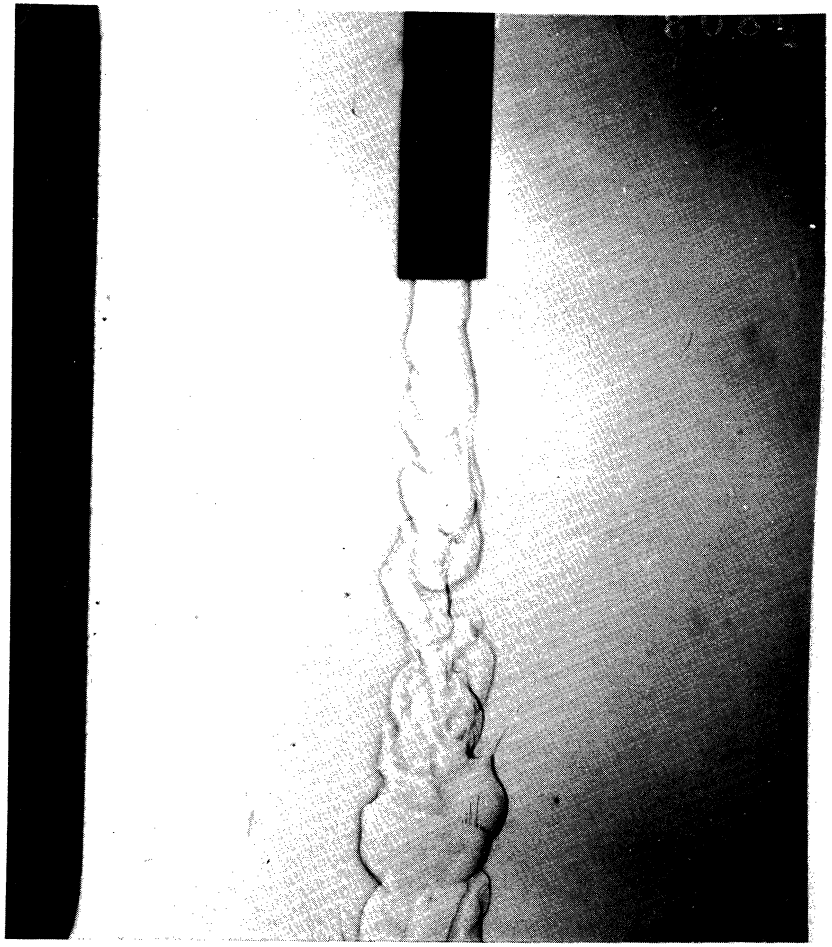

Figure 46. Carbon Tetrachloride into Glycerine - No. 19 Hypodermic Needle, at Orifice - 10X - Re = 39.6.

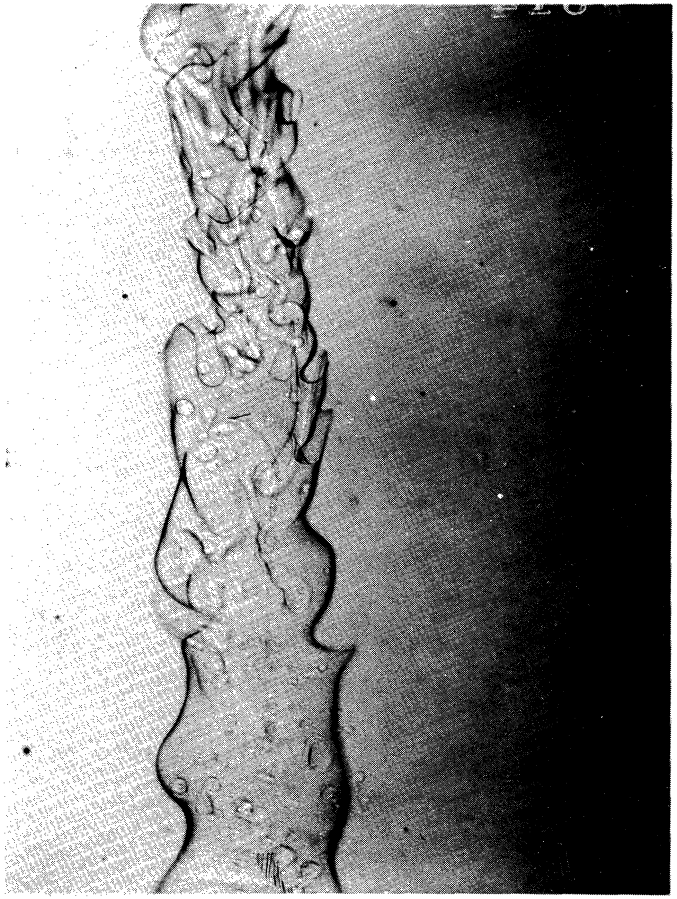

Figure 47. Carbon Tetrachloride into Glycerine - No. 19 Hypodermic Needle, 2.5 cm. From Orifice - 10X - Re = 47.5.

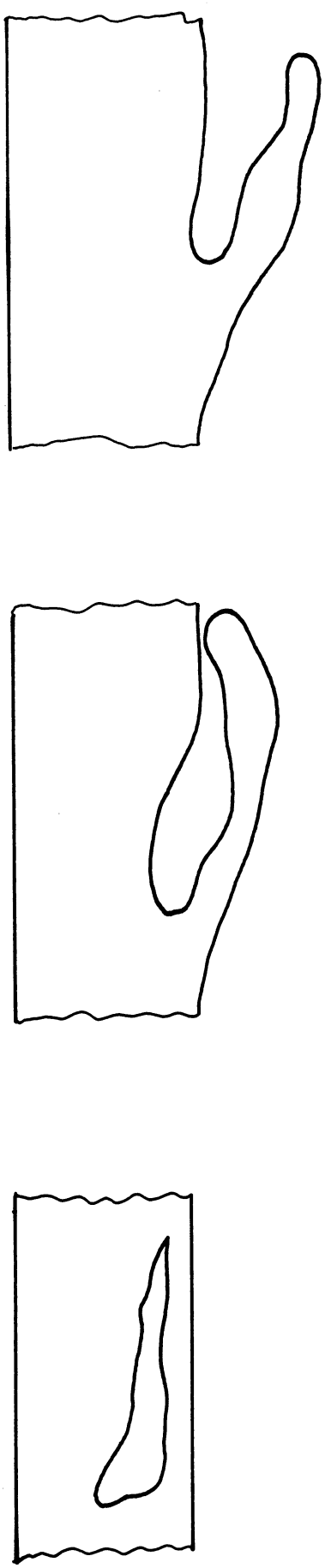

Figure 48. Schematic Depiction of Mechanism.

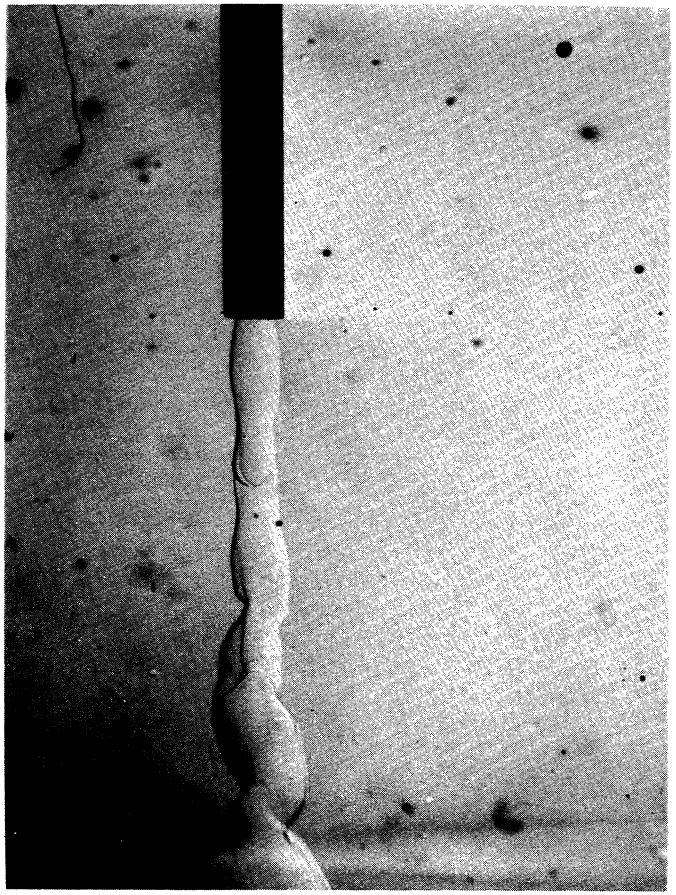

Figure 49. Carbon Tetrachloride into Glycerine - No. 22 Hypodermic Needle - 10X - Re = 8.88.

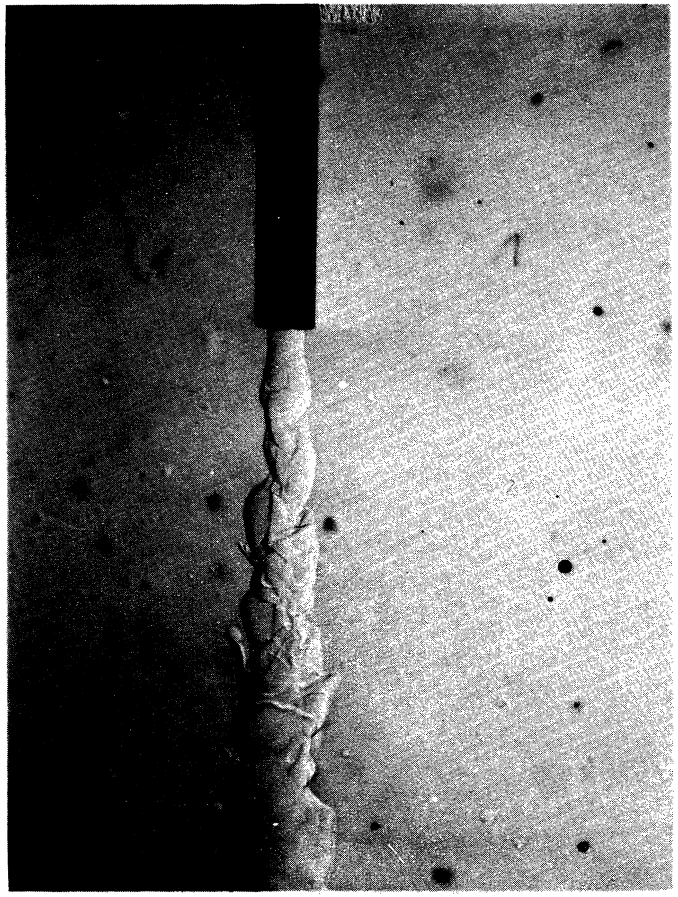

Figure 50. Carbon Tetrachloride into Glycerine - No. 22 Hypodermic Needle - 10X - Re = 30.6.

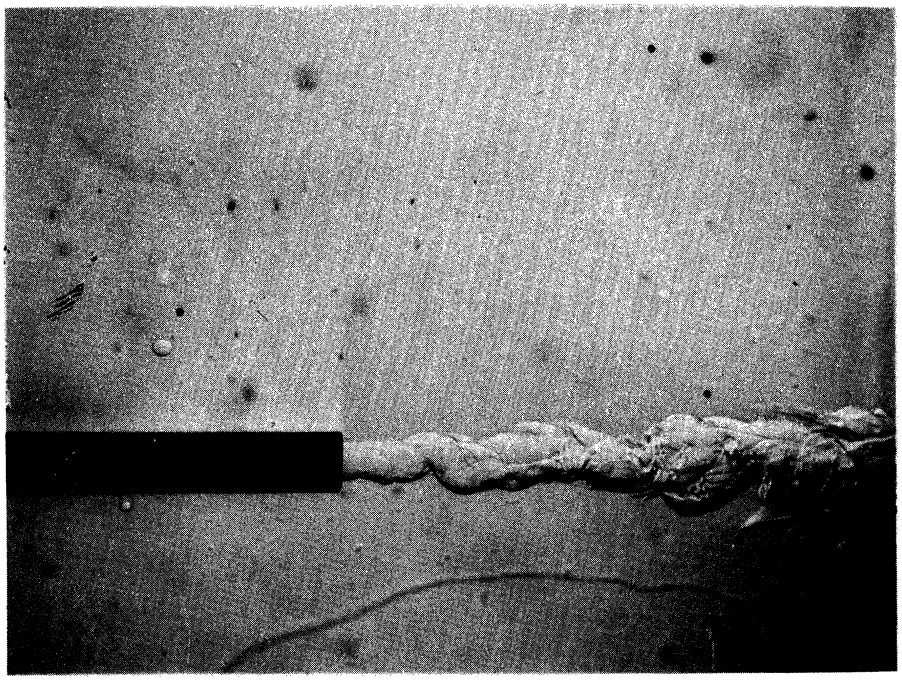

Figure 51. Carbon Tetrachloride into Glycerine - No. 22 Hypodermic Needle - 10X - Re = 42.0.

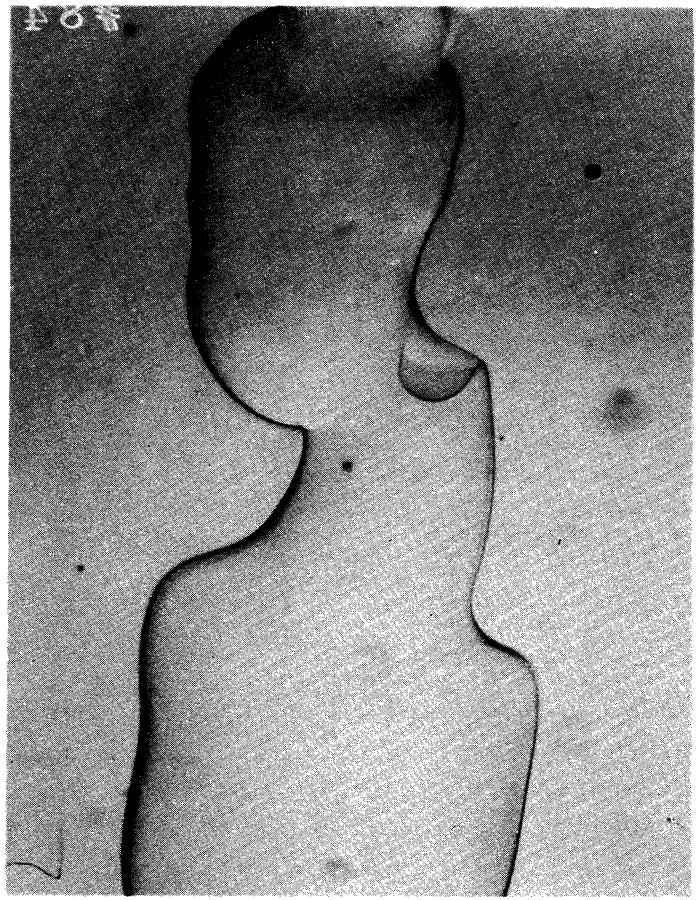

Figure 52. Carbon Tetrachloride into Glycerine - No. 17 Hypodermic Needle - 10X - 4 cm. From Orifice - Re = 24.6.

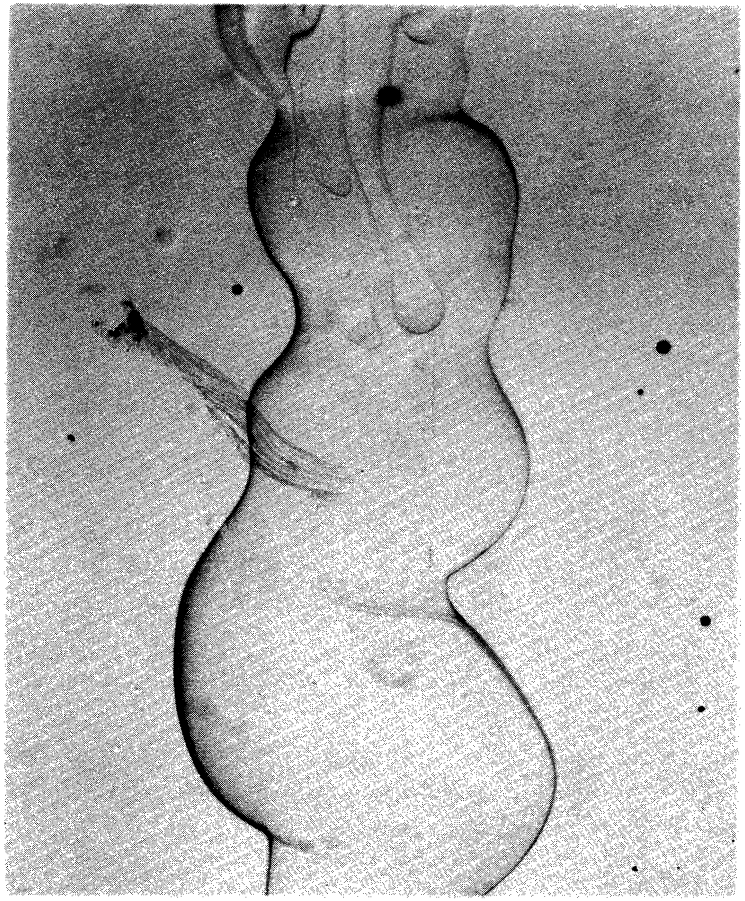

Figure 53. Carbon Tetrachloride into Glycerine - No. 17 Hypodermic Needle - 10X - 4 cm. From Orifice - Re = 33.8.

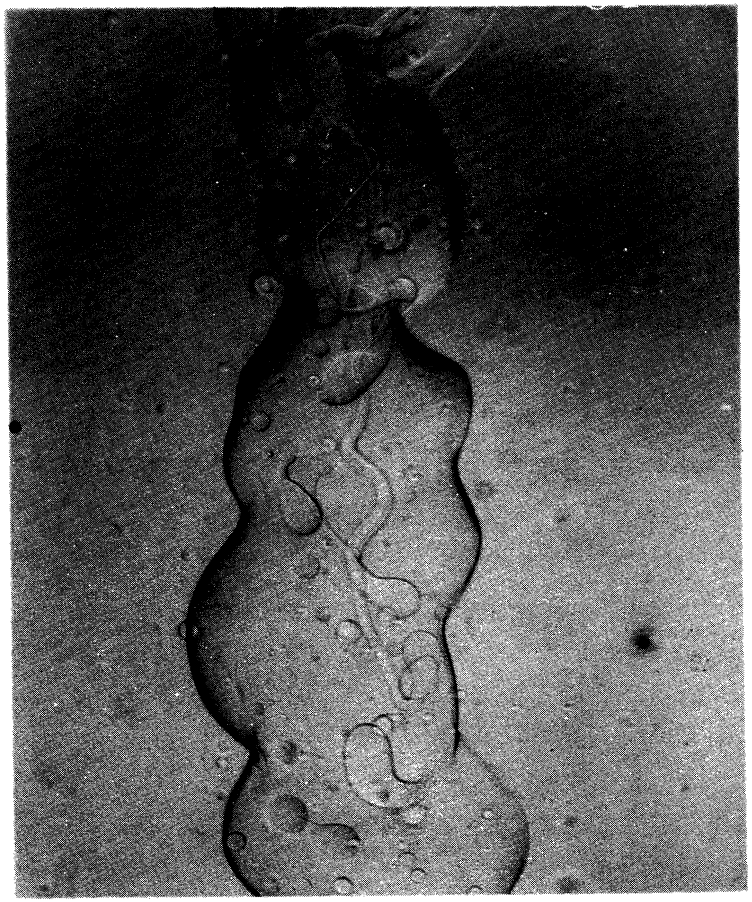

Figure 54. Carbon Tetrachloride into Glycerine - No. 17 Hypodermic Needle - 10X - 4 cm. From Orifice - Re = 60.3.

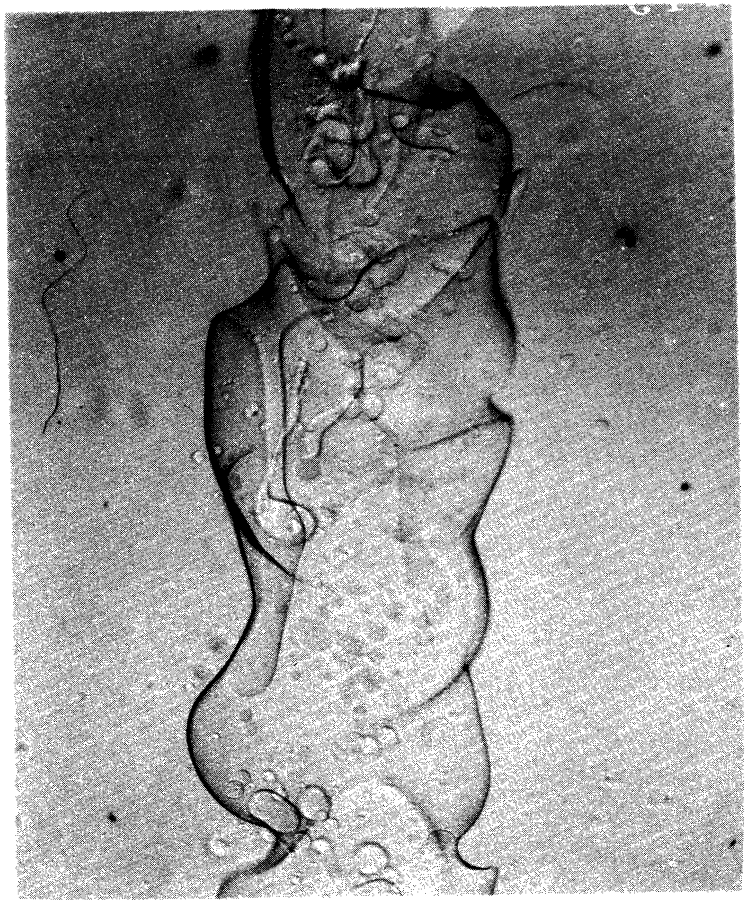

Figure 55. Carbon Tetrachloride into Glycerine - No. 17 Hypodermic Needle - 10X - 4 cm. From Orifice - Re = 71.4.

Another important observation that could be made using this viscous system was that the coalescence of the inclusions was extremely rapid. From a jet literally packed full of included drops as shown in Figure 45, a large drop would detach with much the appearance shown in Figure 56a. The inclusions coalesce rapidly out through the large drop wall, and by the time the drop reaches the bottom of the cell, it has an appearance much as shown in Figure 56c, all in a time of the order of one second.

The rapid coalescence rate indicates that this is perhaps the reason that multiple emulsions are so seldom observed in liquid-liquid work. Measurements are usually taken on a stagnant system rather than a dynamic one, and by the time the observation is made, the inclusions have disappeared. The systems where multiple emulsions have been observed, as in the work by Boll and that by Pavloshenko and Yanishevskii discussed earlier, have either been very viscous systems or heterogeneous systems with possible stabilizing surfactants.

A logical conclusion would seem to be that the flow pattern which spawns inclusion formation probably occurs in very nearly all liquid-liquid processes, but that coalescence is so rapid in most cases that the inclusions are never observed. For any sort of macroscopic approach, inclusion surface area would merely be lumped in the mass transfer coefficient, and coalescence would give observed effects which would be regarded as anomalies in the transfer coefficient rather than the interfacial area.

It is instructive to examine some more of the counted data in light of the proposed mechanism. Since the inclusions are formed

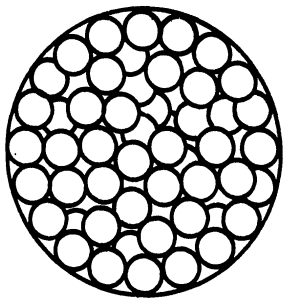

a.

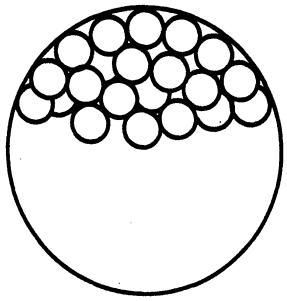

b.

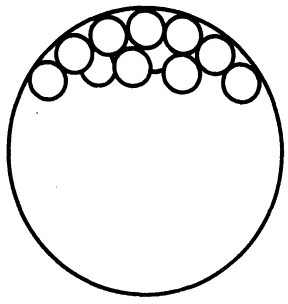

c.

Figure 56. Schematic Diagram of Inclusion Coalescence.

more or less independently of the large drops, we would expect little or no relationship between the diameter of a large drop and the mean diameter of the inclusion within that drop, other than the obvious limitation that inclusion diameter cannot exceed large drop diameter. Shown in Figure 57 is such a plot, with the observed relation very nearly flat as would be expected.

The specific flow field which leads to inclusion formation would seem to be an eddy which forms in the receiving phase at the jet boundary, and rotates similarly to the vortex rings which exist in the atmosphere. Such a flow will obviously be induced by the moments existing in the viscous fluids. This type of rotating motion would be supplied with energy by the deceleration of the jet; the magnitude of this deceleration is obvious from the jet swelling observable in Figures 46 and 47. Such an eddy would also give a velocity field which tends to return the free end of a ligament to the jet body. Strong interfacial tension would tend to prevent such recoalescence, in agreement with the observed data.

It is also interesting to note that inclusion mean diameter does not change with (Re)(We) (see Figure 58). Since we observed that the percent included volume and area do change with (Re)(We), this indicates that the number of inclusions increases but not the diameter. In other words, we are led to the speculation that the scale of turbulence which forms inclusions is relatively constant, although the intensity must change to supply the energy for the additional surface formation.

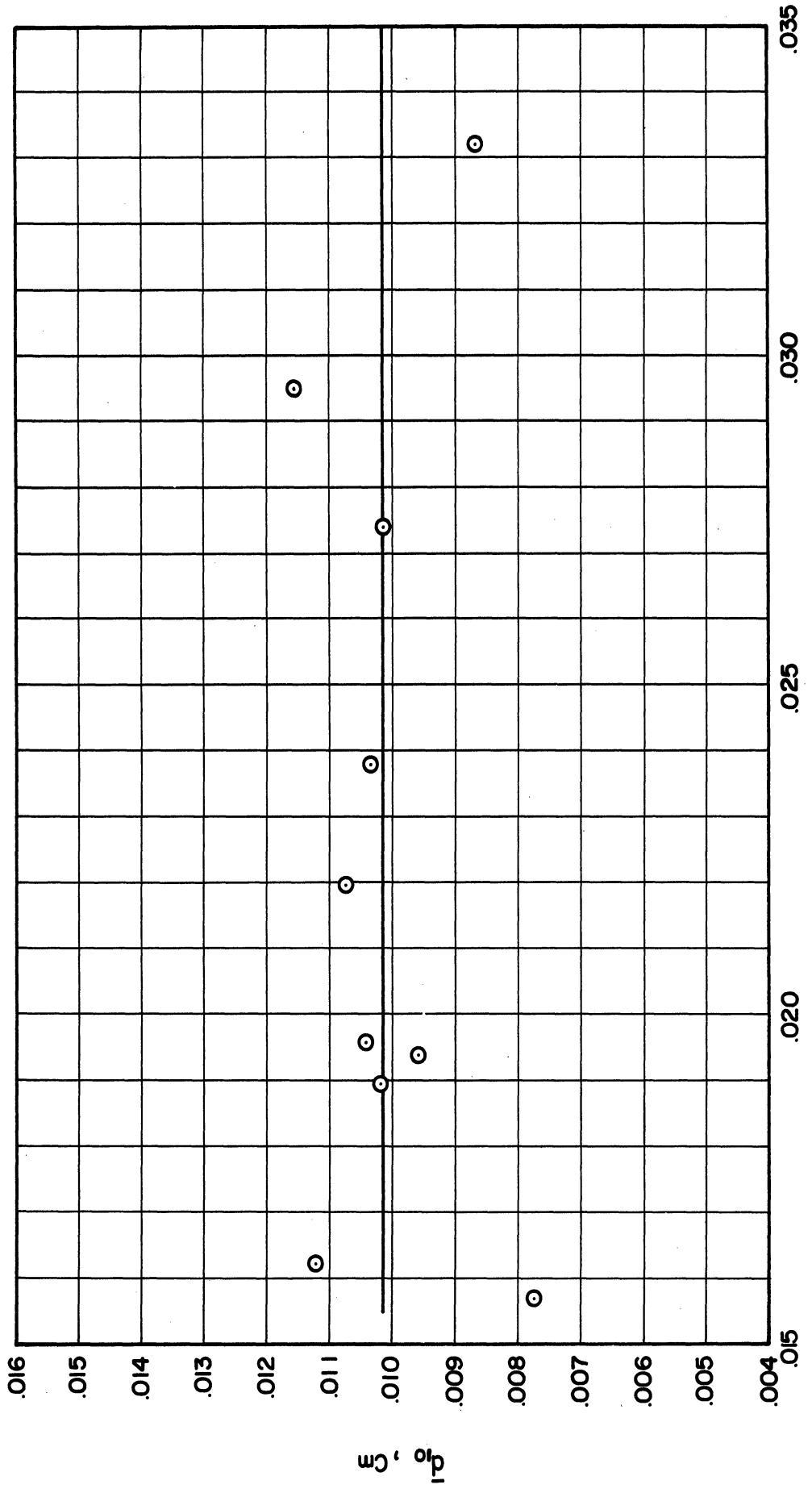

Figure 57. $\overline{D_{10}}$ versus $\overline{d_{10}}$.

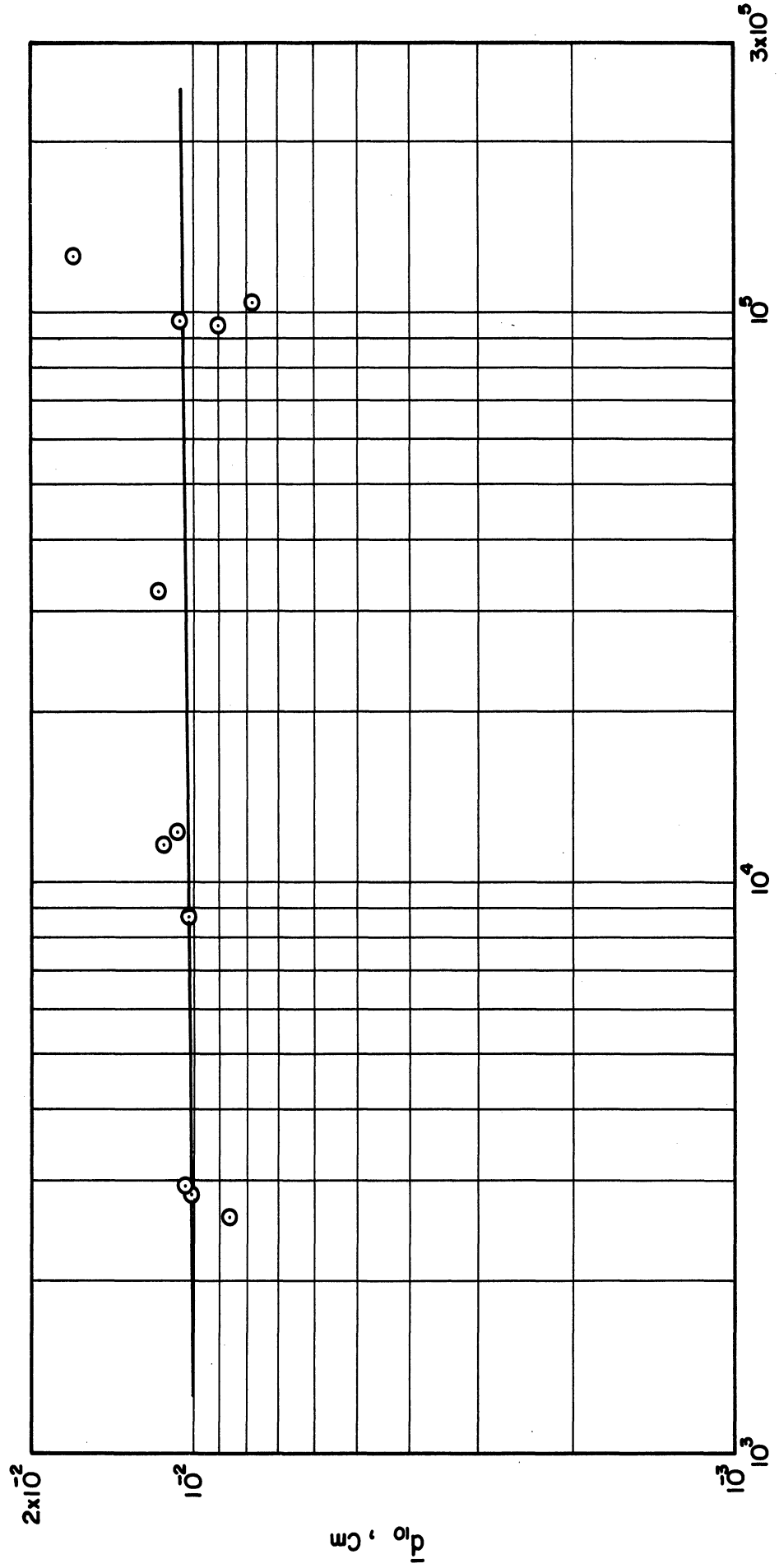

Figure 58. $\overline{d}_{10}$ versus Re x We.

We should note at this time that a lower limit for inclusion formation is observable. We must also say there may be an upper limit. It may be that at sufficiently high injection pressures the internal pressure of the jet will cause disruption before the flow field observed here has time to develop. Equipment limitations prevent investigation of possible upper limits at this time.

A further understanding of the interfacial forces involved will be necessary before it will be possible to construct a realistic mathematical model for the mechanism proposed, particularly with regard to coalescence and with regard to the interfacial tension of an interface under dynamic conditions. It is well known that interfacial tension can show a strong time dependence. The extreme length to which the external phase can penetrate the jet may indicate that the interfacial tension drops sharply when an interface is being strained. When it is possible to make some reasonable assumptions with regard to surface forces, one can postulate a variety of eddy strengths and initial jet disturbance configurations and attempt to see what configurations will grow and bend back toward the jet. The existence of the large velocity gradients in real systems will probably require that such modeling be very naive at the outest.

IX. CONCLUSIONS

This work, as is typical with investigations in relatively unexplored fields, has frequently grown back two questions for every one that has been cut off. There are, however, several general conclusions which appear well motivated.

Both the mechanism proposed and the data taken indicate that multiple emulsion formation is not only possible in pure phases, but probably exists in many present day operations with rapid coalescence preventing its observation as such. It appears that hydrodynamics controls multiple emulsion formation, although stabilization is necessary to its observation.

The application of the log-normal distribution to the large drops, and to the inclusion marginal and conditional distributions seems well indicated. The possibility of a one-parameter characterization would seem worthy of further investigation.

The proposed model for percent included area and volume as a function of nozzle parameters will probably furnish order of magnitude results for a given liquid pair; however, caution should be used in extrapolating. It can be said that inertial forces predominate in the inclusion formation process, and that the five variables in Reynolds number and Weber number must all be considered in future work.

X. RECOMMENDATIONS FOR FUTURE WORK

There are several directions in which future work should be directed. First, since the experimental error is fairly large compared to the differences one desires to measure, there are three alternatives:

1) Re-design of experimental equipment to permit work over a wider range of independent variables so that changes in dependent variables are larger with respect to experimental error.
2) Improved analytical technique.
3) Experimental runs with many replicates so as to permit reduction of experimental error by averaging.

Alternatives 1 and 2 are preferable to alternative 3; however, to redesign the equipment to permit working over a larger range requires certain additional knowledge. The most important limitation is the clouding of the sample cell at high liquid velocities through the nozzle. In order to circumvent this, a larger, deeper, sample cell could be used to permit photographing the spray farther from the nozzle where spray density is less. To do this, one must know the coalescence rate of the inclusions, and the validity of the spray sample taken. It will probably be necessary to traverse across the spray to get a representive sample. Longer focal length lenses will be required.

To improve analytical techniques will be very difficult unless some way is found to eliminate the human factor in counting, perhaps by a light transmittance technique.

In order to remove variation by averaging, it will be necessary to determine experimental error precisely. This also involves consideration of variation of error at high percent included area or volume because of obscuring of inclusions, etc.

After resolving the experimental error problem in one of the three ways suggested, the next logical step is a designed experiment, probably a partial factorial, to test a model of the form:

$$\begin{aligned}\log (\%\text{ included volume}) = {} & m_1 \log D_n + m_2 \log v_n \\ & + m_3 \log \rho_s + m_4 \log \rho_n \\ & + m_5 \log \mu_s + m_6 \log \mu_n \\ & + m_7 \log \gamma + b\end{aligned} \qquad (X.1)$$

Results from checking this model at two or three levels should suggest more realistic dimensionless groups for correlation purposes.

With respect to the suggested mechanism, the first step should be an investigation of dynamic, as opposed to static, coalescence. Initial study can probably be done with a drop approaching a flat interface at various velocities.

Finally, there are any number of independent variables which suggest themselves for study, such as:

1) nozzle configuration - producing sheets, cones, etc.
2) nozzle roughness and wettability,
3) sharp versus blunt edge nozzles,
4) vibration of nozzle,
5) effect of surfactant type,
6) effect of chemical properties of the liquids.

A P P E N D I C E S

APPENDIX A

BIBLIOGRAPHY

A. BIBLIOGRAPHY

1. Allan, R. S., and Mason, S. G. "Effects of Electrical Fields on Coalescence in Liquid + Liquid Systems," Trans. Far. Soc., 57, (1961) 2027-40.

2. Albers, W., and Overbeek, J. T. G. "Floccuation and Re-Dispersion of Water Droplets Covered by Amphi Polar Mono Layers," Colloid Science, 15, (1960) 489-502.

3. Asset, G. M., and Bales, P. D. "Hydraulic Jets at Low Reynolds Numbers and Constant Weber Number," Research Report 69, Chemical Corps Medical Laboratory, Army Chemical Center, Maryland (June, 1951).

4. Balje, O. E., and Larson, L. F. "The Mechanism of Jet Disintegration," Air Material Command Engineering Division Memorandum Rep. MCREXE-664-531B GS USAF Wright Pat. No. 179 (August 29, 1949).

5. Baron, T. "Atomization of Liquid Jets and Droplets," Tech. Rep. No. 4 on Contr. N6-Ori-71, Eng. Expt. Station, University of Illinois (1949).

6. Batchelor, G. K., and Davies, R. M. Surveys in Mechanics, Cambridge: New York (1956).

7. Bennett, C. A., and Franklin, N. L. Statistical Analysis in Chemistry and the Chemical Industry, Wiley: New York (1954).

8. Boll, R. H. "A Rapid Technique for Determining Specific Surface in Liquid-Liquid Sprays," Doctoral Dissertation, The University of Michigan (1955).

9. Borisenko, A. J. "The Problem of the Influence of Turbulence of a Liquid Jet on Its Atomization," Zhur. Tekh. Fizik., 23, (1953) 195-6.

10. Borodin, V. A., and Dityakin, Y. F. "Unstable Capillary Waves on the Surface of Separation of Two Viscous Fluids," NACA Memo 1281 (April, 1951).

11. Boucher, P. E. Fundamentals of Photography, Van Nostrand: New York (1947).

12. Brown, E. B. Optical Instruments, Chemical Publishing Company: Brooklyn (1945).

13. Chamberlain, Katherine, An Introduction to the Science of Photography, MacMillian: New York (1951).

14. Charles, G. E., and Mason, S. G. "The Coalescence of Liquid Drops with Flat Liquid-Liquid Interfaces," J. Colloid Sci., 15, (1960) 236.

15. Charles, G. E., and Mason, S. G. "The Mechanism of Partial Coalescence of Liquid Drops at Liquid/Liquid Interfaces," J. Colloid Sci., 15, (1960) 105.

16. Cheesman, D. F. and King, A. "The Properties of Dual Emulsions," Trans. Far. Soc., 34, (1938) 594-8.

17. Christiansen, R. M. and Hixson, A. N. "Breakup of a Liquid Jet in a Denser Liquid," Industrial and Engineering Chemistry, 49, No. 6, (1957) 1017-24.

18. Clay, P. H. "The Mechanism of Emulsion Formation in Turbulent Flow," Proc. Nederl. Akad. Wetensch., 42, (1940) 852-65, 979, 990.

19. Clayton, W. The Theory of Emulsions and Their Technical Treatment, 5th ed., Churchill: London (1954).

20. Clerk, L. P. Photography Theory and Practice, Pitman: New York (1954).

21. Cochran, W. G., and Cox, G. M. Experimental Designs, 2nd ed., Wiley: New York (1957).

22. Colloid Science (Symposium), Chemical Pub. Co.: Brooklyn (1947).

23. Dallavalle, J. M., Orr, C., Jr., and Blocker, H. G. "Fitting Bimodal Size Distribution Curves," Industrial and Engineering Chemistry, (June, 1951) 1377-80.

24. Debye, P., and Daen, J. "Stability Considerations on Nonviscous Jets Exhibiting Surface or Body Tension," Phys. Fluids, 2, (1959) 416-21.

25. De Juhasz, K. J. (ed.) Spray Literature Abstracts, ASME: New York (1959).

26. Du Nouy, P. Surface Equilibria of Biological and Organic Colloids, The Chemical Catalog Co.: New York (1926).

27. Eriksen, J. L. "Thin Liquid Jets," Journal of Rational Mechanics and Analysis, 1, (1952) 521-38.

28. Fraser, D. A. S. Statistics: An Introduction, Wiley: New York (1958).

29. Fuhs, A. E. "Spray Formation and Breakup, and Spray Combustion," Air Force Office of Sce. Res., Rept. TN-58-514, AMF/TD No. 1199, Tech. Note 4 (February, 1958).

30. Gelalles, A. G. "The Effect of Orifice L/D Ratio on Fuel Sprays for Compression Ignition Engines," NACA Tech. Rept. 402 (1931).

31. Gelalles, A. G., and Marsh, E. T. "The Effect of Orifice L/D Ratio on the Coefficient of Discharge of Fuel Injection Nozzles," NACA Techn. Note 369 (1931).

32. Gelalles, A. G. "The Effect of Orifice L/D Ratio on Spray Characteristics," NACA Tech. Note 352 (1930).

33. Gel'perin, N. I., and Vil'nits, S. A. "Dispersion of Liquids Flowing Through Nozzles Into Air and Liquid Media," Trudy. Moskov. Inst. Tonkoi Khim. Tedhnol. Im. M.V. Lomonosova, 6, (1956) 111-16.

34. Giffen, E., and Muraszew, A. The Atomization of Liquid Fuels, Wiley: New York (1953).

35. Glasstone, S. Textbook of Physical Chemistry, 2nd ed., Van Nostrand: New York (1948).

36. Harmon, D. B. "Drop Sizes from Low Speed Jets," Journal of the Franklin Institute, 259, No. 6 (June, 1955) 519-22.

37. Hayworth, C. B., and Treybal, R. E. "Drop Formation in Two Liquid-Phase Systems," Industrial and Engineering Chemistry, 42, (June, 1950) 1174.

38. Herdan, G. Small Particle Statistics, Elsevier: New York (1953).

39. Hermans, J. J. Flow Properties of Disperse Systems, Interscience: New York (1953).

40. Hill, T. L. "Concerning the Dependence of the Surface Energy and Surface Tension of Spherical Drops and Bubbles on Radius," Journal of the American Chemical Society, 72, (1950) 3923-27.

41. Hinze, J. O. "Critical Speeds and Sizes of Liquid Globules," J. Appl. Sci. Res., Vol. A1, (1949) 273-88.

42. Hinze, J. O. "Forced Deformations of Viscous Liquid Globules," J. Appl. Sci. Res., Vol. A1, (1949) 263-72.

43. Hinze, J. O. "Fundamentals of the Hydrodynamic Mechanism of Splitting in Dispersion Processes," A.I.Ch.E. Journal, (September, 1955). 289-95.

44. Hinze, J. O. "On the Mechanism of Disintegration of High Speed Liquid Jets," 6th International Congress on Applied Mechanincs, Paris (July, 1946).

45. Holroyd, H. B. "On the Atomization of Liquid Jets," Journal of the Franklin Institute, 215, (1933) 93-7.

46. Hughes, R. R., and Gilliland, E. R. "The Mechanics of Drops," 1951 Heat Transfer and Fluid Mechanics Institute, Stanford, 53-72.

47. Jacobs, D. H. Fundamentals of Optical Engineering, McGraw Hill: New York (1954).

48. Jirgensons, B., and Straumanis, M. E. A Short Textbook of Colloid Chemistry, Wiley: New York (1954).

49. Keith, F. W., and Hixson, A. N. "Liquid-Liquid Extraction Spray Columns - Drop Formation and Interfacial Transfer Area," Industrial and Engineering Chemistry, 47, No. 2, (January, 1955) 258.

50. Knelman, F. H., Dombrowski, N., and Newitt, D. M. "Mechanism of the Bursting of Bubbles," Nature, 173, (February 6, 1954) 261-2.

51. Lange, N. A. Handbook of Chemistry, 8th ed., Handbook Publishers: Sandusky (1952).

52. Lapple, C. E. Fluid and Particle Dynamics, Stanford Res. Inst.: Menlo Park (1951).

53. Magarvey, R. H., and Taylor, B. W. "Free Fall Breakup of Large Drops," J. Appl. Phys., 27, (October, 1956) 1129-35.

54. McDonald, J. E. "The Shape of Raindrops," Scientific American, 190, (February, 1954) 64-8.

55. McDonough, J. A. "Formation of Interfacial Area in Immiscible Liquids by Orifice Mixers," A.I.Ch.E. Journal, 6, (1960) 615-18.

56. Merrington, A. C., and Richardson, E. G. "The Breakup of Liquid Jets," Proc. Phys. Soc. (England), 59, (1947) 1-13.

57. Miesse, C. C. "Correlation of Experimental Data on the Disintegration of Liquid Jets," Industrial and Engineering Chemistry, 47, (September, 1955) 1690-1701.

58. Miesse, C. C. "Recent Advances in Spray Technology," Appl. Mech. Rev., 9 (August, 1956) 321-3.

59. Mugele, R. A., and Evans, H. D. "Droplet Size Distribution in Sprays," Industrial and Engineering Chemistry, 43, (1951) 1317-24.

60. Newitt, D. M., Dombrowski, N., and Knelman, F. H. "Liquid Entrainment - The Mechanism of Drop Formation from Gas or Vapor Bubbles," Trans. Inst. Chem. Engrs., 32, No. 4, (1954) 244-61.

61. Null, H. R., and Johnson, H. F. "Drop Formation in Liquid-Liquid Systems from Single Nozzles," A.I.Ch.E. Journal, 4, No. 3, (September, 1958) 273-81.

62. Pai, S. Fluid Dynamics of Jets, Van Nostrand: New York (1954).

63. Pavloshenko, I. S., and Yanishevskii, A. V. "Interfacial Surface Area of Mechanically Stirred Mutually Immiscible Liquids," Zhur. Priklad. Khim., 32, (1959) 1495-1502.

64. Perry, J. H. (ed.) Chemical Engineers' Handbook, 3rd ed., McGraw Hill: New York (1950).

65. Putnam, A. A. et al. "Injection and Combustion of Liquid Fuels," WADC Tech. Rept. 56-344 (March, 1957).

66. Ranz, W. E. "On Sprays and Spraying," Bulletin No. 65, Dept. of Eng. Res., Penn State U. (1956).

67. Ranz, W. E. "Some Experiments on Orifice Sprays," Can. Jl. of Chem. Eng., 36, No. 4, (August, 1958).

68. Redding, T. H. Flow Through Orifices and Parallel Throated Nozzles-A Bibliographic Survey, Chapman and Hall: London (1952).

69. "Reversal of Emulsion Type," Chem. Soc. Jl., (September, 1934) 1360-1.

70. Richardson, E. G. "Mechanics of the Disruption of Liquid Jets," Appl. Sci. Res., 4, Section A, (1954) 374-80.

71. Rideal, E. K. An Introduction to Surface Chemistry, Cambridge U. Press: Cambridge (1926).

72. Robertson, G. R. (ed.) Modern Chemistry for the Engineer and Scientist, McGraw Hill: New York (1957).

73. Rouse, H., and Abul-Fetough, A. "Characteristics of Irrotational Flow Through Axially Symmetric Orifices," Jl. Appl. Mech., 17, No. 4, (December, 1950) 421-6.

74. Rumscheidt, F. D., and Mason, S. G. "Particle Motion in Sheared Suspensions," J. Colloid Sci., 16, (1961) 210-61.

75. Rutgers, A. J. Physical Chemistry, Interscience: New York (1954)

76. Savic, P. "Circulation and Distortion of Liquid Drops Falling Through a Viscous Medium," Rept. No. MT22, National Research Council of Canada (July, 1953).

77. Savic, P. "Hydrodynamical and Heat Transfer Problems of Liquid Spray Droplets," National Research Council of Canada, Div. of Mech. Eng. Quarterly Bull. (January - March, 1953).

78. Schlicting, H. Boundary Layer Theory, 4th ed., McGraw Hill: New York (1960).

79. Schwartz, A. M., and Perry, J. W. Surface Active Agents, Their Chemistry and Technology, Interscience: New York (1949).

80. Schwarz, N., and Bezemer, C. "A New Equation for Size Distribution of Emulsion Particles," Kolloid Zeitschrift, 146, No. 1-3 (1956) 139-51.

81. Scott, L. S., Hayes, W. B., and Holland, C. D. "The Formation of Interfacial Area in Immiscible Liquids by Orifice Mixers," A.I.Ch.E. Journal, 4, No. 3, (1958) 346.

82. Shafer, M. R., and Bovey, H. L. "Applications of Dimensional Analysis to Spray Nozzle Performance Data," NBS Jl. of Research, 52, No. 3 (March, 1954) 141-7.

83. Siemes, W., and Kauffmann, J. F. "Drop Formation in Liquids on Nozzles at High Rates of Flow," Chimie-Ing. Techn., 29, No. 1 (1957) 32-8.

84. Squire, H. B. "The Round Laminar Jet," Quart. Jl. Mech. Appl. Math., 4, pt. 3, (September, 1951) 321-29.

85. Squire, H. B. "Some Viscous Fluid Flow Problems: Jet Emerging from a Hole in a Plane Wall," Phil. Mag., VIIth Series, No. 344, (September, 1932) 942-5.

86. Treybal, R. E. Liquid Extraction, McGraw Hill: New York (1951).

87. Tyler, E., and Watkin, F. "Experiments with Capillary Jets," Phil. Mag., 14, Series VII, No. 94, (1932) 849-81.

88. Van Deemter, J. J., and Van der Laan, E. T. "Momentum and Energy Balances for Dispersed Two-Phase Flow," Appl. Sci. Res., 10A, (1961) 102-8.

89. Washburn, E. W. (ed.) International Critical Tables, McGraw Hill: New York (1928).

90. Wiley, R. M. "Limited Coalescence of Oil Droplets in Coarse Oil-in-Water Emulsions," J. Colloid Sci., 9, No. 5, (October, 1954) 427-37.

91. Woodman, R. M. "Notes on Dual Emulsions," J. Phys. Chem., 33, (1929) 88-94.

92. Woodman, R. M. "Studies in Dual Emulsions," Chem. Age. 25, (1931) 146-7.

93. York, J. L. "Photographic Analysis of Sprays," Ph.D. Dissertation, The University of Michigan (1949).

94. Zucrow, M. J. "Discharge Characteristics of Submerged Jets," Purdue Univ. Eng. Expt. Sta. Bull. No. 31 (June, 1928).

APPENDIX B

COMPUTER PROGRAM

COMPUTER PROGRAM

Shown on the following pages (Table XI) is the computer program used in this work. The program is written in the MAD language developed at the University of Michigan. Information regarding this language and instructions for its use can be obtained from the Computing Center, University of Michigan, Ann Arbor, Michigan. Execution was by an IBM 709 machine.

Shown in Table XII are the input variables for the program. In Table XIII are the corresponding values for Run 10. In Table XIV is the computer output for Run 10. Note the raw data for Run 10 is contained in Table II. We will consider in order the calculation of the items shown in the computer output for Run 10.

The nozzle diameter, flow rate, interfacial tension, and viscosity are input variables. The Reynolds number is calculated as:

$$R_E = \frac{(\text{CONST 7})(4.)(\text{FLOW})(\text{DENSTY})}{(3.14159)(\text{NOZD})(\text{VISC})} \qquad (B.1)$$

and the Weber number as:

$$W_E = \frac{\left[\frac{(\text{FLOW})(4.)}{3.14159}\right]^2 (\text{DENSTY})}{(\text{GAMMA})(\text{NOZD})^3} \qquad (B.2)$$

Velocity through the nozzle is given by:

$$\text{Nozzle Velocity} = \frac{(4.)(\text{FLOW})}{(3.14159)(\text{NOZD})^2} \qquad (B.3)$$

```
$COMPILE MAD, EXECUTE, DUMP, PUNCH OBJECT, PRINT OBJECT                    01/

      DIMENSION CELL(30),MOMENT(20),ENDPT(35),DIAM(30),MEAN(20),      1DPK  *001
     ONUM(10),DEN(10),DIST(30),NUMBER(30),PCT(30),CUMPCT(30),PCTINT   2DPK  *001
     1(30),F(30),X(30),Y(30),DELAY(30),W(30),SPEED(30),G(30),PR(30)   3DPK  *001
     2,CUPR(30),        REM1(60),REM2(60),REM3(60),REM4(60),REM5(60)  4DPK  *001
      DIMENSION NIN(600,D),UC600,D)                                    DPK  *002
      DIMENSION EDPTIN(20),W1(20),ALPHA(30),BETA(20),SIZIN(20)         DPK  *003
START CONTINUE                                                         5DPK  *004
      READ FORMAT DCARD1, HEIGTH,WIDTH,DEPTH,CONST1,CONST2,CONST3,C    6DPK  *005
     OONST4                                                            7DPK  *005
      VECTOR VALUES DCARD1=$(4E20.5)*$                                 8DPK  *006
      READ FORMAT DCARD2,M,S,T,L,DOGEM,ENDREM,PHOTOS                   9DPK  *007
      VECTOR VALUES DCARD2=$6I3,F10.5*$                               10DPK  *008
      INTEGER M,S,DOGEM,I,R,T,H,L,ENDREM                              11DPK  *009
      INTEGER N,J,DOLOG,MOMIN                                         11DPKA *010
      INTEGER REM1,REM2,REM3,REM4,REM5                                12DPK  *011
      READ FORMAT DCARD3,NUMBER(1)...NUMBER(M)                        15DPK  *012
      VECTOR VALUES DCARD3=$(4F20.5)*$                                16DPK  *013
      READ FORMAT DCARD4,DIST(1)...DIST(M)                            17DPK  *014
      VECTOR VALUES DCARD4=$(4E20.5)*$                                18DPK  *015
      READ FORMAT DCARD5,DELAY(1)...DELAY(M)                          19DPK  *016
      VECTOR VALUES DCARD5=$(4E20.5)*$                                20DPK  *017
      READ FORMAT DCARD6,ENDPT(1)...ENDPT(M+1)                        21DPK  *018
      VECTOR VALUES DCARD6=$(4E20.5)*$                                22DPK  *019
      READ FORMAT DCARD7,NUM(1)...NUM(T)                              23DPK  *020
      VECTOR VALUES DCARD7=$(4E20.5)*$                                24DPK  *021
      READ FORMAT DCARD8,DEN(1)...DEN(T)                              25DPK  *022
      VECTOR VALUES DCARD8=$(4E20.5)*$                                26DPK  *023
      READ FORMAT DCARD9,REM1(1)...REM1(ENDREM)                       27DPK  *024
      VECTOR VALUES DCARD9=$(13C6)*$                                  28DPK  *025
      READ FORMAT DCAR10,REM2(1)...REM2(ENDREM)                       29DPK  *026
      VECTOR VALUES DCAR10=$(13C6)*$                                  30DPK  *027
      READ FORMAT DCAR11,REM3(1)...REM3(ENDREM)                       31DPK  *028
      VECTOR VALUES DCAR11=$(13C6)*$                                  32DPK  *029
      READ FORMAT DCAR12,REM4(1)...REM4(ENDREM)                       33DPK  *030
      VECTOR VALUES DCAR12=$(13C6)*$                                  34DPK  *031
      READ FORMAT DCAR13,REM5(1)...REM5(ENDREM)                       35DPK  *032
      VECTOR VALUES DCAR13=$(13C6)*$                                  36DPK  *033
      READ FORMAT DCAR17,DENSTY,CONST5,CONST6                         42DPKA *034
      VECTOR VALUES DCAR17=$3E20.5*$                                  42DPKB *035
      READ FORMAT DCAR18,N,DOLOG,MOMIN                                 DPK  *036
      VECTOR VALUES DCAR18=$3I3*$                                           *037
      VECTOR VALUES D=2,1,0                                                 *038
      D(2)=N                                                           DPK  *039
      READ FORMAT DCAR19,NIN(1,1)...NIN(M,N)                           DPK  *040
      VECTOR VALUES DCAR19=$(4F20.2)*$                                 DPK  *041
      READ FORMAT DCAR20,EDPTIN(1)...EDPTIN(N+1)                       DPK  *042
      VECTOR VALUES DCAR20=$(4E20.5)*$                                 DPK  *043
      READ FORMAT DCAR21,NOZD,FLOW,GAMMA,VISC                          DPK  *044
      VECTOR VALUES DCAR21=$4E20.5*$                                   DPK  *045
      READ FORMAT DCAR22,CONST7,CONST8,CONST9                          DPK  *046
      VECTOR VALUES DCAR22=$3E20.5*$                                   DPK  *047
      PRINT FORMAT SPACE                                                    *048
      VECTOR VALUES SPACE=$1H1*$                                            *049
      PRINT FORMAT RES18,REM1(1)...REM1(ENDREM)                       43DPK  *050
```

```
          VECTOR VALUES RES18=$1H , 13C6/,(1HO,13C6)*$                    44DPK  *051
          RE=(CONST7*4.*FLOW*DENSTY)/(3.14159*NOZD*VISC)                         *052
          WE=((FLOW*4./3.141592.P.2.)*DENSTY/(GAMMA*(NOZD.P.3.))           DPK  *053
          PRINT FORMAT RES43,NOZD,FLOW,GAMMA,VISC,RE,WE                    DPK  *054
          VECTOR VALUES RES43=$19HONOZZLE DIAMETER =,E20.5/,                DPK  *055
         012H FLOW RATE =,E20.5/,                                           DPK  *055
         122H INTERFACIAL TENSION =,E20.5/,                                 DPK  *055
         212H VISCOSITY =,E20.5/,                                           DPK  *055
         318H REYNOLDS NUMBER =,E20.5/,                                     DPK  *055
         415H WEBER NUMBER =,E20.5*$                                        DPK  *055
          SPDN = 4.*FLOW/(3.14159*(NOZD.P.2.))                                  *056
          PRINT FORMAT SPDNF, SPDN                                              *057
          VECTOR VALUES SPDNF =$27H VELOCITY THROUGH NOZZLE = ,E20.5*$          *058
          ADJUST=0.                                                             *059
          THROUGH RET1,FOR I=1,1,I.G.M                                  45DPK   *060
          ADJUST=ADJUST+NUMBER(I)                                               *061
          CELL(I)=ENDPT(I+1)-ENDPT(I)                                   46DPK   *062
          WHENEVER DOGEM.E.0, TRANSFER TO AMEAN                         47DPK   *063
          W(I)=(ENDPT(I)*ENDPT(I+1)).P.(.5)                             48DPK   *064
          WHENEVER I.G.1, TRANSFER TO AWAY1                                     *065
          PRINT FORMAT RES1                                             49DPK   *066
          VECTOR VALUES RES1=$38HOTHIS COMPUTATION USES GEOMETRIC MEANS 50DPK   *067
         0*$                                                            51DPK   *067
AWAY1     CONTINUE                                                              *068
          TRANSFER TO OUT                                               52DPK   *069
AMEAN     W(I)=(ENDPT(I)+ENDPT(I+1))/2.                                 53DPK   *070
          WHENEVER I.G.1, TRANSFER TO AWAY2                                     *071
          PRINT FORMAT RES2                                             54DPK   *072
          VECTOR VALUES RES2=$39HOTHIS COMPUTATION USES ARITHMETIC MEAN 55DPK   *073
         0S*$                                                           56DPK   *073
AWAY2     CONTINUE                                                              *074
OUT       CONTINUE                                                      57DPK   *075
          WHENEVER DOLOG.E.0,TRANSFER TO OUT14                                  *076
          PRINT FORMAT RES5O                                                    *077
          VECTOR VALUES RES5O=$44HOTHIS COMPUTATION USES LOGARITHMIC DI         *078
         0AMETERS*$                                                             *078
OUT14     CONTINUE                                                              *079
          Y(0)=0.                                                       58DPK   *080
          X(I)=(NUMBER(I)*DIST(I)*CONST1)/(PHOTOS*DELAY(I))             59DPK   *081
          Y(I)=X(I)+Y(I-1)                                              60DPK   *082
RET1      CONTINUE                                                      61DPK   *083
          PRINT FORMAT RES3                                             62DPK   *084
          VECTOR VALUES RES3=$30H1VELOCITY WEIGHTED PERCENTAGES*$       63DPK   *085
          PRINT FORMAT RES18, REM2(1)...REM2(ENDREM)                    88DPK   *086
          PRINT FORMAT RES4                                             64DPK   *087
          VECTOR VALUES RES4=$11HOSIZE RANGE,S24,6HNUMBER,S10,5HSPEED,S 65DPK   *088
         08,7HPERCENT,S2,18HCUMULATIVE PERCENT,S2,18HPERCENT/SIZE RANGE 66DPK   *088
         1*$                                                            67DPK   *088
          THROUGH RET2,FOR I=1,1,I.G.M                                  69DPK   *089
          ALPHA(I)=W(I)                                                         *090
          WHENEVER DOLOG.E.0, TRANSFER TO OUT12                                 *091
          W(I)= ELOG.(W(I))                                                     *092
          CELL(I)=ELOG.(ENDPT(I+1))-ELOG.(ENDPT(I))                             *093
OUT12     CONTINUE                                                              *094
          SPEED(I)=DIST(I)*CONST1/DELAY(I)                              70DPK   *095
          PCT(I)=X(I)*100./Y(M)                                         71DPK   *096
          CUMPCT(I)=Y(I)*100./Y(M)                                      72DPK   *097
          PCTINT(I)=PCT(I)/CELL(I)                                      73DPK   *098
          PRINT FORMAT RES5,ENDPT(I),ENDPT(I+1),NUMBER(I),SPEED(I),     74DPK   *099
         0PCT(I),CUMPCT(I),PCTINT(I)                                    75DPK   *099
```

```
          VECTOR VALUES RES5=$1H ,F10.5,4H TO ,F10.5,S6,F10.1,S5,F10.5,      76DPK  *100
         0S5,F10.5,S10,F10.5,S10,F10.5*$                                     77DPK  *100
RET2      CONTINUE                                                           77DPKA *101
          MOMENT(0)=1.                                                       77DPKB *102
          THROUGH RET3, FOR R=1,1,R.G.S                                      78DPK  *103
          MOMENT(R)=0.                                                       79DPK  *104
          G(0)=0.                                                            80DPK  *105
          THROUGH RET4, FOR I=1,1,I.G.M                                      81DPK  *106
          F(I)=(PCT(I)*(W(I).P.R))/100.                                      82DPK  *107
          MOMENT(R)=F(I)+MOMENT(R)                                           83DPK  *108
RET4      G(I)=F(I)+G(I-1)                                                   84DPK  *109
          WHENEVER CONST3.G.10., TRANSFER TO RET3                                   *110
          PRINT FORMAT RES8, R                                               85DPK  *111
          VECTOR VALUES RES8=$60H2PROBABILITY DENSITY AND DISTRIBUTION       86DPK  *112
         0FUNCTIONS WEIGHTED BY ,I3,27HTH POWER OF RANDOM VARIABLE*$         87DPK  *112
          PRINT FORMAT RES9                                                  90DPK  *113
          VECTOR VALUES RES9=$11HOSIZE RANGE,S19,11HPROBABILITY,S8,          91DPK  *114
         022HCUMULATIVE PROBABILITY*$                                        92DPK  *114
          THROUGH RET5, FOR I=1,1,I.G.M                                      94DPK  *115
          PR(I)=F(I)/G(M)                                                    95DPK  *116
          CUPR(I)=G(I)/G(M)                                                  96DPK  *117
          PRINT FORMAT RES10,ENDPT(I),ENDPT(I+1),PR(I),CUPR(I)               97DPK  *118
          VECTOR VALUES RES10=$1H ,F10.5,4H TO ,F10.5,S6,F10.5,S20,F10.      98DPK  *119
         05*$                                                                99DPK  *119
RET5      CONTINUE                                                          100DPK  *120
RET3      CONTINUE                                                          101DPK  *121
          Q=50.                                                                     *122
IN1       CONTINUE                                                                  *123
          PRINT FORMAT RES11                                                102DPK  *124
          VECTOR VALUES RES11=$33H4MOMENTS OF WEIGHTED DISTRIBUTION*$       103DPK  *125
          PRINT FORMAT RES18,REM3(1)...REM3(ENDREM)                         104DPK  *126
          WHENEVER Q.G.25, TRANSFER TO OUT5                                         *127
          THROUGH RET6, FOR R=0,1,R.G.MOMIN                                         *128
OUT5      WHENEVER Q.L.25, TRANSFER TO OUT6                                         *129
          THROUGH RET6, FOR R=0,1,R.G.S                                     106DPK  *130
OUT6      PRINT FORMAT RES12,R,MOMENT(R)                                    107DPK  *131
          VECTOR VALUES RES12=$1H ,I3,12HTH MOMENT = ,E15.5*$               108DPK  *132
RET6      CONTINUE                                                          109DPK  *133
          PRINT FORMAT RES13                                                110DPK  *134
          VECTOR VALUES RES13=$14H4MOMENT RATIOS*$                                  *135
          THROUGH RET7,FOR I=1,1,I.G.T                                      112DPK  *136
          K=MOMENT(NUM(I))/MOMENT(DEN(I))                                   113DPK  *137
          PRINT FORMAT RES14,NUM(I),DEN(I),K                                114DPK  *138
          VECTOR VALUES RES14=$10H RATIO OF ,F5.2,13HTH MOMENT TO ,F5.2     115DPK  *139
         0,12HTH MOMENT = ,E15.5*$                                          116DPK  *139
RET7      CONTINUE                                                          117DPK  *140
OUT7      PRINT FORMAT RES15                                                118DPK  *141
          VECTOR VALUES RES15=$53H4COMPUTATION OF MEANS, VARIANCES, AND     119DPK  *142
         0 STD. DEVIATIONS*$                                                120DPK  *142
          PRINT FORMAT RES18, REM4(1)...REM4(ENDREM)                        120DPKA *143
          WHENEVER Q.G.25, TRANSFER TO OUT8                                         *144
          THROUGH RET8, FOR I=0,1,I.G.(MOMIN-2)                                     *145
OUT8      WHENEVER Q.L.25, TRANSFER TO OUT9                                         *146
          THROUGH RET8, FOR I=0,1,I.G.(S-2)                                         *147
OUT9      MEAN=MOMENT(I+1)/MOMENT(I)                                        122DPK  *148
          VAR=(MOMENT(I+2)/MOMENT(I))-((MOMENT(I+1)/MOMENT(I)).P.2.)        123DPK  *149
          WHENEVER ADJUST.L.2., ADJUST = 2.                                         *150
          VAR=VAR*ADJUST/(ADJUST-1.)                                                *151
          WHENEVER VAR.L.0., VAR = .000001                                          *152
          DEV=(VAR.P.(.5))                                                  124DPK  *153
```

```
CHECK4    CONTINUE                                                          *154
          PRINT FORMAT RES35,I                                    125DPK    *155
          VECTOR VALUES RES35=$4OH FOR THE RANDOM VARIABLE DIAMETER ON      126DPK    *156
         0THE,I5,24HTH WEIGHTED DISTRIBUTION*$                    127DPK    *156
          PRINT FORMAT RES36,MEAN,VAR,DEV                         128DPK    *157
          VECTOR VALUES RES36=$7H MEAN =,E15.5,S5,10HVARIANCE =,E15.5,      129DPK    *158
         0S5,16HSTD. DEVIATION =,E15.5*$                          130DPK    *158
RET8      CONTINUE                                                131DPK    *159
          WHENEVER Q.G.25, TRANSFER TO OUT10                                *160
          THROUGH RET11, FOR I=0,1,I.G.(MOMIN/2)                            *161
OUT10     WHENEVER Q.L.25, TRANSFER TO OUT11                                *162
          THROUGH RET11; FOR I=0,1,I.G.(S/2)                                *163
OUT11     PRINT FORMAT RES19,I                                    133DPK    *164
          VECTOR VALUES RES19=$47H FOR THE RANDOM VARIABLE (DIAMETER TO     134DPK    *165
         0 THE POWER,I5,34H) ON THE NON-WEIGHTED DISTRIBUTION*$   134DPKA   *165
          MEAN=MOMENT(I)                                          134DPKB   *166
          VAR=MOMENT(2.*I)-((MOMENT(I)).P.2.)                     134DPKC   *167
          VAR=VAR*ADJUST/(ADJUST-1.)                                        *168
          WHENEVER VAR.L.0., VAR = .000001                                  *169
          DEV=VAR.P.(.5)                                          134DPKD   *170
          PRINT FORMAT RES36,MEAN,VAR,DEV                         134DPKE   *171
RET11     CONTINUE                                                134DPKF   *172
          WHENEVER Q.L.25., TRANSFER TO OUT1                                *173
          WHENEVER Q.G.75., TRANSFER TO OUT2                                *174
          PRINT FORMAT RES22                                      135DPK    *175
          VECTOR VALUES RES22=$2544SURFACE AND VOLUME RATES*$     136DPK    *176
          PRINT FORMAT RES18,REM5(1)...REM5(ENDREM)               137DPK    *177
          PRINT FORMAT RES50                                                *178
          VECTOR VALUES RES50=$9H DIAMETER,S16,12HSURFACE RATE,S13,          *179
         011HVOLUME RATE*$                                                  *179
          SUMSUR=0.                                                         *180
          SUMVOL=0.                                                         *181
          THROUGH RET23, FOR I=1,1,I.G.M                                    *182
          SUR=(3.14159*(ALPHA(I).P.2.)*SPEED(I)*NUMBER(I))/(PHOTOS*HEIG     *183
         0TH)                                                               *183
          VOL=(3.14159*(ALPHA(I).P.3.)*SPEED(I)*NUMBER(I))/(6.*PHOTOS*H     *184
         0EIGTH)                                                            *184
          SUMSUR=SUR+SUMSUR                                                 *185
          SUMVOL=VOL+SUMVOL                                                 *186
          PRINT FORMAT RES31,ALPHA(I),SUR,VOL                               *187
          VECTOR VALUES RES24=$16H SURFACE RATE = ,E15.5,S25,14HVOLUME      142DPK    *188
         0RATE = ,E20.5*$                                         143DPK    *188
RET23     CONTINUE                                                           *189
          PRINT FORMAT RES51                                                *190
          VECTOR VALUES RES51=$12HOTOTAL RATES*$                            *191
          PRINT FORMAT RES24,SUMSUR,SUMVOL                                  *192
          PRINT FORMAT RES29                                      164DPK    *193
          VECTOR VALUES RES29=$5642MOMENTUM AND ENERGY TRANSFER RATES T     165DPK    *194
         0HROUGH SAMPLE SPACE*$                                   166DPK    *194
          PRINT FORMAT RES18,REM5(1)...REM5(ENDREM)               167DPK    *195
          PRINT FORMAT RES32                                      169DPK    *196
          VECTOR VALUES RES32=$9HODIAMETER,S20,8HMOMENTUM,S10,      170DPK    *197
         014HKINETIC ENERGY*$                                     171DPK    *197
          SUMOM=0.                                                          *198
          SUMEN=0.                                                          *199
          THROUGH RET10,FORI=1,1,I.G.M                            172DPK    *200
          Y(I)=3.14159*(ALPHA(I).P.3.)*DENSTY*CONST5*SPEED(I)*NUMBER(I)     *201
         0/(6.*PHOTOS)                                                      *201
          X(I)=Y(I)*SPEED(I)*CONST6/2.                            174DPK    *202
          SUMOM=Y(I)+SUMOM                                                  *203
```

```
                SUMEN=X(I)+SUMEN                                                *204
                PRINT FORMAT RES31, W(I), Y(I), X(I)                            *205
                VECTOR VALUES RES31=$1H ,E15.5,S6,E15.5,S9,E15.5*$      176DPK  *206
RET10           CONTINUE                                                177DPK  *207
                PRINT FORMAT RES51                                              *208
                PRINT FORMAT RES52,SUMOM,SUMEN                                  *209
                VECTOR VALUES RES52=$11H MOMENTUM =,E20.5,S10,16HKINETIC ENER   *210
               0GY =,E20.5*$                                                    *210
                WHENEVER L.E.0, TRANSFER TO END                                 *211
                THROUGH RET12,FOR I=1,1,I.G.N                           DPK     *212
                W1(I)=(EDPTIN(I)+EDPTIN(I+1))/2.                        DPK     *213
                SIZIN(I)=EDPTIN(I+1)-EDPTIN(I)                                  *214
                BETA(I)=W1(I)                                                   *215
                WHENEVER DOLOG.E.0, TRANSFER TO OUT13                           *216
                W1(I)= ELOG.(W1(I))                                             *217
                SIZIN(I)=ELOG.(EDPTIN(I+1)) - ELOG.(EDPTIN(I))                  *218
OUT13           CONTINUE                                                        *219
RET12           CONTINUE                                                DPK     *220
                ADD1=0.                                                         *221
                ADD2=0.                                                         *222
                THROUGH RET13,FOR H=1,1,H.G.M                           DPK     *223
                WHENEVER CONST8.L.(5.), TRANSFER TO NO1                         *224
                PRINT FORMAT RES37,ALPHA(H)                                     *225
                VECTOR VALUES RES37=$4944CALCULATIONS FOR INCLUSIONS IN DROPS    DPK     *226
               0 OF DIAMETER,E20.5*$                                            DPK     *226
                WHENEVER NUMBER(H).L.(.005), TRANSFER TO NOGO                   *227
                PRINT FORMAT RES38                                      DPK     *228
                VECTOR VALUES RES38=$1940INCLUSION DIAMETER,S14,7HPERCENT,S7,    DPK     *229
               018HCUMULATIVE PERCENT,S7,18HPERCENT/SIZE RANGE*$                *229
                U(H,1)=NIN(H,1)                                                 *230
                THROUGH RET14,FOR J=2,1,J.G.N                           DPK     *231
                U(H,J)=NIN(H,J)+U(H,J-1)                                DPK     *232
RET14           CONTINUE                                                        *233
                WHENEVER U(H,N).L.CONST2, TRANSFER TO NOGO                      *234
                ADJUST=0.                                                       *235
                THROUGH RET15, FOR J=1,1,J.G.N                          DP      *236
                ADJUST=ADJUST+NIN(H,J)                                          *237
                PCT(J)=100.*NIN(H,J)/U(H,N)                                     *238
                CUMPCT(J)=U(H,J)*100./U(H,N)                            DPK     *239
RET15           CONTINUE                                                DPK     *240
IN2             CONTINUE                                                        *241
                THROUGH RET20, FOR J=1,1,J.G.N                                  *242
                PCTINT(J)=PCT(J)/SIZIN(J)                                       *243
                PRINT FORMAT RES39,W1(J),PCT(J),CUMPCT(J),PCTINT(J)             *244
                VECTOR VALUES RES39=$1H ,E15.5,S9,F15.5,S10,F15.5,S10,F15.7*$    *245
RET20           CONTINUE                                                        *246
                MOMENT(0)=1.                                            DP      *247
                WHENEVER Q.G.75, TRANSFER TO OUT3                               *248
                THROUGH RET17, FOR R=1,1,R.G.MOMIN                              *249
OUT3            WHENEVER Q.L.75, TRANSFER TO OUT4                               *250
                THROUGH RET17, FOR R=1,1,R.G.S                          DPK     *251
OUT4            MOMENT(R)=0.                                            DP      *252
                G(0)=0.                                                 DP      *253
                THROUGH RET16, FOR J=1,1,J.G.N                          DP      *254
                F(J)=PCT(J)*(W1(J).P.R)/100.                            DP      *255
                MOMENT(R)=F(J)+MOMENT(R)                                DP      *256
RET16           G(J)=F(J)+G(J-1)                                        DP      *257
                WHENEVER CONST4.G.10., TRANSFER TO RET17                        *258
                PRINT FORMAT RES8,R                                     DP      *259
                PRINT FORMAT RES40                                      DP      *260
```

```
          VECTOR VALUES RES40=$19HOINCLUSION DIAMETER,S10,11HPROBABILIT                *261
         0Y,S3,22HCUMULATIVE PROBABILITY*$                                    DP     *261
          THROUGH RET17, FOR J=1,1,J.G.N                                      DP     *262
          PR(J)=F(J)/G(N)                                                     DP     *263
          CUPR(J)=G(J)/G(N)                                                   DP     *264
          PRINT FORMAT RES41,BETA(J),PR(J),CUPR(J)                                   *265
          VECTOR VALUES RES41=$1H ,E15.5,S9,F15.5,S10,F15.5*$                 DP     *266
RET17     CONTINUE                                                            DP     *267
          WHENEVER Q.G.75., TRANSFER TO IN1                                          *268
NO1       CONTINUE                                                                   *269
          Y(H)=0.                                                                    *270
          X(H)=0.                                                                    *271
          THROUGH RET9, FOR J=1,1,J.G.N                                              *272
          X(H)=((BETA(J).P.2.)*NIN(H,J)*SPEED(H))+X(H)                               *273
          Y(H)=((BETA(J).P.3.)*NIN(H,J)*SPEED(H))+Y(H)                               *274
RET9      CONTINUE                                                                   *275
          ADD1=X(H)+ADD1                                                             *276
          ADD2=Y(H)+ADD2                                                             *277
          X(H)=(X(H)*100.)/((ALPHA(H).P.2.)*NUMBER(H)*SPEED(H))                      *278
          Y(H)=(Y(H)*100.)/((ALPHA(H).P.3.)*NUMBER(H)*SPEED(H))                      *279
          Q=1.                                                                       *280
          WHENEVER CONST8.L.(5.), TRANSFER TO RET13                                  *281
          WHENEVER Q.L.25., TRANSFER TO IN1                                          *282
OUT1      CONTINUE                                                                   *283
NOGO      CONTINUE                                                                   *284
RET13     CONTINUE                                                            DP     *285
          Q=100.                                                                     *286
          SUM=0.                                                              DP     *287
          PRINT FORMAT CHECK                                                         *288
          VECTOR VALUES CHECK=$2391TOTAL NUMBERS OF DROPS*$                          *289
          PRINT FORMAT CHECK2                                                        *290
          VECTOR VALUES CHECK2=$11HOSIZE RANGE,S21,9HNO. DROPS,S16,                  *291
         014HNO. INCLUSIONS*$                                                        *291
          THROUGH CHECK1, FOR I=1,1,I.G.M                                            *292
          PRINT FORMAT RES10, ENDPT(I),ENDPT(I+1),NUMBER(I),U(I,N)                   *293
CHECK1    CONTINUE                                                                   *294
          ADJUST=0.                                                                  *295
          THROUGH RET18, FOR J=1,1,J.G.N                                      DP     *296
          U(1,J)=0.                                                           DPK    *297
          THROUGH RET19, FOR I=1,1,I.G.M                                      DP     *298
          ADJUST=ADJUST + NIN(I,J)                                                   *299
          U(1,J)=NIN(I,J)*SPEED(I)/PHOTOS+U(1,J)                                     *300
RET19     CONTINUE                                                            DP     *301
          SUM=U(1,J)+SUM                                                      DPK    *302
RET18     CONTINUE                                                            DP     *303
          CUMPCT(0)=0.                                                        DP     *304
          THROUGH RET21, FOR J=1,1,J.G.N                                      DP     *305
          PCT(J)=100.*U(1,J)/SUM                                              DP     *306
RET21     CUMPCT(J)=PCT(J)+CUMPCT(J-1)                                        DP     *307
          PRINT FORMAT RES42                                                  DP     *308
          VECTOR VALUES RES42=$49H1CALCULATIONS FOR INCLUSIONS BASED ON       DP     *309
         0 WHOLE SPRAY*$                                                      DP     *309
          PRINT FORMAT RES38                                                  DPK    *310
          WHENEVER Q.G.75., TRANSFER TO IN2                                          *311
OUT2      CONTINUE                                                                   *312
          PRINT FORMAT RES25                                                         *313
          ADD3=0.                                                                    *314
          ADD4=0.                                                                    *315
          THROUGH RET22, FOR I=1,1,I.G.M                                             *316
          ADD3=(ALPHA(I).P.2.)*NUMBER(I)*SPEED(I)+ADD3                               *317
```

```
                ADD4=(ALPHA(I).P.3.)*NUMBER(I)*SPEED(I)+ADD4                    *318
RET22           CONTINUE                                                        *319
                PRINT FORMAT RES25                                              *320
                VECTOR VALUES RES25=$7141CALCULATION OF PERCENT OF SURFACE AN    *321
               OD VOLUME REPRESENTED BY INCLUSIONS*$                            *321
                PRINT FORMAT RES26                                              *322
                VECTOR VALUES RES26=$14HODROP DIAMETER,S14,21HPERCENT INCLUDE    *323
               OD AREA, S6,23HPERCENT INCLUDED VOLUME*$                         *323
                THROUGH CHECK3, FOR H=1,1,H.G.M                                 *324
                PRINT FORMAT RES27,ALP49(H),X(H),Y(H)                           *325
                VECTOR VALUES RES27=$1H ,F10.5,S10,E20.5, S7,E20.5*$            *326
CHECK3          CONTINUE                                                        *327
                ADD1=ADD1*100./ADD3                                             *328
                ADD2=ADD2*100./ADD4                                             *329
                PRINT FORMAT RES44,ADD1,ADD2                                    *330
                VECTOR VALUES RES44=$44H PERCENT SURFACE REPRESENTED BY INCLU    *331
               OSIONS =,F10.5/,43H PERCENT VOLUME REPRESENTED BY INCLUSIONS =   *331
               1,F10.5*$                                                        *331
END             CONTINUE                                                        *332
                TRANSFER TO START                          178DPK               *333
                END OF PROGRAM                             179DPK               *334

THE FOLLOWING NAMES HAVE OCCURRED ONLY ONCE IN THIS PROGRAM.
THEY WILL ALL BE ASSIGNED TO THE SAME LOCATION, AND
COMPILATION WILL CONTINUE.

      CHECK4
      CONST9
      DEPTH
      OUT7
      WIDTH
```

TABLE XII

INPUT VARIABLES FOR COMPUTER PROGRAM

HEIGHT - Dimension of camera field of view in the direction of spray flow.

WIDTH - Dimension of camera field of view normal to spray flow and normal to camera lens principal axis.

DEPTH - Dimension of camera field of view normal to spray flow and parallel to camera lens principal axis.

CONST1 - Arbitrary constant which can be used to change units in which spray drop velocity is printed out.

CONST2 - Control variable: calculations for inclusion conditional distributions are not calculated if total inclusions $\sum_{J=1}^{N} N,N(m,J) <$ CONST2 $(1 \leq m \leq M)$.

CONST3 - Control variable: for CONST3 $\geq$ 10, calculation and printing of weighted large drop distributions is suppressed.

CONST4 - Control variable: for CONST4 $\geq$ 10, calculation and printing of weighted inclusion conditional distributions are suppressed.

M - Number of large drop size ranges.

S - Highest moment of large drop distribution to be calculated.

T - Maximum number of moment ratios to be computed.

L - Control variable: for L = 0, no calculations involving inclusions are made.

DOGEM - Control variable: when DOGEM = 0, arithmetic means of diameter size intervals for large drops are used as D_i - for other values of DOGEM, geometric means are used.

TABLE XII

INPUT VARIABLES FOR COMPUTER PROGRAM (Continued)

ENDREM - Control variable: ENDREM controls the length of the remark statements REM1...REM5.

PHOTOS - The number of photos counted for the drop distribution data.

NUMBER(1)...(M) - Total number of large drops counted from the single exposure photos: $y_1 \ldots y_M$ in Figure 23.

DIST(1)...(M) - Distance traveled by the large drops in the respective size ranges, obtained from a plot such as Figure 22 - $\ell_1 \ldots \ell_M$ in Figure 23.

DELAY(1)...(M) - Time delay used: for this work, DELAY(1) = DELAY(2) = ... = DELAY(M).

ENDPT(1)...(M+1) - Endpoints of the large drop size ranges.

NUM(1)...(T) - Selected moments for numerator of moment ratios.

DEN(1)...(T) - Selected moments for denominator of moment ratios.

REM1(1)...(ENDREM)
REM2(1)...(ENDREM)
REM3(1)...(ENDREM)
REM4(1)...(ENDREM)
REM5(1)...(ENDREM)

} Remarks which may be printed out at various places in the output

DENSTY - Density of flowing phase.

CONST5 - Arbitrary constant used to adjust units on momentum for output.

CONST6 - Arbitrary constant used to adjust units on energy for output.

N - Number of inclusion diameter size ranges.

TABLE XII

INPUT VARIABLES FOR COMPUTER PROGRAM (Continued)

DOLOG - Control variable: for DOLOG not equal to zero, log (D_i) is substituted for D_i and log (d_j) for d_j.

MOMIN - The highest moment to be calculated for the inclusion conditional distributions.

NIN(1,1)...(M,N) - Total numbers of inclusions counted from the single flash photographs: $x_{11}...x_{MN}$ in Figure 23.

EDPTIN(1)...(N+1) - Endpoints for the inclusion size ranges.

NOZD - Nozzle diameter.

FLOW - Flow rate of sprayed phase.

GAMMA - Interfacial tension.

CONST7 - Arbitrary constant which may be used to rationalize units in Reynolds number.

CONST8 - Control variable: when CONST8 < .5, conditional distributions of inclusions are not calculated or printed.

CONST9 - Not used in program: eliminated in a revision.

TABLE XIII

COMPUTER INPUT DATA FOR RUN 10

HEIGHT = 1.2

WIDTH = .96

DEPTH = .10

CONST1 = 1.0

CONST2 = .50

CONST3 = 1.0

CONST4 = 100.

M = 12

S = 3

T = 4

L = 10

DOGEM = 0

ENDREM = 26

PHOTOS = 7.0

NUMBER(1)...(M) = $y_1 \ldots y_M$ in Table II

DIST(1)...(M) = $\ell_1 \ldots \ell_M$ in Table II

DELAY(1)...(M) = all values are 1.55×10^{-3}

ENDPT(1)...(M+1) = 0, 1×10^{-2}, 2×10^{-2} ... 12×10^{-2}

NUM(1)...(T) = 1, 2, 3, 3

DEN(1)...(T) = 0, 1, 1, 2

REM1(1)...(ENDREM) = RUN NUMBER
10 NO 19 HYPO, 130 CC/MIN
SEE RUNS 8, 9 CGS UNITS
SAT. CCl_4 INTO SAT. H_2O

REM2(1)...(ENDREM) = LENGTH = CENTIMETERS MASS = GRAMS TIME = SECONDS

REM3(1)...(ENDREM) = blank

REM4(1)...(ENDREM) = blank

REM5(1)...(ENDREM) = same as REM2

DENSITY = 1.595

CONST5 = 1.0

CONST6 = 1.0

N = 9

DOLOG = 0

MOMIN = 3

NIN(1,1)...(M,N) = see $x_{11} \ldots x_{MN}$ in Table II

TABLE XIII

COMPUTER INPUT DATA FOR RUN 10 (Continued)

EDPTIN(1)...(N+1) = 0, $.5 \times 10^{-2}$, 1.0×10^{-2}... 4.5×10^{-2}

NOZD = 6.42×10^{-2}

FLOW = 130.

GAMMA = 32.

VISC = 1.0

CONST7 = 1.0

CONST8 = 1000.

CONST9 = 1.0

RUN NUMBER 10 NO. 19 HYPO, 130 CC/MIN SEE RUNS 8, 9 CGS UNITS

SAT. CCL4 INTO SAT. H2O

NOZZLE DIAMETER = .64200E-01
FLOW RATE = .21700E 01
INTERFACIAL TENSION = .32000E 02
VISCOSITY = .10000E 01
REYNOLDS NUMBER = .68643E 02
WEBER NUMBER = .14380E 04
VELOCITY THROUGH NOZZLE = .67035E 03

THIS COMPUTATION USES ARITHMETIC MEANS

VELOCITY WEIGHTED PERCENTAGES
LENGTH = CENTIMETERS MASS = GRAMS TIME = SECONDS

SIZE RANGE		NUMBER	SPEED	PERCENT	CUMULATIVE PERCENT	PERCENT/SIZE RANGE
.00000 TO	.01000	193.0	11.29032	18.55260	18.55260	1855.25957
.01000 TO	.02000	304.0	13.54839	35.06729	53.61989	3506.72894
.02000 TO	.03000	140.0	15.80645	18.84098	72.46086	1884.09778
.03000 TO	.04000	63.0	18.06452	9.68965	82.15051	968.96461
.04000 TO	.05000	36.0	20.00000	6.13018	88.28069	613.01839
.05000 TO	.06000	15.0	21.93548	2.80143	91.08212	280.14283
.06000 TO	.07000	11.0	24.19355	2.26586	93.34798	226.58611
.07000 TO	.08000	11.0	26.45161	2.47734	95.82532	247.73415
.08000 TO	.09000	7.0	28.38710	1.69184	97.51717	169.18428
.09000 TO	.10000	4.0	30.64516	1.04367	98.56083	104.36694
.10000 TO	.11000	3.0	32.90323	.84043	99.40126	84.04285
.11000 TO	.12000	2.0	35.16129	.59874	100.00000	59.87366

PROBABILITY DENSITY AND DISTRIBUTION FUNCTIONS WEIGHTED BY 1TH POWER OF RANDOM VARIABLE

SIZE RANGE		PROBABILITY	CUMULATIVE PROBABILITY
.00000 TO	.01000	.03579	.03579
.01000 TO	.02000	.20294	.23872
.02000 TO	.03000	.18172	.42045
.03000 TO	.04000	.13084	.55128
.04000 TO	.05000	.10643	.65771
.05000 TO	.06000	.05944	.71715
.06000 TO	.07000	.05682	.77398
.07000 TO	.08000	.07168	.84566
.08000 TO	.09000	.05548	.90114
.09000 TO	.10000	.03825	.93939
.10000 TO	.11000	.03405	.97344
.11000 TO	.12000	.02656	1.00000

PROBABILITY DENSITY AND DISTRIBUTION FUNCTIONS WEIGHTED BY 2TH POWER OF RANDOM VARIABLE

SIZE RANGE		PROBABILITY	CUMULATIVE PROBABILITY
.00000 TO	.01000	.00403	.00403
.01000 TO	.02000	.06848	.07250
.02000 TO	.03000	.10220	.17470
.03000 TO	.04000	.10302	.27772
.04000 TO	.05000	.10774	.38545
.05000 TO	.06000	.07355	.45900
.06000 TO	.07000	.08309	.54209
.07000 TO	.08000	.12094	.66303
.08000 TO	.09000	.10609	.76911
.09000 TO	.10000	.08175	.85086
.10000 TO	.11000	.08042	.93128
.11000 TO	.12000	.06872	1.00000

PROBABILITY DENSITY AND DISTRIBUTION FUNCTIONS WEIGHTED BY 3TH POWER OF RANDOM VARIABLE

SIZE RANGE		PROBABILITY	CUMULATIVE PROBABILITY
.00000 TO	.01000	.00032	.00032
.01000 TO	.02000	.01612	.01644
.02000 TO	.03000	.04011	.05655
.03000 TO	.04000	.05660	.11315
.04000 TO	.05000	.07611	.18926
.05000 TO	.06000	.06350	.25276
.06000 TO	.07000	.08478	.33753
.07000 TO	.08000	.14239	.47992
.08000 TO	.09000	.14156	.62148
.09000 TO	.10000	.12191	.74339
.10000 TO	.11000	.13255	.87594
.11000 TO	.12000	.12406	1.00000

PROBABILITY DENSITY AND DISTRIBUTION FUNCTIONS WEIGHTED BY 4TH POWER OF RANDOM VARIABLE

SIZE RANGE		PROBABILITY	CUMULATIVE PROBABILITY
.00000 TO	.01000	.00002	.00002
.01000 TO	.02000	.00310	.00312
.02000 TO	.03000	.01283	.01595
.03000 TO	.04000	.02535	.04130
.04000 TO	.05000	.04383	.08514
.05000 TO	.06000	.04470	.12984
.06000 TO	.07000	.07053	.20036
.07000 TO	.08000	.13668	.33704
.08000 TO	.09000	.15400	.49104
.09000 TO	.10000	.14823	.63927
.10000 TO	.11000	.17813	.81740
.11000 TO	.12000	.18260	1.00000

MOMENTS OF WEIGHTED DISTRIBUTION

0TH MOMENT =	.10000E 01
1TH MOMENT =	.25920E-01
2TH MOMENT =	.11522E-02
3TH MOMENT =	.73399E-04
4TH MOMENT =	.57349E-05

MOMENT RATIOS

RATIO OF	1.00TH MOMENT TO	.00TH MOMENT =	.25920E-01
RATIO OF	2.00TH MOMENT TO	1.00TH MOMENT =	.44453E-01
RATIO OF	3.00TH MOMENT TO	1.00TH MOMENT =	.28318E-02
RATIO OF	3.00TH MOMENT TO	2.00TH MOMENT =	.63702E-01

COMPUTATION OF MEANS, VARIANCES, AND STD. DEVIATIONS

FOR THE RANDOM VARIABLE DIAMETER ON THE 0TH WEIGHTED DISTRIBUTION

MEAN = .25920E-01 VARIANCE = .48098E-03 STD. DEVIATION = .21931E-01

FOR THE RANDOM VARIABLE DIAMETER ON THE 1TH WEIGHTED DISTRIBUTION

MEAN = .44453E-01 VARIANCE = .85677E-03 STD. DEVIATION = .29271E-01

FOR THE RANDOM VARIABLE DIAMETER ON THE 2TH WEIGHTED DISTRIBUTION

MEAN = .63702E-01 VARIANCE = .92042E-03 STD. DEVIATION = .30338E-01

FOR THE RANDOM VARIABLE (DIAMETER TO THE POWER 0) ON THE NON-WEIGHTED DISTRIBUTION

MEAN = .10000E 01 VARIANCE = .00000E 00 STD. DEVIATION = .00000E 00

FOR THE RANDOM VARIABLE (DIAMETER TO THE POWER 1) ON THE NON-WEIGHTED DISTRIBUTION

MEAN = .25920E-01 VARIANCE = .48037E-03 STD. DEVIATION = .21917E-01

FOR THE RANDOM VARIABLE (DIAMETER TO THE POWER 2) ON THE NON-WEIGHTED DISTRIBUTION

MEAN = .11522E-02 VARIANCE = .44073E-05 STD. DEVIATION = .20993E-02

SURFACE AND VOLUME RATES

LENGTH = CENTIMETERS MASS = GRAMS TIME = SECONDS

DIAMETER	SURFACE RATE	VOLUME RATE
.50000E-02	.20374E-01	.16978E-04
.15000E-01	.34659E 00	.86647E-03
.25000E-01	.51726E 00	.21553E-02
.35000E-01	.52140E 00	.30415E-02
.45000E-01	.54529E 00	.40897E-02
.55000E-01	.37225E 00	.34123E-02
.65000E-01	.42052E 00	.45557E-02
.75000E-01	.61212E 00	.76515E-02
.85000E-01	.53694E 00	.76067E-02
.95000E-01	.41375E 00	.65511E-02
.10500E 00	.40701E 00	.71227E-02
.11500E 00	.34782E 00	.66666E-02

TOTAL RATES

SURFACE RATE = .50613E 01 VOLUME RATE = .53736E-01

MOMENTUM AND ENERGY TRANSFER RATES THROUGH SAMPLE SPACE
LENGTH = CENTIMETERS MASS = GRAMS TIME = SECONDS

DIAMETER	MOMENTUM	KINETIC ENERGY
.50000E-02	.32496E-04	.18345E-03
.15000E-01	.16584E-02	.11234E-01
.25000E-01	.41252E-02	.32602E-01
.35000E-01	.58215E-02	.52581E-01
.45000E-01	.78276E-02	.78276E-01
.55000E-01	.65311E-02	.71632E-01
.65000E-01	.87195E-02	.10548E 00
.75000E-01	.14645E-01	.19369E 00
.85000E-01	.14559E-01	.20665E 00
.95000E-01	.12539E-01	.19213E 00
.10500E 00	.13633E-01	.22428E 00
.11500E 00	.12760E-01	.22433E 00

TOTAL RATES
MOMENTUM = .10285E 00 KINETIC ENERGY = .13931E 01

CALCULATIONS FOR INCLUSIONS IN DROPS OF DIAMETER .50000E-02

INCLUSION DIAMETER	PERCENT	CUMULATIVE PERCENT

CALCULATIONS FOR INCLUSIONS IN DROPS OF DIAMETER .15000E-01

INCLUSION DIAMETER	PERCENT	CUMULATIVE PERCENT
.25000E-02	84.61538	84.61538
.75000E-02	15.38462	100.00000
.12500E-01	.00000	100.00000
.17500E-01	.00000	100.00000
.22500E-01	.00000	100.00000
.27500E-01	.00000	100.00000
.32500E-01	.00000	100.00000
.37500E-01	.00000	100.00000
.42500E-01	.00000	100.00000

MOMENTS OF WEIGHTED DISTRIBUTION

0TH MOMENT = .10000E 01
1TH MOMENT = .32692E-02
2TH MOMENT = .13942E-04
3TH MOMENT = .78125E-07
4TH MOMENT = .51983E-09

MOMENT RATIOS
RATIO OF 1.00TH MOMENT TO .00TH MOMENT = .32692E-02
RATIO OF 2.00TH MOMENT TO 1.00TH MOMENT = .42647E-02
RATIO OF 3.00TH MOMENT TO 1.00TH MOMENT = .23897E-04
RATIO OF 3.00TH MOMENT TO 2.00TH MOMENT = .56034E-02

COMPUTATION OF MEANS, VARIANCES, AND STD. DEVIATIONS

FOR THE RANDOM VARIABLE DIAMETER ON THE 0TH WEIGHTED DISTRIBUTION
MEAN = .32692E-02 VARIANCE = .35256E-05 STD. DEVIATION = .18777E-02
FOR THE RANDOM VARIABLE DIAMETER ON THE 1TH WEIGHTED DISTRIBUTION
MEAN = .42647E-02 VARIANCE = .61851E-05 STD. DEVIATION = .24870E-02
FOR THE RANDOM VARIABLE DIAMETER ON THE 2TH WEIGHTED DISTRIBUTION
MEAN = .56034E-02 VARIANCE = .63763E-05 STD. DEVIATION = .25251E-02
FOR THE RANDOM VARIABLE (DIAMETER TO THE POWER 0) ON THE NON-WEIGHTED DISTRIBUTION
MEAN = .10000E 01 VARIANCE = .00000E 00 STD. DEVIATION = .00000E 00
FOR THE RANDOM VARIABLE (DIAMETER TO THE POWER 1) ON THE NON-WEIGHTED DISTRIBUTION
MEAN = .32692E-02 VARIANCE = .32544E-05 STD. DEVIATION = .18040E-02
FOR THE RANDOM VARIABLE (DIAMETER TO THE POWER 2) ON THE NON-WEIGHTED DISTRIBUTION
MEAN = .13942E-04 VARIANCE = .32544E-09 STD. DEVIATION = .18040E-04

CALCULATIONS FOR INCLUSIONS IN DROPS OF DIAMETER .25000E-01

INCLUSION DIAMETER	PERCENT	CUMULATIVE PERCENT
.25000E-02	43.58974	43.58974
.75000E-02	35.89744	79.48718
.12500E-01	20.51282	100.00000
.17500E-01	.00000	100.00000
.22500E-01	.00000	100.00000
.27500E-01	.00000	100.00000
.32500E-01	.00000	100.00000
.37500E-01	.00000	100.00000
.42500E-01	.00000	100.00000

MOMENTS OF WEIGHTED DISTRIBUTION

0TH MOMENT = .10000E 01
1TH MOMENT = .63462E-02
2TH MOMENT = .54968E-04
3TH MOMENT = .55889E-06
4TH MOMENT = .61609E-08

MOMENT RATIOS
RATIO OF 1.00TH MOMENT TO .00TH MOMENT = .63462E-02
RATIO OF 2.00TH MOMENT TO 1.00TH MOMENT = .86616E-02
RATIO OF 3.00TH MOMENT TO 1.00TH MOMENT = .88068E-04
RATIO OF 3.00TH MOMENT TO 2.00TH MOMENT = .10168E-01

COMPUTATION OF MEANS, VARIANCES, AND STD. DEVIATIONS

FOR THE RANDOM VARIABLE DIAMETER ON THE 0TH WEIGHTED DISTRIBUTION
MEAN = .63462E-02 VARIANCE = .15081E-04 STD. DEVIATION = .38834E-02
FOR THE RANDOM VARIABLE DIAMETER ON THE 1TH WEIGHTED DISTRIBUTION
MEAN = .86616E-02 VARIANCE = .13388E-04 STD. DEVIATION = .36589E-02
FOR THE RANDOM VARIABLE DIAMETER ON THE 2TH WEIGHTED DISTRIBUTION
MEAN = .10168E-01 VARIANCE = .89290E-05 STD. DEVIATION = .29881E-02
FOR THE RANDOM VARIABLE (DIAMETER TO THE POWER 0) ON THE NON-WEIGHTED DISTRIBUTION
MEAN = .10000E 01 VARIANCE = .00000E 00 STD. DEVIATION = .00000E 00
FOR THE RANDOM VARIABLE (DIAMETER TO THE POWER 1) ON THE NON-WEIGHTED DISTRIBUTION
MEAN = .63462E-02 VARIANCE = .14694E-04 STD. DEVIATION = .38333E-02
FOR THE RANDOM VARIABLE (DIAMETER TO THE POWER 2) ON THE NON-WEIGHTED DISTRIBUTION
MEAN = .54968E-04 VARIANCE = .31394E-08 STD. DEVIATION = .56030E-04

CALCULATIONS FOR INCLUSIONS IN DROPS OF DIAMETER .35000E-01

INCLUSION DIAMETER	PERCENT	CUMULATIVE PERCENT
.25000E-02	13.15789	13.15789
.75000E-02	31.57895	44.73684
.12500E-01	34.21053	78.94737
.17500E-01	15.78947	94.73684
.22500E-01	5.26316	100.00000
.27500E-01	.00000	100.00000
.32500E-01	.00000	100.00000
.37500E-01	.00000	100.00000
.42500E-01	.00000	100.00000

MOMENTS OF WEIGHTED DISTRIBUTION

0TH MOMENT = .10000E 01
1TH MOMENT = .10921E-01
2TH MOMENT = .14704E-03
3TH MOMENT = .22492E-05
4TH MOMENT = .37654E-07

MOMENT RATIOS

RATIO OF 1.00TH MOMENT TO .00TH MOMENT = .10921E-01
RATIO OF 2.00TH MOMENT TO 1.00TH MOMENT = .13464E-01
RATIO OF 3.00TH MOMENT TO 1.00TH MOMENT = .20595E-03
RATIO OF 3.00TH MOMENT TO 2.00TH MOMENT = .15296E-01

COMPUTATION OF MEANS, VARIANCES, AND STD. DEVIATIONS

FOR THE RANDOM VARIABLE DIAMETER ON THE 0TH WEIGHTED DISTRIBUTION
MEAN = .10921E-01 VARIANCE = .28521E-04 STD. DEVIATION = .53405E-02
FOR THE RANDOM VARIABLE DIAMETER ON THE 1TH WEIGHTED DISTRIBUTION
MEAN = .13464E-01 VARIANCE = .25340E-04 STD. DEVIATION = .50339E-02
FOR THE RANDOM VARIABLE DIAMETER ON THE 2TH WEIGHTED DISTRIBUTION
MEAN = .15296E-01 VARIANCE = .22699E-04 STD. DEVIATION = .47643E-02
FOR THE RANDOM VARIABLE (DIAMETER TO THE POWER 0) ON THE NON-WEIGHTED DISTRIBUTION
MEAN = .10000E 01 VARIANCE = .00000E 00 STD. DEVIATION = .00000E 00
FOR THE RANDOM VARIABLE (DIAMETER TO THE POWER 1) ON THE NON-WEIGHTED DISTRIBUTION
MEAN = .10921E-01 VARIANCE = .27770E-04 STD. DEVIATION = .52697E-02
FOR THE RANDOM VARIABLE (DIAMETER TO THE POWER 2) ON THE NON-WEIGHTED DISTRIBUTION
MEAN = .14704E-03 VARIANCE = .16034E-07 STD. DEVIATION = .12662E-03

CALCULATIONS FOR INCLUSIONS IN DROPS OF DIAMETER .45000E-01

INCLUSION DIAMETER	PERCENT	CUMULATIVE PERCENT
.25000E-02	17.46032	17.46032
.75000E-02	14.28571	31.74603
.12500E-01	44.44444	76.19048
.17500E-01	9.52381	85.71428
.22500E-01	11.11111	96.82540
.27500E-01	1.58730	98.41270
.32500E-01	1.58730	100.00000
.37500E-01	.00000	100.00000
.42500E-01	.00000	100.00000

MOMENTS OF WEIGHTED DISTRIBUTION

0TH MOMENT =	.10000E 01
1TH MOMENT =	.12183E-01
2TH MOMENT =	.19276E-03
3TH MOMENT =	.35821E-05
4TH MOMENT =	.75505E-07

MOMENT RATIOS

RATIO OF 1.00TH MOMENT TO .00TH MOMENT =	.12183E-01
RATIO OF 2.00TH MOMENT TO 1.00TH MOMENT =	.15822E-01
RATIO OF 3.00TH MOMENT TO 1.00TH MOMENT =	.29404E-03
RATIO OF 3.00TH MOMENT TO 2.00TH MOMENT =	.18583E-01

COMPUTATION OF MEANS, VARIANCES, AND STD. DEVIATIONS

FOR THE RANDOM VARIABLE DIAMETER ON THE 0TH WEIGHTED DISTRIBUTION

MEAN = .12183E-01 VARIANCE = .45059E-04 STD. DEVIATION = .67126E-02

FOR THE RANDOM VARIABLE DIAMETER ON THE 1TH WEIGHTED DISTRIBUTION

MEAN = .15822E-01 VARIANCE = .44389E-04 STD. DEVIATION = .66625E-02

FOR THE RANDOM VARIABLE DIAMETER ON THE 2TH WEIGHTED DISTRIBUTION

MEAN = .18583E-01 VARIANCE = .47117E-04 STD. DEVIATION = .68642E-02

FOR THE RANDOM VARIABLE (DIAMETER TO THE POWER 0) ON THE NON-WEIGHTED DISTRIBUTION

MEAN = .10000E 01 VARIANCE = .00000E 00 STD. DEVIATION = .00000E 00

FOR THE RANDOM VARIABLE (DIAMETER TO THE POWER 1) ON THE NON-WEIGHTED DISTRIBUTION

MEAN = .12183E-01 VARIANCE = .44344E-04 STD. DEVIATION = .66591E-02

FOR THE RANDOM VARIABLE (DIAMETER TO THE POWER 2) ON THE NON-WEIGHTED DISTRIBUTION

MEAN = .19276E-03 VARIANCE = .38350E-07 STD. DEVIATION = .19583E-03

CALCULATIONS FOR INCLUSIONS IN DROPS OF DIAMETER .55000E-01

INCLUSION DIAMETER	PERCENT	CUMULATIVE PERCENT
.25000E-02	31.91489	31.91489
.75000E-02	27.65957	59.57447
.12500E-01	8.51064	68.08511
.17500E-01	12.76596	80.85106
.22500E-01	10.63830	91.48936
.27500E-01	2.12766	93.61702
.32500E-01	4.25532	97.87234
.37500E-01	.00000	97.87234
.42500E-01	2.12766	100.00000

MOMENTS OF WEIGHTED DISTRIBUTION

0TH MOMENT =	.10000E 01
1TH MOMENT =	.11436E-01
2TH MOMENT =	.22327E-03
3TH MOMENT =	.57204E-05
4TH MOMENT =	.17126E-06

MOMENT RATIOS

RATIO OF 1.00TH MOMENT TO .00TH MOMENT =	.11436E-01
RATIO OF 2.00TH MOMENT TO 1.00TH MOMENT =	.19523E-01
RATIO OF 3.00TH MOMENT TO 1.00TH MOMENT =	.50020E-03
RATIO OF 3.00TH MOMENT TO 2.00TH MOMENT =	.25621E-01

COMPUTATION OF MEANS, VARIANCES, AND STD. DEVIATIONS

FOR THE RANDOM VARIABLE DIAMETER ON THE 0TH WEIGHTED DISTRIBUTION
MEAN = .11436E-01 VARIANCE = .94496E-04 STD. DEVIATION = .97209E-02

FOR THE RANDOM VARIABLE DIAMETER ON THE 1TH WEIGHTED DISTRIBUTION
MEAN = .19523E-01 VARIANCE = .12163E-03 STD. DEVIATION = .11029E-01

FOR THE RANDOM VARIABLE DIAMETER ON THE 2TH WEIGHTED DISTRIBUTION
MEAN = .25621E-01 VARIANCE = .11303E-03 STD. DEVIATION = .10632E-01

FOR THE RANDOM VARIABLE (DIAMETER TO THE POWER 0) ON THE NON-WEIGHTED DISTRIBUTION
MEAN = .10000E 01 VARIANCE = .00000E 00 STD. DEVIATION = .00000E 00

FOR THE RANDOM VARIABLE (DIAMETER TO THE POWER 1) ON THE NON-WEIGHTED DISTRIBUTION
MEAN = .11436E-01 VARIANCE = .92485E-04 STD. DEVIATION = .96169E-02

FOR THE RANDOM VARIABLE (DIAMETER TO THE POWER 2) ON THE NON-WEIGHTED DISTRIBUTION
MEAN = .22327E-03 VARIANCE = .12141E-06 STD. DEVIATION = .34844E-03

CALCULATIONS FOR INCLUSIONS IN DROPS OF DIAMETER .65000E-01

INCLUSION DIAMETER	PERCENT	CUMULATIVE PERCENT
.25000E-02	25.00000	25.00000
.75000E-02	20.45455	45.45455
.12500E-01	34.09091	79.54545
.17500E-01	11.36364	90.90909
.22500E-01	2.27273	93.18182
.27500E-01	.00000	93.18182
.32500E-01	6.81818	100.00000
.37500E-01	.00000	100.00000
.42500E-01	.00000	100.00000

MOMENTS OF WEIGHTED DISTRIBUTION

0TH MOMENT = .10000E 01
1TH MOMENT = .11136E-01
2TH MOMENT = .18466E-03
3TH MOMENT = .39645E-05
4TH MOMENT = .10153E-06

MOMENT RATIOS
RATIO OF 1.00TH MOMENT TO .00TH MOMENT = .11136E-01
RATIO OF 2.00TH MOMENT TO 1.00TH MOMENT = .16582E-01
RATIO OF 3.00TH MOMENT TO 1.00TH MOMENT = .35599E-03
RATIO OF 3.00TH MOMENT TO 2.00TH MOMENT = .21469E-01

COMPUTATION OF MEANS, VARIANCES, AND STD. DEVIATIONS

FOR THE RANDOM VARIABLE DIAMETER ON THE 0TH WEIGHTED DISTRIBUTION
MEAN = .11136E-01 VARIANCE = .62051E-04 STD. DEVIATION = .78772E-02
FOR THE RANDOM VARIABLE DIAMETER ON THE 1TH WEIGHTED DISTRIBUTION
MEAN = .16582E-01 VARIANCE = .82929E-04 STD. DEVIATION = .91065E-02
FOR THE RANDOM VARIABLE DIAMETER ON THE 2TH WEIGHTED DISTRIBUTION
MEAN = .21469E-01 VARIANCE = .90966E-04 STD. DEVIATION = .95376E-02
FOR THE RANDOM VARIABLE (DIAMETER TO THE POWER 0) ON THE NON-WEIGHTED DISTRIBUTION
MEAN = .10000E 01 VARIANCE = .00000E 00 STD. DEVIATION = .00000E 00
FOR THE RANDOM VARIABLE (DIAMETER TO THE POWER 1) ON THE NON-WEIGHTED DISTRIBUTION
MEAN = .11136E-01 VARIANCE = .60640E-04 STD. DEVIATION = .77872E-02
FOR THE RANDOM VARIABLE (DIAMETER TO THE POWER 2) ON THE NON-WEIGHTED DISTRIBUTION
MEAN = .18466E-03 VARIANCE = .67432E-07 STD. DEVIATION = .25968E-03

CALCULATIONS FOR INCLUSIONS IN DROPS OF DIAMETER .75000E-01

INCLUSION DIAMETER	PERCENT	CUMULATIVE PERCENT
.25000E-02	26.92308	26.92308
.75000E-02	11.53846	38.46154
.12500E-01	32.69231	71.15385
.17500E-01	9.61538	80.76923
.22500E-01	9.61538	90.38461
.27500E-01	1.92308	92.30769
.32500E-01	3.84615	96.15385
.37500E-01	1.92308	98.07692
.42500E-01	1.92308	100.00000

MOMENTS OF WEIGHTED DISTRIBUTION

0TH MOMENT = .10000E 01
1TH MOMENT = .12788E-01
2TH MOMENT = .25433E-03
3TH MOMENT = .65126E-05
4TH MOMENT = .19670E-06

MOMENT RATIOS
RATIO OF 1.00TH MOMENT TO .00TH MOMENT = .12788E-01
RATIO OF 2.00TH MOMENT TO 1.00TH MOMENT = .19887E-01
RATIO OF 3.00TH MOMENT TO 1.00TH MOMENT = .50926E-03
RATIO OF 3.00TH MOMENT TO 2.00TH MOMENT = .25607E-01

COMPUTATION OF MEANS, VARIANCES, AND STD. DEVIATIONS

FOR THE RANDOM VARIABLE DIAMETER ON THE 0TH WEIGHTED DISTRIBUTION
MEAN = .12788E-01 VARIANCE = .92562E-04 STD. DEVIATION = .96209E-02
FOR THE RANDOM VARIABLE DIAMETER ON THE 1TH WEIGHTED DISTRIBUTION
MEAN = .19887E-01 VARIANCE = .11599E-03 STD. DEVIATION = .10770E-01
FOR THE RANDOM VARIABLE DIAMETER ON THE 2TH WEIGHTED DISTRIBUTION
MEAN = .25607E-01 VARIANCE = .11998E-03 STD. DEVIATION = .10954E-01
FOR THE RANDOM VARIABLE (DIAMETER TO THE POWER 0) ON THE NON-WEIGHTED DISTRIBUTION
MEAN = .10000E 01 VARIANCE = .00000E 00 STD. DEVIATION = .00000E 00
FOR THE RANDOM VARIABLE (DIAMETER TO THE POWER 1) ON THE NON-WEIGHTED DISTRIBUTION
MEAN = .12788E-01 VARIANCE = .90782E-04 STD. DEVIATION = .95280E-02
FOR THE RANDOM VARIABLE (DIAMETER TO THE POWER 2) ON THE NON-WEIGHTED DISTRIBUTION
MEAN = .25433E-03 VARIANCE = .13202E-06 STD. DEVIATION = .36334E-03

CALCULATIONS FOR INCLUSIONS IN DROPS OF DIAMETER .85000E-01

INCLUSION DIAMETER	PERCENT	CUMULATIVE PERCENT
.25000E-02	7.54717	7.54717
.75000E-02	5.66038	13.20755
.12500E-01	41.50943	54.71698
.17500E-01	18.86792	73.58491
.22500E-01	22.64151	96.22641
.27500E-01	.00000	96.22641
.32500E-01	3.77358	100.00000
.37500E-01	.00000	100.00000
.42500E-01	.00000	100.00000

MOMENTS OF WEIGHTED DISTRIBUTION

0TH MOMENT = .10000E 01
1TH MOMENT = .15425E-01
2TH MOMENT = .28078E-03
3TH MOMENT = .57214E-05
4TH MOMENT = .12814E-06

MOMENT RATIOS
RATIO OF 1.00TH MOMENT TO .00TH MOMENT = .15425E-01
RATIO OF 2.00TH MOMENT TO 1.00TH MOMENT = .18203E-01
RATIO OF 3.00TH MOMENT TO 1.00TH MOMENT = .37093E-03
RATIO OF 3.00TH MOMENT TO 2.00TH MOMENT = .20377E-01

COMPUTATION OF MEANS, VARIANCES, AND STD. DEVIATIONS

FOR THE RANDOM VARIABLE DIAMETER ON THE 0TH WEIGHTED DISTRIBUTION
MEAN = .15425E-01 VARIANCE = .43686E-04 STD. DEVIATION = .66096E-02
FOR THE RANDOM VARIABLE DIAMETER ON THE 1TH WEIGHTED DISTRIBUTION
MEAN = .18203E-01 VARIANCE = .40327E-04 STD. DEVIATION = .63504E-02
FOR THE RANDOM VARIABLE DIAMETER ON THE 2TH WEIGHTED DISTRIBUTION
MEAN = .20377E-01 VARIANCE = .41948E-04 STD. DEVIATION = .64767E-02
FOR THE RANDOM VARIABLE (DIAMETER TO THE POWER 0) ON THE NON-WEIGHTED DISTRIBUTION
MEAN = .10000E 01 VARIANCE = .00000E 00 STD. DEVIATION = .00000E 00
FOR THE RANDOM VARIABLE (DIAMETER TO THE POWER 1) ON THE NON-WEIGHTED DISTRIBUTION
MEAN = .15425E-01 VARIANCE = .42862E-04 STD. DEVIATION = .65469E-02
FOR THE RANDOM VARIABLE (DIAMETER TO THE POWER 2) ON THE NON-WEIGHTED DISTRIBUTION
MEAN = .28078E-03 VARIANCE = .49304E-07 STD. DEVIATION = .22205E-03

CALCULATIONS FOR INCLUSIONS IN DROPS OF DIAMETER .95000E-01

INCLUSION DIAMETER	PERCENT	CUMULATIVE PERCENT
.25000E-02	15.15152	15.15152
.75000E-02	27.27273	42.42424
.12500E-01	18.18182	60.60606
.17500E-01	15.15152	75.75758
.22500E-01	12.12121	87.87879
.27500E-01	6.06061	93.93939
.32500E-01	3.03030	96.96970
.37500E-01	.00000	96.96970
.42500E-01	3.03030	100.00000

MOMENTS OF WEIGHTED DISTRIBUTION

0TH MOMENT =	.10000E 01
1TH MOMENT =	.14015E-01
2TH MOMENT =	.28504E-03
3TH MOMENT =	.72921E-05
4TH MOMENT =	.21792E-06

MOMENT RATIOS

RATIO OF	1.00TH MOMENT TO	.00TH MOMENT =	.14015E-01
RATIO OF	2.00TH MOMENT TO	1.00TH MOMENT =	.20338E-01
RATIO OF	3.00TH MOMENT TO	1.00TH MOMENT =	.52030E-03
RATIO OF	3.00TH MOMENT TO	2.00TH MOMENT =	.25583E-01

COMPUTATION OF MEANS, VARIANCES, AND STD. DEVIATIONS

FOR THE RANDOM VARIABLE DIAMETER ON THE 0TH WEIGHTED DISTRIBUTION		
MEAN = .14015E-01	VARIANCE = .91383E-04	STD. DEVIATION = .95594E-02
FOR THE RANDOM VARIABLE DIAMETER ON THE 1TH WEIGHTED DISTRIBUTION		
MEAN = .20338E-01	VARIANCE = .11001E-03	STD. DEVIATION = .10489E-01
FOR THE RANDOM VARIABLE DIAMETER ON THE 2TH WEIGHTED DISTRIBUTION		
MEAN = .25583E-01	VARIANCE = .11347E-03	STD. DEVIATION = .10652E-01
FOR THE RANDOM VARIABLE (DIAMETER TO THE POWER 0) ON THE NON-WEIGHTED DISTRIBUTION		
MEAN = .10000E 01	VARIANCE = .00000E 00	STD. DEVIATION = .00000E 00
FOR THE RANDOM VARIABLE (DIAMETER TO THE POWER 1) ON THE NON-WEIGHTED DISTRIBUTION		
MEAN = .14015E-01	VARIANCE = .88613E-04	STD. DEVIATION = .94135E-02
FOR THE RANDOM VARIABLE (DIAMETER TO THE POWER 2) ON THE NON-WEIGHTED DISTRIBUTION		
MEAN = .28504E-03	VARIANCE = .13667E-06	STD. DEVIATION = .36969E-03

CALCULATIONS FOR INCLUSIONS IN DROPS OF DIAMETER .10500E 00

INCLUSION DIAMETER	PERCENT	CUMULATIVE PERCENT
.25000E-02	.00000	.00000
.75000E-02	.00000	.00000
.12500E-01	30.00000	30.00000
.17500E-01	55.00000	85.00000
.22500E-01	.00000	85.00000
.27500E-01	5.00000	90.00000
.32500E-01	5.00000	95.00000
.37500E-01	.00000	95.00000
.42500E-01	5.00000	100.00000

MOMENTS OF WEIGHTED DISTRIBUTION

0TH MOMENT =	.10000E 01
1TH MOMENT =	.18500E-01
2TH MOMENT =	.39625E-03
3TH MOMENT =	.10128E-04
4TH MOMENT =	.30641E-06

MOMENT RATIOS

RATIO OF	1.00TH MOMENT TO	.00TH MOMENT =	.18500E-01
RATIO OF	2.00TH MOMENT TO	1.00TH MOMENT =	.21419E-01
RATIO OF	3.00TH MOMENT TO	1.00TH MOMENT =	.54747E-03
RATIO OF	3.00TH MOMENT TO	2.00TH MOMENT =	.25560E-01

COMPUTATION OF MEANS, VARIANCES, AND STD. DEVIATIONS

FOR THE RANDOM VARIABLE DIAMETER ON THE 0TH WEIGHTED DISTRIBUTION
MEAN = .18500E-01 VARIANCE = .56842E-04 STD. DEVIATION = .75394E-02
FOR THE RANDOM VARIABLE DIAMETER ON THE 1TH WEIGHTED DISTRIBUTION
MEAN = .21419E-01 VARIANCE = .93364E-04 STD. DEVIATION = .96625E-02
FOR THE RANDOM VARIABLE DIAMETER ON THE 2TH WEIGHTED DISTRIBUTION
MEAN = .25560E-01 VARIANCE = .12629E-03 STD. DEVIATION = .11238E-01
FOR THE RANDOM VARIABLE (DIAMETER TO THE POWER 0) ON THE NON-WEIGHTED DISTRIBUTION
MEAN = .10000E 01 VARIANCE = .00000E 00 STD. DEVIATION = .00000E 00
FOR THE RANDOM VARIABLE (DIAMETER TO THE POWER 1) ON THE NON-WEIGHTED DISTRIBUTION
MEAN = .18500E-01 VARIANCE = .54000E-04 STD. DEVIATION = .73485E-02
FOR THE RANDOM VARIABLE (DIAMETER TO THE POWER 2) ON THE NON-WEIGHTED DISTRIBUTION
MEAN = .39625E-03 VARIANCE = .14940E-06 STD. DEVIATION = .38652E-03

CALCULATIONS FOR INCLUSIONS IN DROPS OF DIAMETER .11500E 00

INCLUSION DIAMETER	PERCENT	CUMULATIVE PERCENT
.25000E-02	.00000	.00000
.75000E-02	6.66667	6.66667
.12500E-01	53.33333	60.00000
.17500E-01	26.66667	86.66667
.22500E-01	.00000	86.66667
.27500E-01	.00000	86.66667
.32500E-01	13.33333	100.00000
.37500E-01	.00000	100.00000
.42500E-01	.00000	100.00000

MOMENTS OF WEIGHTED DISTRIBUTION

0TH MOMENT = .10000E 01
1TH MOMENT = .16167E-01
2TH MOMENT = .30958E-03
3TH MOMENT = .70760E-05
4TH MOMENT = .18700E-06

MOMENT RATIOS
RATIO OF 1.00TH MOMENT TO .00TH MOMENT = .16167E-01
RATIO OF 2.00TH MOMENT TO 1.00TH MOMENT = .19149E-01
RATIO OF 3.00TH MOMENT TO 1.00TH MOMENT = .43769E-03
RATIO OF 3.00TH MOMENT TO 2.00TH MOMENT = .22857E-01

COMPUTATION OF MEANS, VARIANCES, AND STD. DEVIATIONS

FOR THE RANDOM VARIABLE DIAMETER ON THE 0TH WEIGHTED DISTRIBUTION
MEAN = .16167E-01 VARIANCE = .51667E-04 STD. DEVIATION = .71880E-02
FOR THE RANDOM VARIABLE DIAMETER ON THE 1TH WEIGHTED DISTRIBUTION
MEAN = .19149E-01 VARIANCE = .76061E-04 STD. DEVIATION = .87213E-02
FOR THE RANDOM VARIABLE DIAMETER ON THE 2TH WEIGHTED DISTRIBUTION
MEAN = .22857E-01 VARIANCE = .87431E-04 STD. DEVIATION = .93505E-02
FOR THE RANDOM VARIABLE (DIAMETER TO THE POWER 0) ON THE NON-WEIGHTED DISTRIBUTION
MEAN = .10000E 01 VARIANCE = .00000E 00 STD. DEVIATION = .00000E 00
FOR THE RANDOM VARIABLE (DIAMETER TO THE POWER 1) ON THE NON-WEIGHTED DISTRIBUTION
MEAN = .16167E-01 VARIANCE = .48222E-04 STD. DEVIATION = .69442E-02
FOR THE RANDOM VARIABLE (DIAMETER TO THE POWER 2) ON THE NON-WEIGHTED DISTRIBUTION
MEAN = .30958E-03 VARIANCE = .91156E-07 STD. DEVIATION = .30192E-03

TOTAL NUMBERS OF DROPS

SIZE RANGE		NO. DROPS	NO. INCLUSIONS
.00000 TO	.01000	193.00000	.00000
.01000 TO	.02000	304.00000	13.00000
.02000 TO	.03000	140.00000	39.00000
.03000 TO	.04000	63.00000	38.00000
.04000 TO	.05000	36.00000	63.00000
.05000 TO	.06000	15.00000	47.00000
.06000 TO	.07000	11.00000	44.00000
.07000 TO	.08000	11.00000	52.00000
.08000 TO	.09000	7.00000	53.00000
.09000 TO	.10000	4.00000	33.00000
.10000 TO	.11000	3.00000	20.00000
.11000 TO	.12000	2.00000	15.00000

CALCULATIONS FOR INCLUSIONS BASED ON WHOLE SPRAY

INCLUSION DIAMETER	PERCENT	CUMULATIVE PERCENT
.25000E-02	19.77868	19.77868
.75000E-02	17.18145	36.96013
.12500E-01	31.36534	68.32547
.17500E-01	15.66802	83.99349
.22500E-01	9.13588	93.12938
.27500E-01	1.64036	94.76973
.32500E-01	3.83401	98.60374
.37500E-01	.26688	98.87063
.42500E-01	1.12937	100.00000

MOMENTS OF WEIGHTED DISTRIBUTION

0TH MOMENT = .10000E 01
1TH MOMENT = .12778E-01
2TH MOMENT = .23120E-03
3TH MOMENT = .52335E-05
4TH MOMENT = .14060E-06

MOMENT RATIOS
RATIO OF 1.00TH MOMENT TO .00TH MOMENT = .12778E-01
RATIO OF 2.00TH MOMENT TO 1.00TH MOMENT = .18093E-01
RATIO OF 3.00TH MOMENT TO 1.00TH MOMENT = .40956E-03
RATIO OF 3.00TH MOMENT TO 2.00TH MOMENT = .22637E-01

COMPUTATION OF MEANS, VARIANCES, AND STD. DEVIATIONS

FOR THE RANDOM VARIABLE DIAMETER ON THE 0TH WEIGHTED DISTRIBUTION
MEAN = .12778E-01 VARIANCE = .68072E-04 STD. DEVIATION = .82506E-02
FOR THE RANDOM VARIABLE DIAMETER ON THE 1TH WEIGHTED DISTRIBUTION
MEAN = .18093E-01 VARIANCE = .82408E-04 STD. DEVIATION = .90779E-02
FOR THE RANDOM VARIABLE DIAMETER ON THE 2TH WEIGHTED DISTRIBUTION
MEAN = .22637E-01 VARIANCE = .95945E-04 STD. DEVIATION = .97952E-02
FOR THE RANDOM VARIABLE (DIAMETER TO THE POWER 0) ON THE NON-WEIGHTED DISTRIBUTION
MEAN = .10000E 01 VARIANCE = .00000E 00 STD. DEVIATION = .00000E 00
FOR THE RANDOM VARIABLE (DIAMETER TO THE POWER 1) ON THE NON-WEIGHTED DISTRIBUTION
MEAN = .12778E-01 VARIANCE = .67909E-04 STD. DEVIATION = .82407E-02
FOR THE RANDOM VARIABLE (DIAMETER TO THE POWER 2) ON THE NON-WEIGHTED DISTRIBUTION
MEAN = .23120E-03 VARIANCE = .87146E-07 STD. DEVIATION = .29521E-03

CALCULATION OF PERCENT OF SURFACE AND VOLUME REPRESENTED BY INCLUSIONS

DROP DIAMETER	PERCENT INCLUDED AREA	PERCENT INCLUDED VOLUME
.00500	.18345E-03	.32496E-04
.01500	.26499E 00	.98989E-01
.02500	.24500E 01	.99643E 00
.03500	.72400E 01	.31642E 01
.04500	.16658E 02	.68792E 01
.05500	.23127E 02	.10773E 02
.06500	.17483E 02	.57744E 01
.07500	.21374E 02	.72976E 01
.08500	.29424E 02	.70538E 01
.09500	.26056E 02	.70168E 01
.10500	.23961E 02	.58327E 01
.11500	.17557E 02	.34895E 01

PERCENT SURFACE REPRESENTED BY INCLUSIONS = 16.93234
PERCENT VOLUME REPRESENTED BY INCLUSIONS = 6.01691

In the velocity weighted percentages, number is from input data. For the mth size range:

$$\text{Speed}(m) = \frac{[\text{DISTANCE}(m)]\,[\text{CONST1}]}{\text{DELAY}(m)} \qquad (B.4)$$

Percent for the mth size range is figured as:

$$\text{Percent}(m) = \frac{100.\,[\text{NUMBER}(m)]\,[\text{SPEED}(m)]}{\sum_{I=1}^{M} [\text{NUMBER}(I)]\,[\text{SPEED}(I)]} \qquad (B.5)$$

and, for the mth size range, cumulative percent is:

$$\text{Cumulative Percent}(m) = \sum_{I=1}^{M} \text{PERCENT}(I) \qquad (B.6)$$

Percent per size range is:

$$\text{Percent/Size Range}\ (m) = \frac{\text{PERCENT}(m)}{\text{ENDPT}(m+1) - \text{ENDPT}(m)} \qquad (B.7)$$

The probability density and distribution functions represent various weightings of the velocity weighted distribution by the indicated powers of the mean diameter of the size range. For the mth size range in the density (probability) function weighted by the Rth power of the mean diameter, D_m, of that size range:

$$P_R(m) = \frac{(D_m)^R\ \text{PERCENT}(m)}{\sum_{I=1}^{M} (D_I)^R\ \text{PERCENT}(I)} \qquad (B.8)$$

and:

$$\text{CUMULATIVE PROBABILITY}\ (m) = \sum_{I=1}^{M} P_R(I) \qquad (B.9)$$

The moments of the weighted distribution are calculated as, for the Rth moment:

$$\text{MOMENT}(R) = \frac{1}{100.} \sum_{I=1}^{M} [D_I]^R \text{PERCENT}(I) \qquad \text{(B.10)}$$

Moment ratios are self-explanatory.

Means, variances, and standard deviations are calculated for the Rth weighted distribution as:

$$\text{Mean} = \frac{\text{Moment } (R + 1)}{\text{Moment } (R)} \qquad \text{(B.11)}$$

$$\text{Variance} = \left[\frac{\text{MOMENT}(R+2)}{\text{MOMENT}(R)} - \left(\frac{\text{MOMENT}(R+1)}{\text{MOMENT}(R)}\right)^2\right]\left[\frac{\sum_{I=1}^{M} \text{NUMBER}(I)}{\left(\sum_{I=1}^{M} \text{NUMBER}(I)\right) - 1.}\right] \qquad \text{(B.12)}$$

$$\text{Standard Deviation} = (\text{Variance})^{1/2} \qquad \text{(B.13)}$$

For the mean of the variable diameter to the power R on the non-weighted distribution, we have:

$$\text{Mean} = \text{Moment } (R) \qquad \text{(B.14)}$$

$$\text{Variance} = \left[\text{Moment } (2R) - \left[\text{Moment } (R)\right]^2\right]\left[\frac{\sum_{I=1}^{M} \text{NUMBER}(I)}{\left(\sum_{I=1}^{M} \text{NUMBER}(I)\right) - 1.}\right] \qquad \text{(B.15)}$$

It should be noted that whenever the variance = 0., the computer sometimes will retain a very small negative number instead. This is always replaced automatically by a value of 10^{-6} for the variance to avoid stopping the machine by attempting to take the square root of a negative number in computing the standard deviation.

Surface and volume rates are calculated as, for the mth size range (Note D_m comprises the diameter column):

$$\text{Surface}(m) = \frac{(3.14159)(D_m)^2[\text{SPEED}(m)][\text{NUMBER}(m)]}{(\text{PHOTOS})(\text{HEIGTH})} \qquad \text{(B.16)}$$

and

$$\text{Volume}(m) = \frac{(3.14159)(D_m)^3[\text{SPEED}(m)][\text{NUMBER}(m)]}{(6.)(\text{PHOTOS})(\text{HEIGTH})} \qquad \text{(B.17)}$$

and the total rates are simply:

$$\text{Total Surface} = \sum_{I=1}^{M} \text{Surface}(I) \qquad \text{(B.18)}$$

$$\text{Total Volume} = \sum_{I=1}^{M} \text{Volume}(I) \qquad \text{(B.19)}$$

Note these represent the total volume and surface of the large drops passing through the camera field per unit time without regard to the inclusions.

Similarly, the momentum and energy (kinetic energy) transfer rates are calculated without regard to the inclusions as:

$$\text{Momentum}(m) = \frac{(3.14159)(D_m)^3(\text{DENSTY})(\text{CONST5})[\text{NUMBER}(m)][\text{SPEED}(m)]}{(6.)(\text{PHOTOS})} \qquad \text{(B.20)}$$

$$\text{Energy}(m) = \frac{[\text{MOMENTUM}(m)][\text{SPEED}(m)][\text{CONST6}]}{(2.)} \qquad \text{(B.21)}$$

and for the total rates:

$$\text{Total Momentum} = \sum_{I=1}^{M} \text{Momentum}(I) \qquad \text{(B.22)}$$

$$\text{Total Energy} = \sum_{I=1}^{M} \text{Energy}(I) \qquad \text{(B.23)}$$

Now, for the inclusions in the mth size class of large drops, i.e., drops with mean diameter D_m, we have for the nth inclusion diameter:

$$d_n = \frac{EDPTIN(n+1)+EDPTIN(n)}{2} \qquad (1 \leq n \leq N) \tag{B.24}$$

and as in the calculation for the large drop distribution:

$$PERCENT(n) = \frac{[100.][NIN(m,n)]}{\sum_{J=1}^{N} NIN(m,J)} \tag{B.25}$$

$$CUMULATIVE\ PERCENT(n) = \sum_{J=1}^{n} PERCENT(J) \tag{B.26}$$

Although space does not permit the inclusion of the weighted conditional inclusion distributions, the program will also figure these in a fashion similar to that for the large drop distribution; e.g., for the nth inclusion range in the mth large drop range, we have for the Rth weighted distribution:

$$P_R(n) = \frac{[d_n]^R [PERCENT(n)]}{\sum_{J=1}^{N} [d_J]^R [PERCENT(J)]} \tag{B.27}$$

and

$$\text{Cumulative Probability}(n) = \sum_{J=1}^{n} P_R(J) \tag{B.28}$$

Again, as for the distribution of large drops, the Rth moment:

$$MOMENT(R) = \frac{1}{100} \sum_{J=1}^{N} (d_J)^R [PERCENT(J)] \tag{B.29}$$

Note that in the above we have used PERCENT (n), and for the large drops we spoke of PERCENT (m). For inclusions, PERCENT (n) is

defined in Equation (B.25); for large drops, PERCENT (m) is defined in Equation (B.5).

Moment ratios, means, variances, and standard deviations are calculated as for the large drop distribution, except the last factor in the variance becomes:

$$\left[\frac{\sum_{J=1}^{N} NIN(m,J)}{\left[\sum_{J=1}^{N} NIN(m,J)\right] - 1.} \right] \qquad \text{(B.30)}$$

Note that whenever there are no inclusions in a given large drop class, the computations are skipped to save computer time.

Total numbers of drops are tabulated by large drop diameter D_i. For the mth size class:

$$\text{No Drops} = \text{Number (m)} \qquad \text{(B.31)}$$

$$\text{No Inclusions} = \sum_{J=1}^{N} NIN(m,J) \qquad \text{(B.32)}$$

In the calculations for inclusions based on the whole spray, we must weight the inclusions by the velocity of the large drop which contains them. Therefore, in these calculations, for the nth size class of inclusions, of diameter d_n:

$$PERCENT(n) = \frac{(100.)\sum_{I=1}^{M}[SPEED(I)][NIN(I,n)]}{\sum_{I=1}^{M}\sum_{J=1}^{N}[SPEED(I)][NIN(I,J)]} \qquad \text{(B.33)}$$

$$CUMULATIVE\ PERCENT(n) = \sum_{J=1}^{N} PERCENT(J) \qquad \text{(B.34)}$$

Again, there are no weightings of the marginal distribution shown; however, the calculations can be done using this program as they could for the conditional distributions. Calculation of moments, moment ratios, means, variances, and standard deviations is the same as for the conditional distributions, except the last factor in the variance becomes:

$$\left[\frac{\sum_{I=1}^{M} \sum_{J=1}^{N} NIN(I,J)}{\left[\sum_{I=1}^{M} \sum_{J=1}^{N} NIN(I,J) \right] - 1.} \right] \qquad (B.35)$$

Percent surface and volume represented by inclusions is classified by large drop diameter, D_i, and is calculated, for the mth size class, as:

$$\%_o \text{ AREA } (m) = \frac{(100.) \sum_{J=1}^{N} [NIN(m,J)][d_J]^2}{[NUMBER(m)][D_m]^2} \qquad (B.36)$$

$$\%_o \text{ VOLUME } (m) = \frac{(100.) \sum_{J=1}^{N} [NIN(m,J)][d_J]^3}{[NUMBER(m)][D_m]^3} \qquad (B.37)$$

and for the overall spray (last two lines of output):

$$\text{OVERALL } \%_o \text{ AREA} = \frac{(100.) \sum_{I=1}^{M} \sum_{J=1}^{N} [SPEED(I)][NIN(I,J)][d_J]^2}{\sum_{I=1}^{M} [SPEED(I)][NUMBER(I)][D_I]^2} \qquad (B.38)$$

$$\text{OVERALL } \%_o \text{ VOLUME} = \frac{(100.) \sum_{I=1}^{M} \sum_{J=1}^{N} [SPEED(I)][NIN(I,J)][d_J]^3}{\sum_{I=1}^{M} [SPEED(I)][NUMBER(I)][D_I]^3} \qquad (B.39)$$

APPENDIX C

EQUIPMENT CALIBRATIONS

C.1. Rotameter Calibrations

Shown in Figures 59 and 60 are the calibration curves for the Manostat Corporation FM1043T Flowmeter used to measure flow rate of the dispersed phase through the orifice. Flow rate was measured by measurement of the flow of displacing nitrogen, and curves are presented for nitrogen pressures (measured on upstream side of rotameter) of 34.7 psia. and 49.9" mercury absolute.

Calibration curves were drawn from volume-time measurements with a fluid actually flowing from the liquid reservoir. The timing device used was a Hewlitt-Packard counter with an accuracy of .001 second, and samples of the liquid were collected in a graduated cylinder in such quantity as to reduce both time and volume measurement errors to less than 1%. Readings were reproducible, and the presence of two different floats permits averaging the two readings (when both are on scale) while using the calibration curves.

It is possible to make a mathematical prediction of the calibration using a "Predictability Chart" which is supplied by the manufacturer. The values calculated with the aid of this chart for the 34.7 psia pressure are shown in Table XV. Although the agreement is good, the calculated curve falls somewhat above the measured points, and so the measured calibration, since it was representative of actual conditions, was the one used in all cases.

C.2. Calibration of Tensiometer

The tensiometer used in this research was of the DuNouy type, manufactured by the Central Scientific Company, and bore the serial

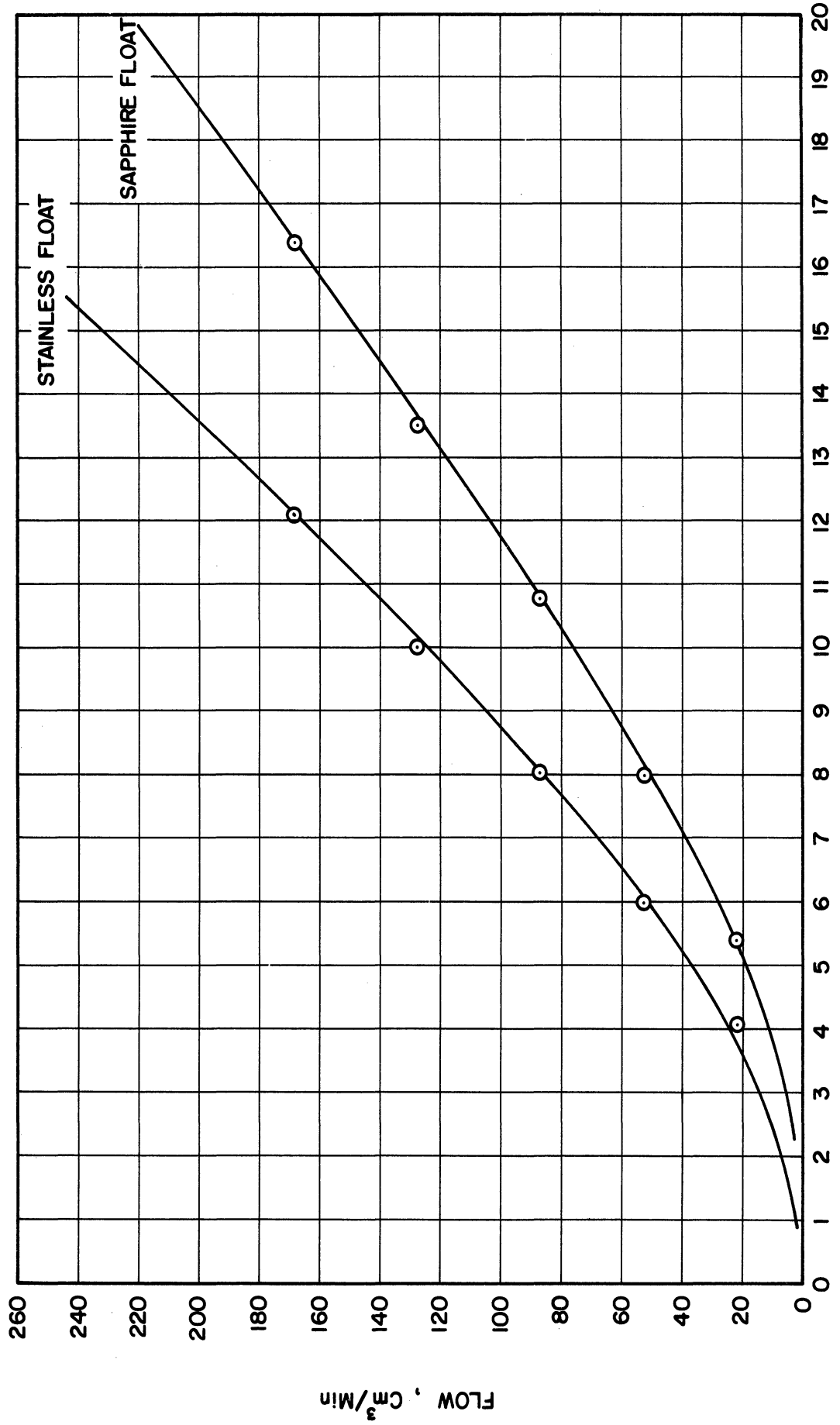

Figure 59. Calibration of 1043B Rotameter at 32.7 Psia.

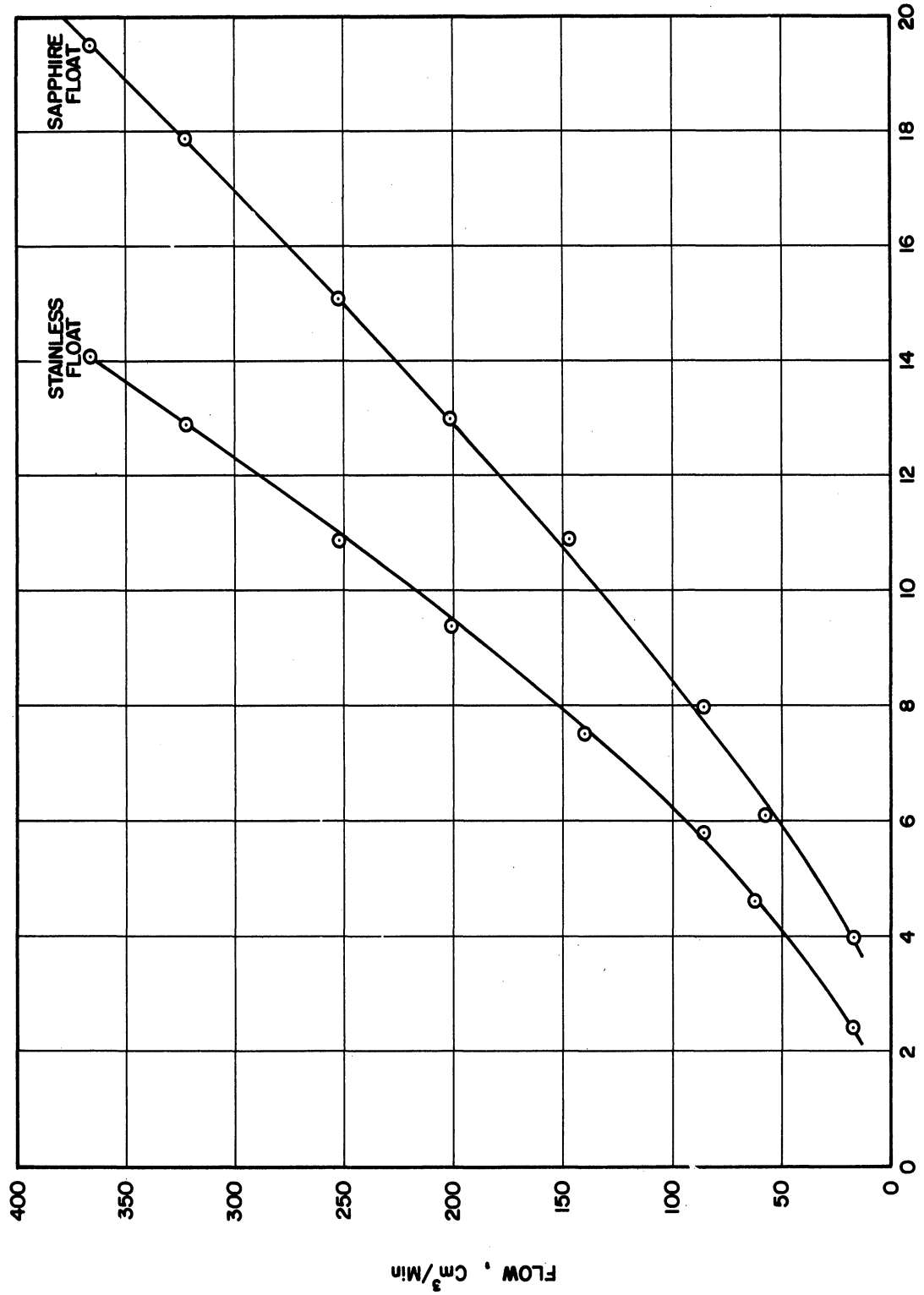

Figure 60. Calibration of 1043B Rotameter at 49.9" Hg Absolute.

TABLE XV

CALCULATED CALIBRATION CURVE FOR ROTAMETER TYPE FM1043T WITH NITROGEN FLOWING AT 70°F AND 34.7 PSIA

Scale Reading	Flow Rate - ml./min. @ 70°F, 34.7 Psia Stainless St. Float	Sapphire Float
1	3.52	1.79
2	7.95	4.04
3	15.4	7.6
4	26.3	13.2
5	41.6	21.1
6	60.6	32.4
7	78.4	42.7
8	99.0	56.6
10	137.0	83.8
12	173.0	110.0
14	222.0	142.0
16	269.0	170.0
18	318.0	181.0
20	359.0	251.0

number C7-8 of the Department of Chemical and Metallurgical Engineering Department of the University of Michigan. The platinum ring used with the tensiometer had a circumference of 5.998 cm., and was also manufactured by the Central Scientific Company. Company catalog number on the interfacial tensiometer is 70545 and on the ring 70542.

Calibration method was as follows: the ring was attached to the tensiometer in the normal fashion, and a small piece of stiff paper placed across the top of the ring to act as a pan for weights. The instrument was zeroed, and then weights from 100 to 1100 gm. were placed on the paper and the tensiometer re-zeroed. This gave a scale reading in dynes/cm. (the instrument is designed to read directly).

Knowing the weight added to the ring, and the diameter of the ring which it was proposed to use, and assuming the gravitational acceleration to be essentially 980 cm./sec.^{2}, one can calculate what the scale reading should actually be. Since the ring is used to rupture two liquid surfaces, the force (mass of weight times acceleration of gravity) is distributed over twice the circumference of the ring. In other words:

$$\text{Calc'd Scale Reading} = \frac{ma}{2cg_c} \qquad (C.2.1)$$

where: Calc'd Scale Reading = Dynes/cm.

m = mass in grams

a = 980 cm/sec^2

c = circumference of ring, cm.

$g_c = \frac{1 \text{ gm.m.cm.}}{\text{dyne sec.}^2}$ (conversion factor)

Results are shown in Figure 61, and the corresponding values shown in Table XVI.

TABLE XVI

CALIBRATION OF TENSIOMETER C7-8

Ring circumference: 5.998 cm.

Mass of Weight mg.	Calculated Scale Reading, Dynes/cm.	Observed Scale Reading, Dynes/cm.
100	8.2	8.3
200	16.3	16.4
300	24.5	24.3
400	32.7	32.4
500	40.8	40.7
600	49.1	48.5
700	57.2	56.7
800	65.4	64.6
900	73.6	72.8
1000	81.7	81.1
1100	90.0	89.1

C.3. Calibration of Pressure Gauges

Pressures involved in the course of this research were measured in two ways - first, by dial-type pressure gauges, and second, by mercury manometer. The mercury manometer obviously needs no calibration other than assurance that the scale is properly graduated and that the proper fluid is used. A commercial mercury manometer was used, model M184 manufactured

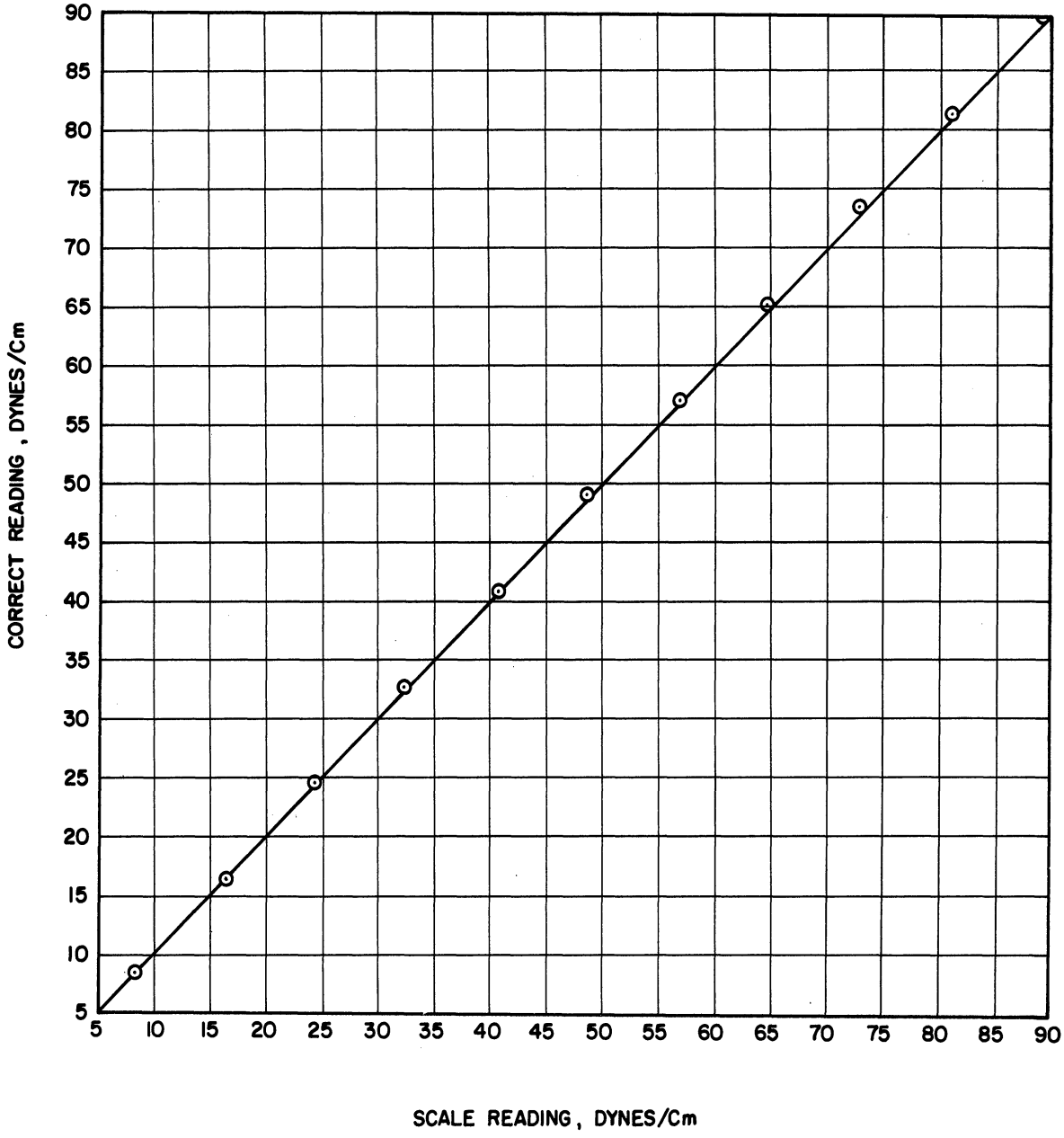

Figure 61. Calibration Curve for Tensiometer.

by the Meriam Instrument Company, serial C17 201 of the Department of Chemical and Metallurgical Engineering of the University of Michigan.

The dial-type pressure gauges used were 0-60 psi, serial C2 111 and 0-30 psi, serial C2 495 - again both serial numbers are from the Chemical and Metallurgical Engineering Department of the University of Michigan. These gauges were both calibrated using a standard dead-weight gauge testing apparatus, with the results shown in Table XVII.

TABLE XVII

CALIBRATION OF DIAL-TYPE PRESSURE GAUGES

	Observed Pressure psi	True Pressure psi
Serial C2 111	4.5	5.
	10.	10.
	15.	15.
	20.	20.
	25.	25.
	30.	30.
	35.	35.
	40.	40.
	45.	45.
	50.	50.
	55.	55.
	60.	60.
Serial C2 495	4.8	5.
	10.	10.
	15.2	15.
	20.2	20.
	25.2	25.
	29.9	30.

C.4. Camera Calibrations

Two calibrations were made on each of the cameras used in this research - one for magnification and one for depth of field. Both cameras

used 50 mm. Argus lenses, the 2.6X camera having f/2.8 to f/22 stops and the 10X camera remaining fixed at f/3.5.

Magnification calibrations were made by photographing the barrel of a hypodermic needle which had been measured with a micrometer. The resulting negative was enlarged by a factor of 10 diameters and the distance measured using a ruler with .01" subdivisions.

It should be further noted that camera magnification will vary slightly depending on the focus setting of the lens. This was checked and not found to be an appreciable consideration, but in order to be systematic all magnifications were measured and all data taken with the lens focus setting on infinity.

Depth of field measurements were made similarly, except that the barrel of the hypodermic needle was inclined at about a 60° angle with the camera axis. From knowledge of the angle and by measuring the length of the barrel shown in focus on the negative, depth of field measurements were obtained. Results are summarized in Table XVIII.

Depth of field was also calculated, and it was found that drops which would appear to be in satisfactory focus can correspond to a sizeable circle of confusion as compared to the sizes of circle of confusion commonly used in photographic work.

TABLE XVIII

DEPTH OF FIELD CALIBRATIONS FOR 2.6X AND 10X CAMERAS

	f stop	depth of field, mm.
10X camera	3.5	1-2
2.6X camera	2.8	2.4
	4.	3.9
	5.6	4.4
	8.	5.4
	11.	6.9
	16.	8.3
	22.	10.3

APPENDIX D

RAW DATA AND DISTRIBUTION PLOTS

TABLE XIX

RAW DATA - RUN NUMBER 1

System: Saturated CCl_4 into saturated H_2O
Flow Rate: 275 $cm^3/min.$
Nozzle Diameter: .1042 cm.
Interfacial Tension: 32.0 Dynes/cm
Viscosity of Flowing Phase: 1.0 cps.
Density of Flowing Phase: 1.595 gm/cm^3
Time Delay: 2.54×10^{-3} sec.

Large Drop Size Range, cm. x 10^2	0.-1.	1.-2.	2.-3.	3.-4.	4.-5.	5.-6.	6.-7.	7.-8.	8.-9.	9.-10.	10.-11.	11.-12.	12.-13.	13.-14.	14.-15.	15.-16.	16.-17.	17.-18.	18.-19.	19.-20.	20.-21.
No. Large Drops	36	86	99	65	32	19	12	6	5	4	7	1	0	0	3	6	0	1	0	0	1
Avg. Distance, cm. x 10^2	3.9	5.3	6.4	7.2	7.7	8.1	8 4	8.7	8.8	8.8	8.8	8.8	8.8	8.8	8.8	8.8	8.8	8.8	8.8	8.8	8.8
Number of Inclusions by Size Range, cm x 10^2 0.-.5	0	0	0	1	0	0	5	0	0	1	1	0	0	0	0	3	0	0	0	0	0
.5-1.0	0	0	0	0	1	2	2	0	3	6	13	0	0	0	0	5	0	3	0	0	0
1.0-1.5	0	0	1	0	7	3	7	1	8	6	18	0	0	0	5	14	0	4	0	0	3
1.5-2.0	0	0	0	1	1	3	4	1	2	2	5	0	0	0	0	6	0	6	0	0	0
2.0-2.5	0	0	0	0	1	4	2	1	7	8	10	1	0	0	11	9	0	6	0	0	2
2.5-3.0	0	0	0	0	0	2	0	1	1	2	0	1	0	0	0	4	0	2	0	0	0
3.0-3.5	0	0	0	0	1	1	1	1	3	0	3	0	0	0	4	4	0	0	0	0	4
3.5-4.0	0	0	0	0	0	0	0	0	0	1	2	1	0	0	0	1	0	0	0	0	0
4.0-4.5	0	0	0	0	0	0	0	0	1	2	4	0	0	0	6	3	0	4	0	0	3

TABLE XX

RAW DATA - RUN NUMBER 2

System: Saturated CCl_4 into Saturated H_2O
Flow Rate: 275 $cm^3/min.$
Nozzle Diameter: .1042 cm.
Interfacial Tension: 32.0 Dynes/cm.
Viscosity of Flowing Phase: 1.0 cps.
Density of Flowing Phase: 1.595 gm/cm^3
Time Delay: 2.54×10^{-3} sec.

Large Drop Size Range, cm. x 10^2	0.-1.	1.-2.	2.-3.	3.-4.	4.-5.	5.-6.	6.-7.	7.-8.	8.-9.	9.-10.	10.-11.	11.-12.	12.-13.	13.-14.	14.-15.	15.-16.	16.-17.	17.-18.
No. Large Drops	16	57	70	40	19	9	7	4	3	3	6	1	0	0	0	4	0	1
Avg. Distance, cm. x 10^2	3.9	5.3	6.4	7.2	7.7	8.1	8.4	8.7	8.8	8.8	8.8	8.8	8.8	8.8	8.8	8.8	8.8	8.8
Number of Inclusions by Size Range, cm. x 10^2 0.-.5	0	0	0	1	0	0	0	0	0	0	1	0	0	0	0	3	0	0
.5-1.0	0	0	0	0	1	1	2	0	3	1	12	0	0	0	0	5	0	3
1.0-1.5	0	0	1	0	6	3	6	0	4	5	15	0	0	0	0	14	0	4
1.5-2.0	0	0	0	1	1	3	3	1	1	2	4	0	0	0	0	5	0	6
2.0-2.5	0	0	0	0	0	2	1	0	1	3	6	1	0	0	0	7	0	6
2.5-3.0	0	0	0	0	0	2	0	1	0	3	0	1	0	0	0	3	0	2
3.0-3.5	0	0	0	0	1	1	0	0	0	0	3	0	0	0	0	2	0	0
3.5-4.0	0	0	0	0	0	0	0	0	0	0	2	1	0	0	0	1	0	0
4.0-4.5	0	0	0	0	0	0	0	0	1	1	4	0	0	0	0	3	0	4

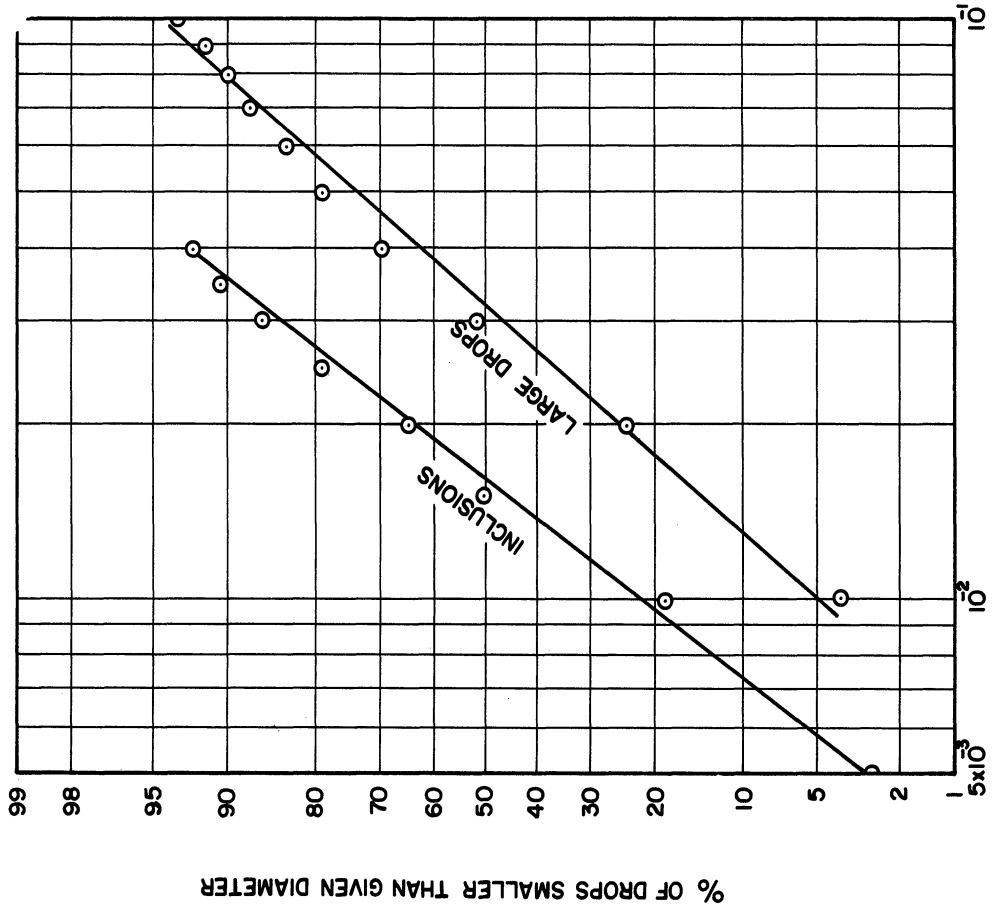

Figure 63. Distribution Plot for Run 2

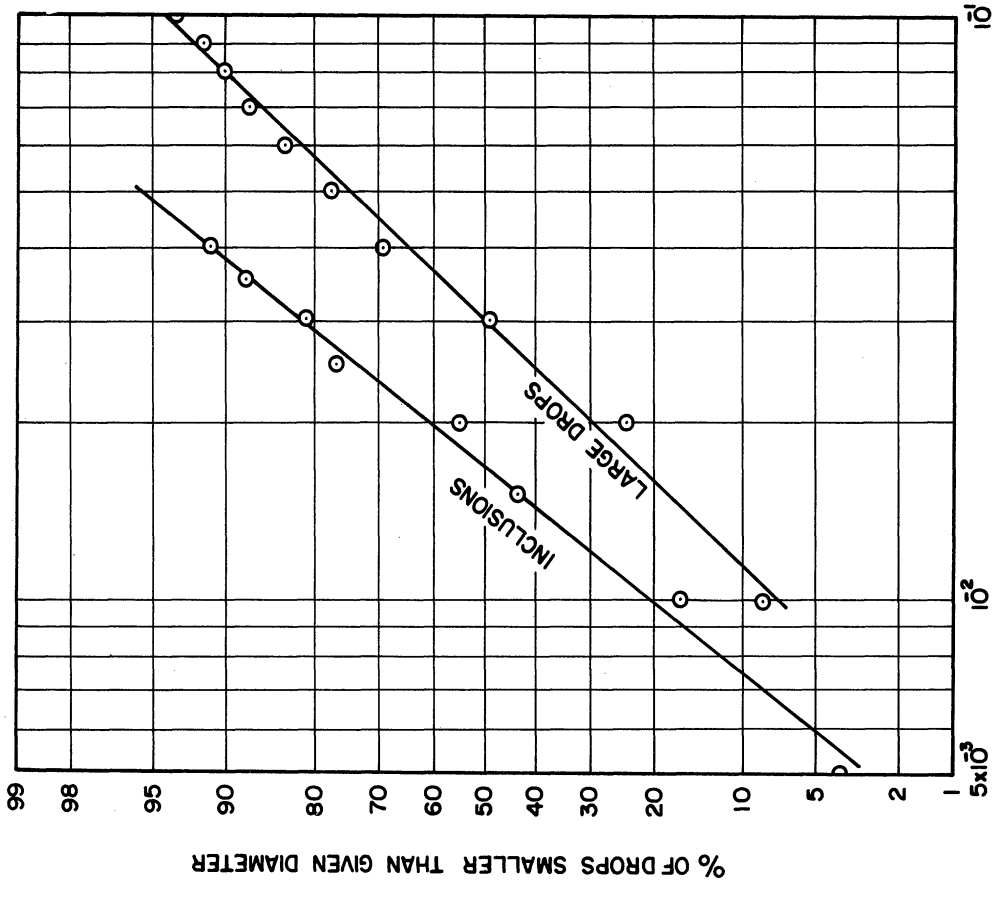

Figure 62. Distribution Plot for Run 1.

TABLE XXI

RAW DATA - RUN NUMBER 4

System: Saturated CCl_4 into saturated H_2O

Flow Rate: 92 cm^3/min.

Nozzle Diameter: .1042 cm.

Interfacial Tension: 32.0 Dynes/cm.

Viscosity of Flowing Phase: 1.0 cps.

Density of Flowing Phase: 1.595 gm/cm^3

Time Delay: 2.52×10^{-3} sec.

Large Drop Size Range, cm. x 10^2	0.- 1.	1.- 2.	2.- 3.	3.- 4.	4.- 5.	5.- 6.	6.- 7.	7.- 8.	8.- 9.	9.- 10.	10.- 11.	11.- 12.	12.- 13.	13.- 14.	14.- 15.	15.- 16.	16.- 17.	17.- 18.	18.- 19.	19.- 20.	20.- 21.	21.- 22.	22.- 23.	23.- 24.	24. 25.
No. Large Drops	3	1	6	1	5	4	3	3	1	3	0	1	0	0	0	0	0	0	0	4	1	0	1	0	1
Avg. Distance cm. x 10^2	2.4	3.2	4.3	4.8	5.0	5.1	5.3	5.4	5.4	5.6	5.6	5.8	5.8	5.8	5.8	5.8	5.8	5.8	5.8	6.8	7.0	7.0	7.2	7.2	7.4

TABLE XXII

RAW DATA - RUN NUMBER 5*

System: Saturated CCl_4 into saturated H_2O
Flow Rate: 20.0 cm^3/min.
Nozzle Diameter: .1042 cm.
Interfacial Tension: 30.0 Dynes/cm.
Viscosity of Flowing Phase: 1.0 cps.
Density of Flowing Phase: 1.595 gm/cm^3
Time Delay: 2.52×10^{-3} sec.

*For Distribution Plot See Figure 29.

Large Drop Size Range, cm. x 10^2	0.- 1.	1.- 2.	2.- 3.	3.- 4.	4.- 5.	5.- 6.	6.- 7.	7.- 8.	8.- 9.	9.- 10.	10.- 11.
No. Large Drops	1	0	2	3	1	4	3	0	0	2	3
Avg. Distance, cm. x 10^2	3.9	3.9	4.2	4.3	4.5	4.6	4.8	4.8	4.8	5.2	5.3

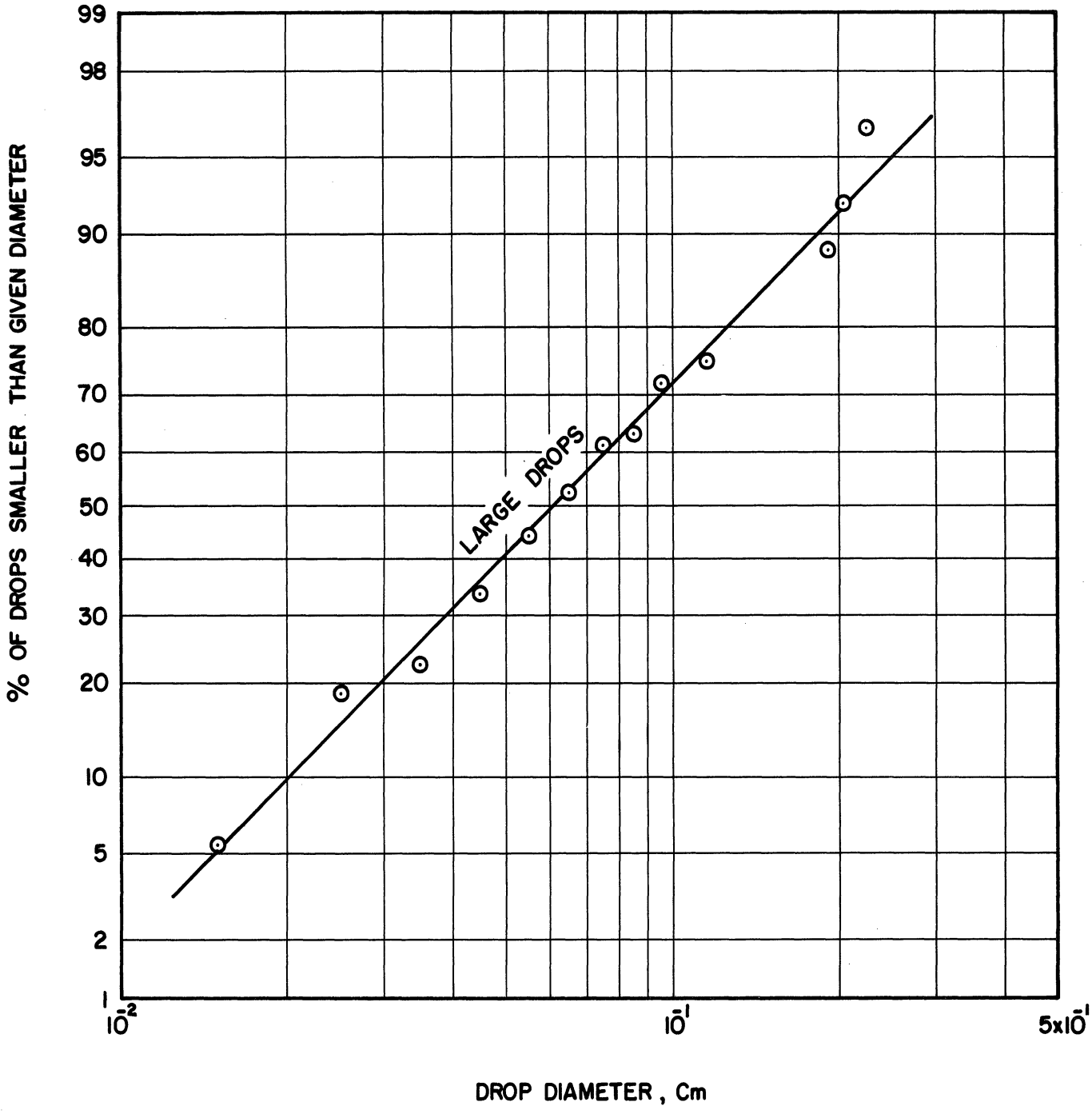

Figure 64. Distribution Plot for Run 4.

TABLE XXIII

RAW DATA - RUN NUMBER 6

System: Saturated CCl_4 into saturated H_2O
Flow Rate: 22 cm^3/min.
Nozzle Diameter: .0420 cm.
Interfacial Tension: 32.0 Dynes/cm.
Viscosity of Flowing Phase: 1.0 cps.
Density of Flowing Phase: 1.595 gm/cm^3
Time Delay: 2.52 x 10^{-6} sec.

Large Drops Size Range, cm. x 10^2		0.-1.	1.-2.	2.-3.	3.-4.	4.-5.	5.-6.	6.-7.	7.-8.	8.-9.	9.-10.	10.-11.	11.-12.
No. Large Drops		61	132	126	78	41	37	30	33	25	25	8	1
Avg. Distance cm. x 10^2		2.4	3.2	4.3	4.8	5.0	5.1	5.3	5.4	5.4	5.6	5.6	5.8
Number of Inclusions by Size Range, cm. x 10^2	0.-.5	0	4	21	13	13	8	8	6	12	10	1	0
	.5-1.0	0	4	15	16	9	9	21	19	12	22	7	3
	1.0-1.5	0	0	1	6	3	10	13	14	20	13	2	0
	1.5-2.0	0	0	1	2	3	3	5	8	6	8	1	0
	2.0-2.5	0	0	0	0	0	2	4	8	8	4	2	1
	2.5-3.0	0	0	0	1	0	1	2	1	1	3	1	0
	3.0-3.5	0	0	0	0	0	0	0	1	1	1	0	0
	3.5-4.0	0	0	0	0	0	0	1	0	0	0	1	0
	4.0-4.5	0	0	0	0	0	0	0	0	0	1	1	0

TABLE XXIV

RAW DATA - RUN NUMBER 7

System: Saturated CCl_4 into saturated H_2O
Flow Rate: 190 cm^3/min.
Nozzle Diameter: .0642 cm.
Interfacial Tension: 32.0 Dynes/cm.
Viscosity of Flowing Phase: 1.0 cps.
Density of Flowing Phase: 1.595 gm/cm^3
Time Delay: 1.10 x 10^{-3} sec

Large Drop Size Range, cm. x 10^2		0.-1.	1.-2.	2.-3.	3.-4.	4.-5.	5.-6.	6.-7.	7.-8.	8.-9.	9.-10.	10.-11.	11.-12.	12.-13.	13.-14.	14.-15.	15.-16.
No. Large Drops		40	67	50	31	17	12	6	6	8	5	4	4	3	3	2	0	1
Avg. Distance, cm. x 10^2		2.0	2.2	2.4	2.6	2.8	3.0	3.2	3.4	3.5	3.7	3.9	4.1	4.3	4.5	4.7	4.9	5.1
Number of Inclusions by Size Range, cm. x 10^2	0.-.5	0	0	0	0	0	0	2	1	2	6	5	4	1	1	1	0	2
	.5-1.0	0	0	2	2	4	5	1	1	11	6	6	6	4	3	1	0	0
	1.0-1.5	0	0	0	2	1	1	2	1	5	4	6	4	5	7	6	0	5
	1.5-2.0	0	0	0	1	0	0	0	0	0	2	2	5	4	1	4	0	0
	2.0-2.5	0	0	0	0	1	1	1	2	3	1	4	5	1	4	2	0	0
	2.5-3.0	0	0	0	0	1	0	0	1	1	0	0	3	0	1	0	0	0
	3.0-3.5	0	0	0	0	0	1	1	0	2	1	0	0	2	0	1	0	0
	3.5-4.0	0	0	0	0	0	0	0	0	0	0	1	0	0	2	2	0	0
	4.0-4.5	0	0	0	0	0	0	0	0	0	0	0	1	0	2	0	0	0

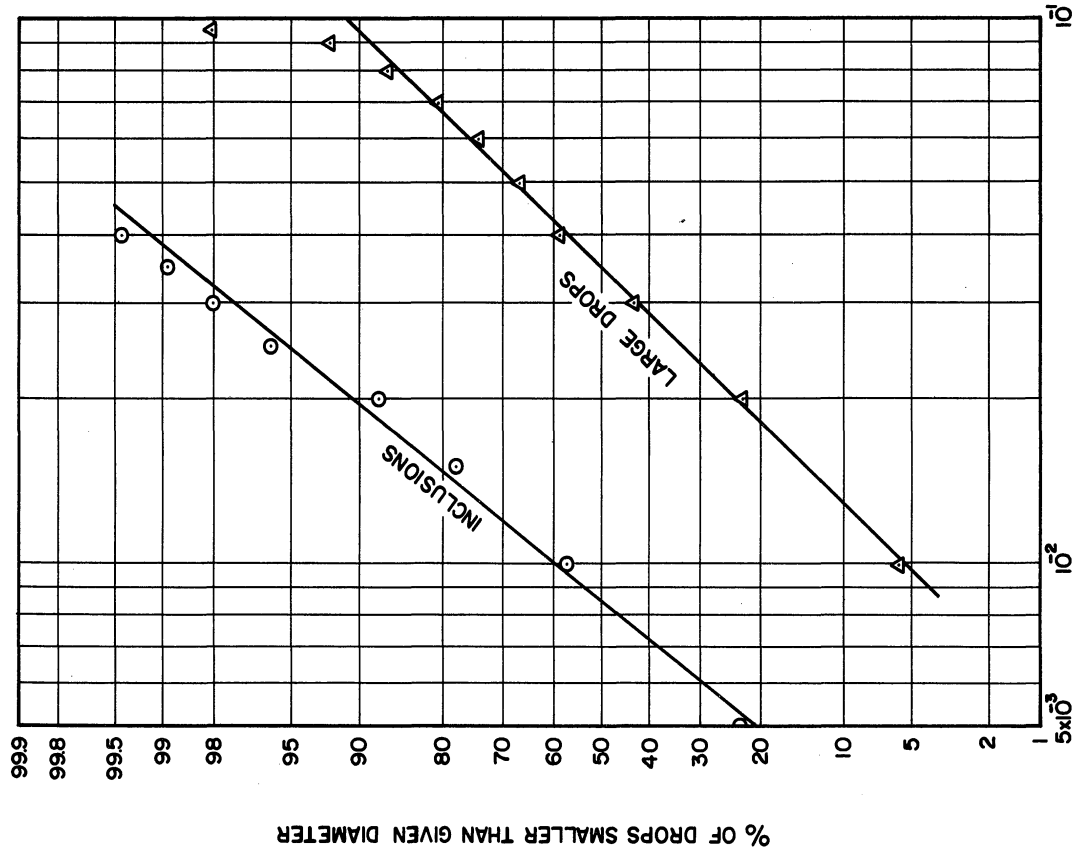

Figure 65. Distribution Plot for Run 6.

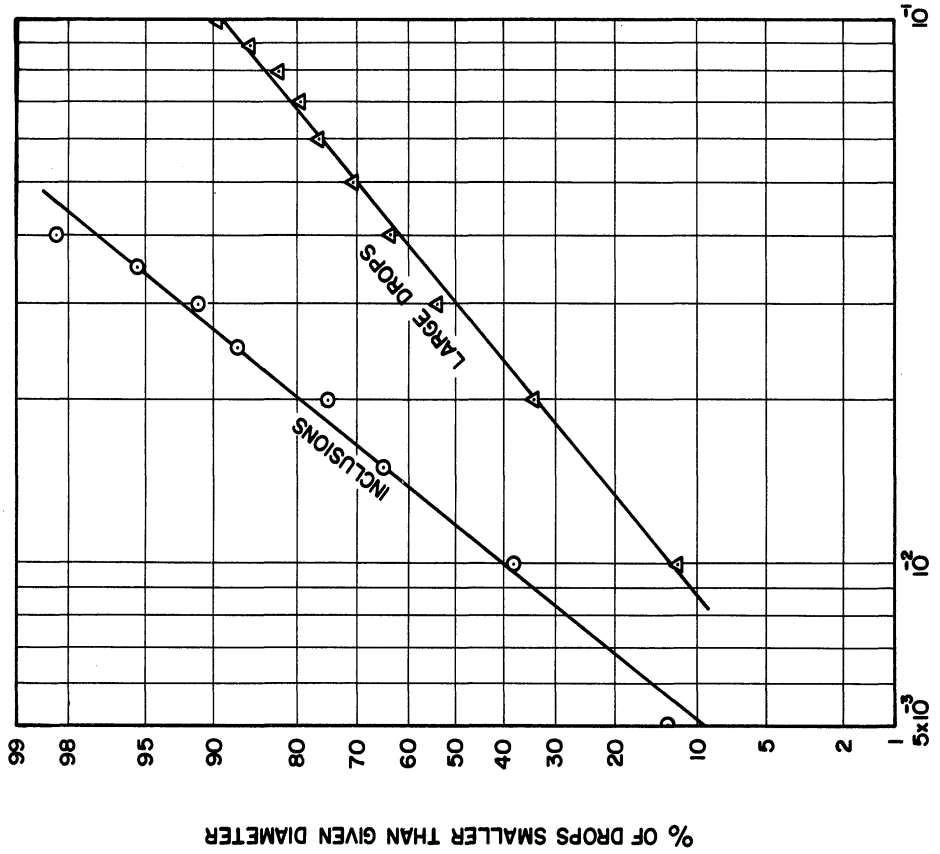

Figure 66. Distribution Plot for Run 7.

TABLE XXV

RAW DATA - RUN NUMBER 8

System: Saturated CCl_4 into saturated H_2O
Flow Rate: 130 cm^3/min.
Nozzle Diameter: .0642 cm.
Interfacial Tension: 32.0 Dynes/cm.
Viscosity of Flowing Phase: 1.0 cps.
Density of Flowing Phase: 1.595 gm/cm^3.
Time Delay: 1.55 x 10^{-3} sec.

Large Drop Size Range, cm. x 10^2		0.-1.	1.-2.	2.-3.	3.-4.	4.-5.	5.-6.	6.-7.	7.-8.	8.-9.	9.-10.	10.-11.	11.-12.
No. Large Drops		108	151	61	31	19	6	6	4	1	3	1	1
Avg. Distance, cm. x 10^2		1.8	2.1	2.5	2.8	3.1	3.4	3.8	4.1	4.4	4.8	5.1	5.5
Number of Inclusions by Size Range, cm. x 10^2	0.-.5	0	7	13	1	5	4	3	7	0	5	0	0
	.5-1.0	0	1	9	8	1	2	7	0	0	9	0	0
	1.0-1.5	0	0	7	7	17	1	14	5	4	5	0	8
	1.5-2.0	0	0	0	4	5	2	5	3	3	5	10	2
	2.0-2.5	0	0	0	1	3	3	0	1	2	3	0	0
	2.5-3.0	0	0	0	0	1	0	0	1	0	2	0	0
	3.0-3.5	0	0	0	0	0	0	1	0	0	1	0	0
	3.5-4.0	0	0	0	0	0	0	0	0	0	0	0	0
	4.0-4.5	0	0	0	0	0	0	0	1	0	0	0	0

TABLE XXVI

RAW DATA - RUN NUMBER 9

System: Saturated CCl_4 into saturated H_2O
Flow Rate: 130 cm^3/min.
Nozzle Diameter: .0642 cm.
Interfacial Tension: 32.0 Dynes/cm.
Viscosity of Flowing Phase: 1.0 cps.
Density of Flowing Phase: 1.595 gm/cm^3
Time Delay: 1.55 x 10^{-3} sec.

Large Drop Size Range, cm. x 10^2		0.-1.	1.-2.	2.-3.	3.-4.	4.-5.	5.-6.	6.-7.	7.-8.	8.-9.	9.-10.	10.-11.	11.-12.
No. Large Drops		85	153	79	32	17	9	5	7	6	1	2	1
Avg. Distance, cm. x 10^2		1.8	2.1	2.5	2.8	3.1	3.4	3.8	4.1	4.4	4.8	5.1	5.5
Number of Inclusions by Size Range, cm. x 10^2	0.-.5	0	4	4	4	6	11	8	7	4	0	0	0
	.5-1.0	0	1	5	4	8	11	2	6	3	0	0	1
	1.0-1.5	0	0	1	6	11	3	1	12	18	1	6	0
	1.5-2.0	0	0	0	2	1	4	0	2	7	0	1	2
	2.0-2.5	0	0	0	1	4	2	1	4	10	1	0	0
	2.5-3.0	0	0	0	0	0	1	0	0	0	0	1	0
	3.0-3.5	0	0	0	0	1	2	2	2	2	0	1	2
	3.5-4.0	0	0	0	0	0	0	0	1	0	0	0	0
	4.0-4.5	0	0	0	0	0	1	0	0	0	1	1	0

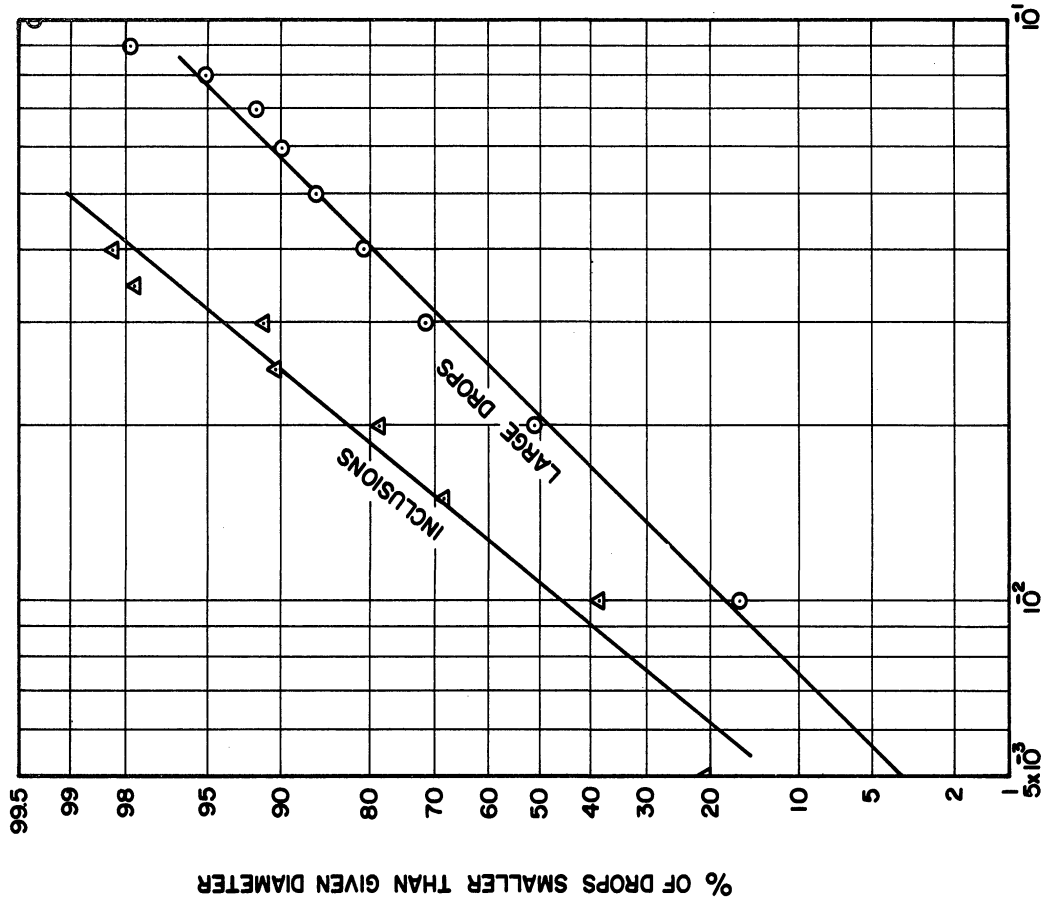

Figure 68. Distribution Plot for Run 9.

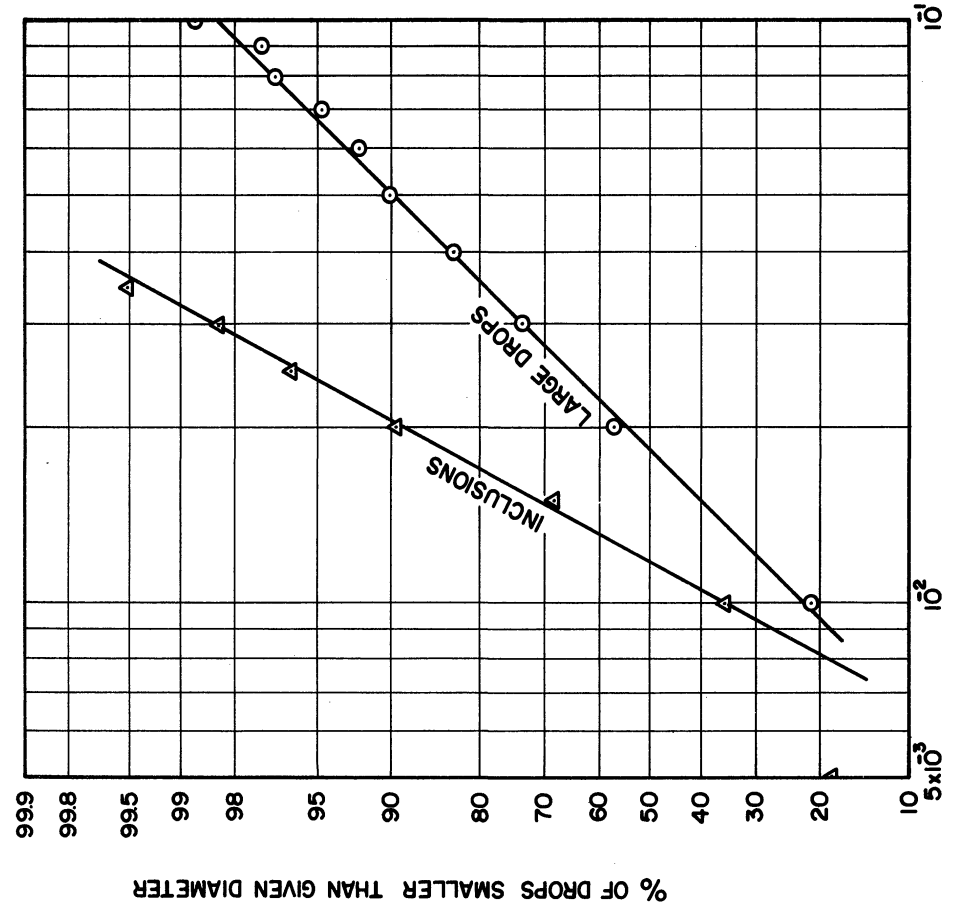

Figure 67. Distribution Plot for Run 8.

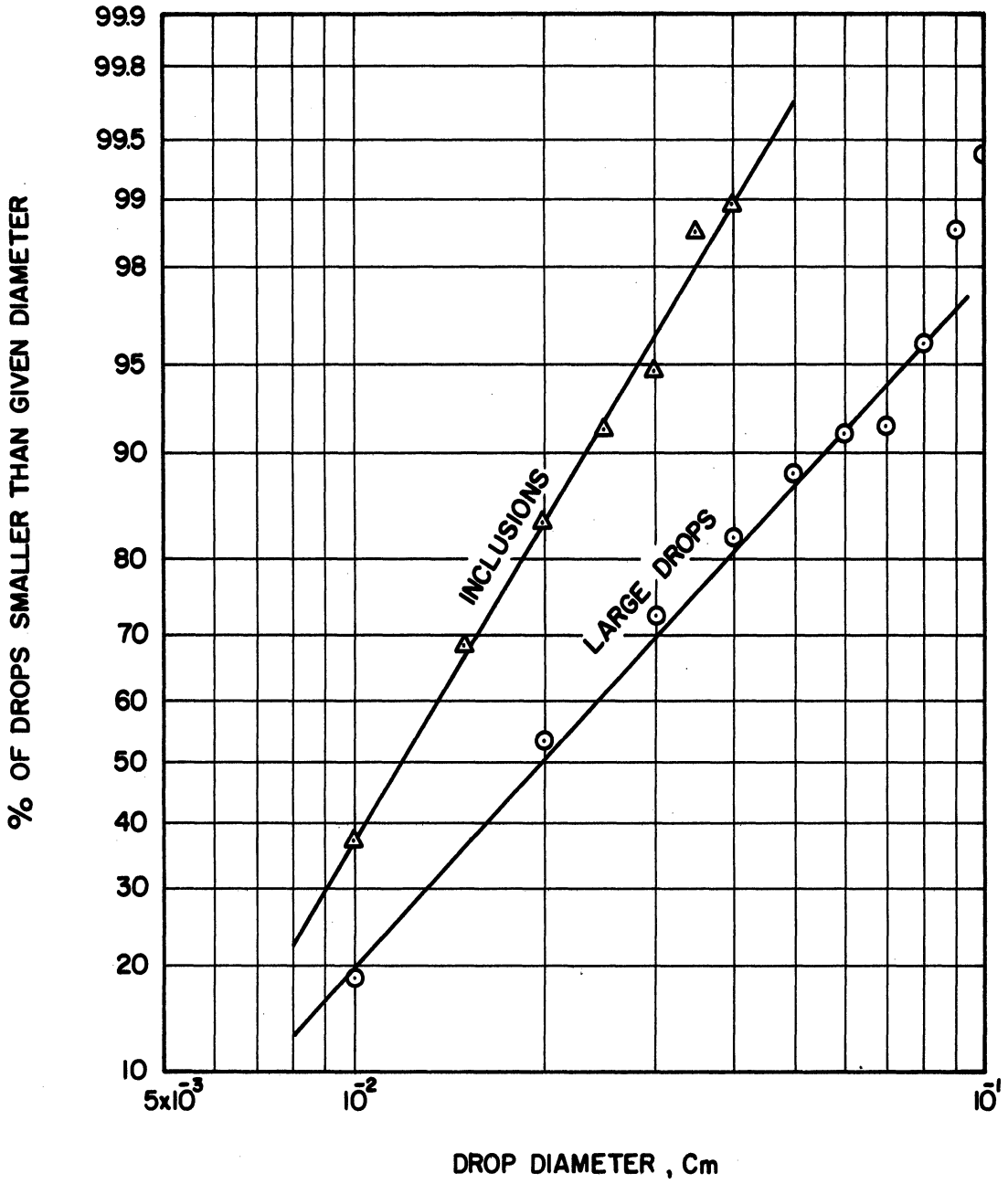

Figure 69. Distribution Plot for Run 10.
(For Raw Data See Table II)

TABLE XXVII

RAW DATA - RUN NUMBER 11

System: Saturated CCl_4 into saturated H_2O

Flow Rate: 50 $cm^3/min.$

Nozzle Diameter: .0642 cm.

Interfacial Tension: 32.0 Dynes/cm.

Viscosity of Flowing Phase: 1.0 cps.

Density of Flowing Phase: 1.595 $gm/cm.^3$

Time Delay: 2.19×10^{-3} sec

Large Drop Size Range, cm. x 10^2	0.-1.	1.-2.	2.-3.	3.-4.	4.-5.	5.-6.	6.-7.	7.-8.	8.-9.	9.-10.	10.-11.	11.-12.	12.-13.	13.-14.	14.-15.	15.-16.	16.-17.	17.-18.	18.-19.	19.-20.	20.-21.
No. Large Drops	22	7	5	1	1	1	3	3	9	10	9	5	1	5	8	5	3	1	2	1	1
Avg. Distance, cm. x 10^{-2}	1.5	1.9	2.2	2.5	2.8	3.1	3.4	3.7	4.0	4.3	4.6	4.9	5.2	5.4	5.5	5.6	5.7	5.8	5.8	5.9	6.0

TABLE XXVIII

RAW DATA - RUN NUMBER 12

System: Saturated CCl_4 into saturated H_2O
Flow Rate: 75 $cm^3/min.$
Nozzle Diameter: .0420 cm.
Interfacial Tension: 32.0 Dynes/cm.
Viscosity of Flowing Phase: 1.0 cps.
Density of Flowing Phase: 1.595 gm/cm^3
Time Delay: 1.70×10^{-3} sec.

Large Drop Size Range, cm. x 10^2		0.-1.	1.-2.	2.-3.	3.-4.	4.-5.	5.-6.	6.-7.	7.-8.	8.-9.	9.-10.	10.-11.
No. Large Drops		139	229	103	54	15	10	4	4	2	0	1
Avg. Distance, cm. x 10^2		2.5	2.5	2.5	2.5	2.5	2.5	2.5	2.5	2.5	2.5	2.5
Number of Inclusions by Size Range, cm. x 10^2	0.-.5	0	14	30	27	14	10	5	0	4	0	1
	.5-1.0	0	6	17	36	24	8	10	8	4	0	1
	1.0-1.5	0	0	6	17	9	15	6	16	8	0	4
	1.5-2.0	0	0	0	8	4	5	4	8	2	0	3
	2.0-2.5	0	0	0	1	4	5	2	2	2	0	2
	2.5-3.0	0	0	0	0	0	0	1	1	0	0	0
	3.0-3.5	0	0	0	0	0	2	0	0	0	0	1

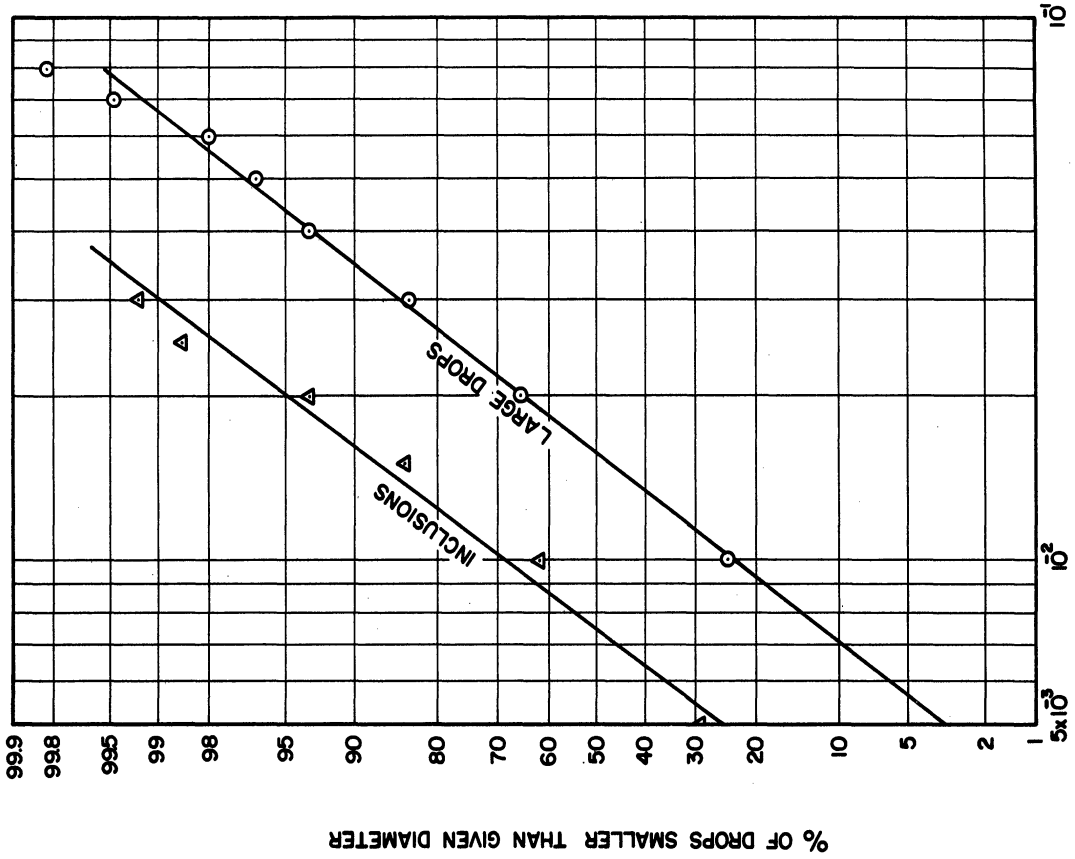

Figure 71. Distribution Plot for Run 12.

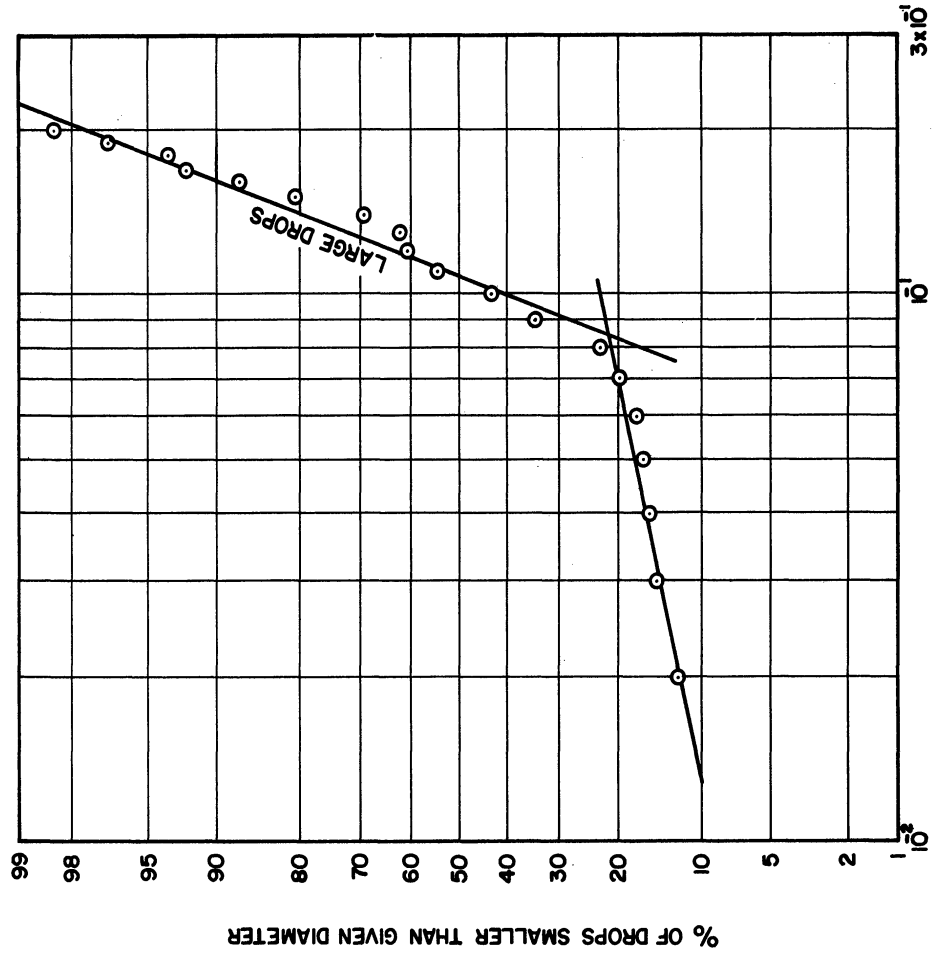

Figure 70. Distribution Plot for Run 11.

TABLE XXIX

RAW DATA - RUN NUMBER 13*

System: Saturated CCl_4 + 6.6 cm^3/gal. "Alkaterge C" into saturated H_2O
Flow Rate: 45 cm^3/min.
Nozzle Diamter: .0642 cm.
Interfacial Tension: 11.7 Dynes/cm.
Viscosity of Flowing Phase: 1.0 cps.
Density of Flowing Phase: 1.595 gm/cm^3
Time Delay: 2.61 x 10^{-3} sec.

*For Distribution Plot See Figure 24.

Large Drop Size Range, cm. x 10^2		0.-1.	1.-2.	2.-3.	3.-4.	4.-5.	5.-6.	6.-7.	7.-8.	8.-9.	9.-10.	10.-11.	11.-12.	12.-13.	13.-14.	14.-15.	15.-16.
No. Large Drops		104	96	87	48	34	20	8	5	7	5	0	3	2	1	2	1
Avg. Distance, cm. x 10^2		4.0	4.2	4.5	4.7	5.0	5.2	5.5	5.7	5.9	6.1	6.3	6.5	6.8	7.0	7.3	7.5
Number	0.-.5	0	1	4	0	8	4	4	2	5	7	0	1	0	0	3	2
of	.5-1.0	0	0	1	3	6	7	6	10	8	10	0	1	4	2	4	3
Inclusions	1.0-1.5	0	0	4	3	7	9	2	3	10	5	0	7	3	1	4	2
by Size	1.5-2.0	0	0	1	0	2	5	1	3	0	2	0	3	1	0	0	1
Range,	2.0-2.5	0	0	0	0	1	2	0	0	0	3	0	4	4	0	2	3
cm. x 10^2	2.5-3.0	0	0	0	0	1	3	0	0	3	0	0	1	3	1	0	2
	3.0-3.5	0	0	0	0	0	0	0	1	1	1	0	0	1	0	3	0
	3.5-4.0	0	0	0	0	0	0	0	0	0	1	0	1	2	0	1	0
	4.0-4.5	0	0	0	0	0	0	0	0	1	0	0	2	0	0	1	1

TABLE XXX

RAW DATA - RUN NUMBER 14

System: Saturated CCl_4 + 6.6 cm^3/gal. "Alkaterge C" into saturated H_2O.
Flow Rate: 90 cm^3/min.
Nozzle Diameter: .0642 cm.
Interfacial Tension: 11.7 Dynes/cm.
Viscosity of Flowing Phase: 1.0 cps.
Density of Flowing Phase: 1.595 gm/cm^3
Time Delay: 2.60 x 10^{-3} sec.

Large Drop Size Range, cm. x 10^2		0.-1.	1.-2.	2.-3.	3.-4.	4.-5.	5.-6.	6.-7.	7.-8.	8.-9.
No. Large Drops		95	162	71	25	24	5	5	2	1
Avg. Distance, cm. x 10^2		1.5	2.2	2.8	3.5	4.0	4.9	5.5	5.5	5.5
Number of	0.-5.	0	2	5	3	7	7	4	4	0
Inclusions	5.-1.0	0	5	5	6	29	17	11	4	2
by Size	1.0-1.5	0	0	7	3	17	8	13	4	3
Range,	1.5-2.0	0	0	1	7	10	4	5	1	2
cm. x 10^2	2.0-2.5	0	0	0	1	3	1	1	2	1
	2.5-3.0	0	0	0	0	2	2	0	2	0
	3.0-3.5	0	0	0	0	1	0	0	0	1

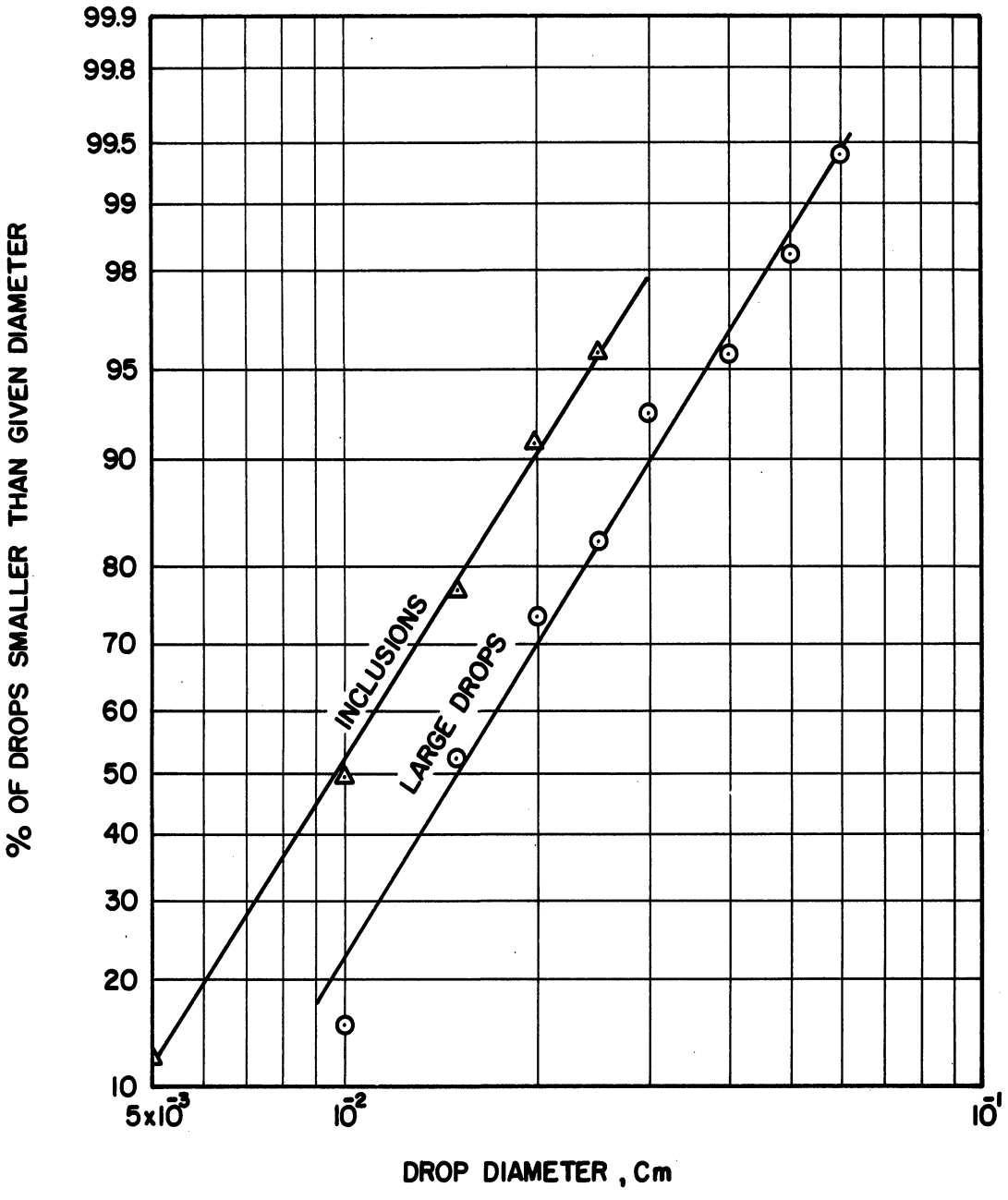

Figure 72. Distribution Plot for Run 14.

TABLE XXXI

RAW DATA - RUN NUMBER 15

System: Saturated H_2O into saturated CCl_4
Flow Rate: 80 $cm^3/min.$
Nozzle Diameter: .0642 cm.
Interfacial Tension: 32.0 Dynes/cm.
Viscosity of Flowing Phase: 1.0 cps.
Density of Flowing Phase: 1.0 gm/cm^3
Time Delay: 1.51 x 10^{-3} sec.

Large Drop Size Range, cm. x 10^2		0.-1.	1.-2.	2.-3.	3.-4.	4.-5.	5.-6.	6.-7.	7.-8.	8.-9.	9.-10.	10.-11.	11.-12.	12.-13.	13.-14.	14.-15.	15.-16.	16.-17.
No. Large Drops		53	119	66	36	14	7	7	3	3	1	2	2	0	0	0	1	1
Avg. Distance, cm. x 10^2		2.0	2.0	2.0	2.0	2.0	2.0	2.0	2.0	2.0	2.0	2.0	2.0	2.0	2.0	2.0	2.0	2.0
Number of Inclusions by Size Range, cm. x 10^2	0.-.5	0	0	2	4	5	2	3	3	1	0	0	1	0	0	0	0	0
	.5-1.0	0	2	13	10	5	5	7	6	9	1	10	18	0	0	0	2	0
	1.0-1.5	0	0	3	8	2	2	6	1	5	2	4	2	0	0	0	3	25
	1.5-2.0	0	0	0	0	1	0	1	5	4	1	3	1	0	0	0	4	25
	2.0-2.5	0	0	0	0	1	0	0	2	1	1	1	1	0	0	0	4	0
	2.5-3.0	0	0	0	0	0	2	0	0	0	0	1	0	0	0	0	1	0
	3.0-3.5	0	0	0	0	0	1	0	0	1	0	0	0	0	0	0	0	0
	3.5-4.0	0	0	0	0	0	0	0	0	0	0	1	0	0	0	0	1	0
	4.0-4.5	0	0	0	0	0	0	0	0	0	1	1	0	0	0	0	0	0

TABLE XXXII

RAW DATA - RUN NUMBER 16

System: Saturated H_2O into saturated CCl_4
Flow Rate: 55 $cm^3/min.$
Nozzle Diameter: .0642 cm.
Interfacial Tension: 32.0 Dynes/cm.
Viscosity of Flowing Phase: 1.0 cps.
Density of Flowing Phase: 1.0 gm/cm^3
Time Delay: 1.51 x 10^{-3} sec.

Large Drop Size Range, cm. x 10^2		0.-1.	1.-2.	2.-3.	3.-4.	4.-5.	5.-6.	6.-7.	7.-8.	8.-9.	9.-10.	10.-11.	11.-12.	12.-13.	13.-14.	14.-15.	15.-16.	16.-17.
No. Large Drops		34	69	57	29	23	6	5	8	6	7	2	1	1	1	0	1	2
Avg. Distance, cm. x 10^2		2.0	2.0	2.0	2.0	2.0	2.0	2.0	2.0	2.0	2.0	2.0	2.0	2.0	2.0	2.0	2.0	2.0
Number of Inclusions By Size Range, cm. x 10^2	0.-.5	0	1	2	0	3	0	0	2	0	3	0	0	1	0	0	3	0
	.5-1.0	0	2	13	4	6	4	6	8	5	19	0	0	4	4	0	3	11
	1.0-1.5	0	0	2	2	2	1	7	5	4	6	1	0	2	0	0	2	5
	1.5-2.0	0	0	0	0	4	0	1	4	2	5	0	0	0	3	0	0	3
	2.0-2.5	0	0	0	0	1	0	0	4	3	0	3	0	2	0	0	2	2
	2.5-3.0	0	0	0	0	0	0	1	0	1	6	1	0	0	1	0	0	1
	3.0-3.5	0	0	0	0	0	0	0	1	0	1	1	0	0	1	0	0	1
	3.5-4.0	0	0	0	0	0	0	0	0	0	0	0	0	0	0	0	0	0
	4.0-4.5	0	0	0	0	0	0	0	0	0	0	0	0	0	0	0	0	1

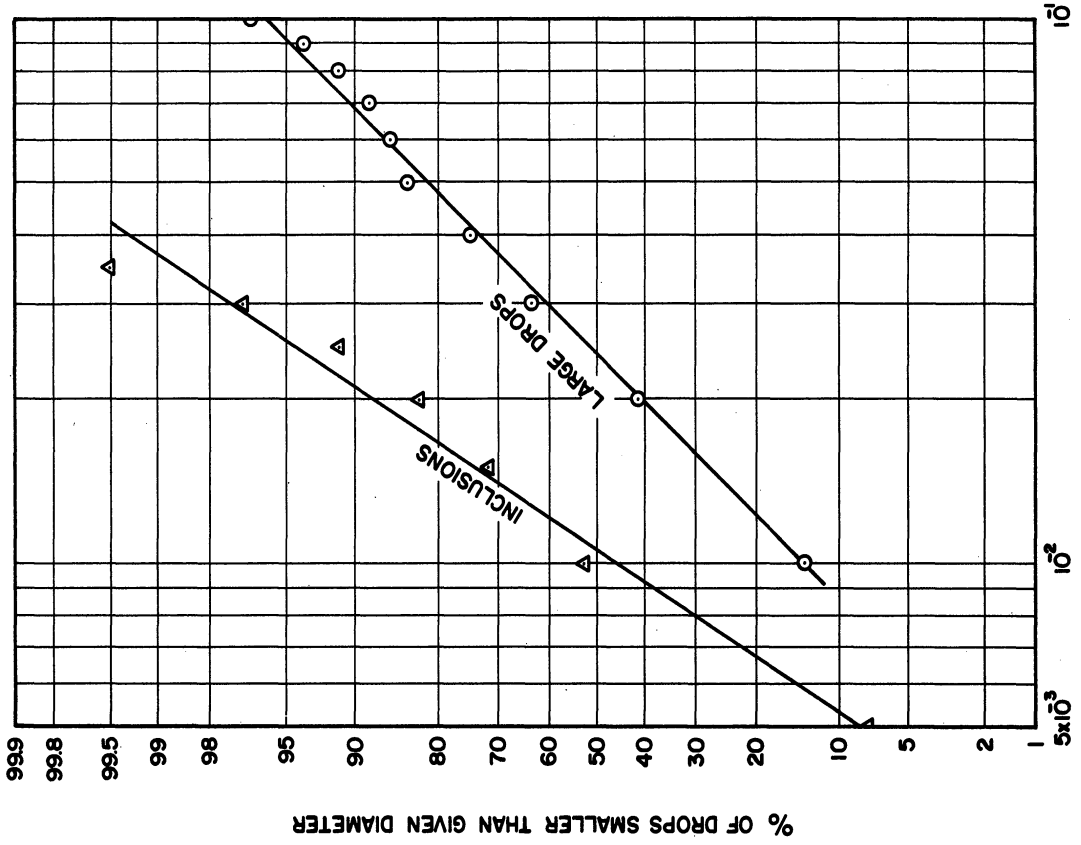

Figure 74. Distribution Plot for Run 16.

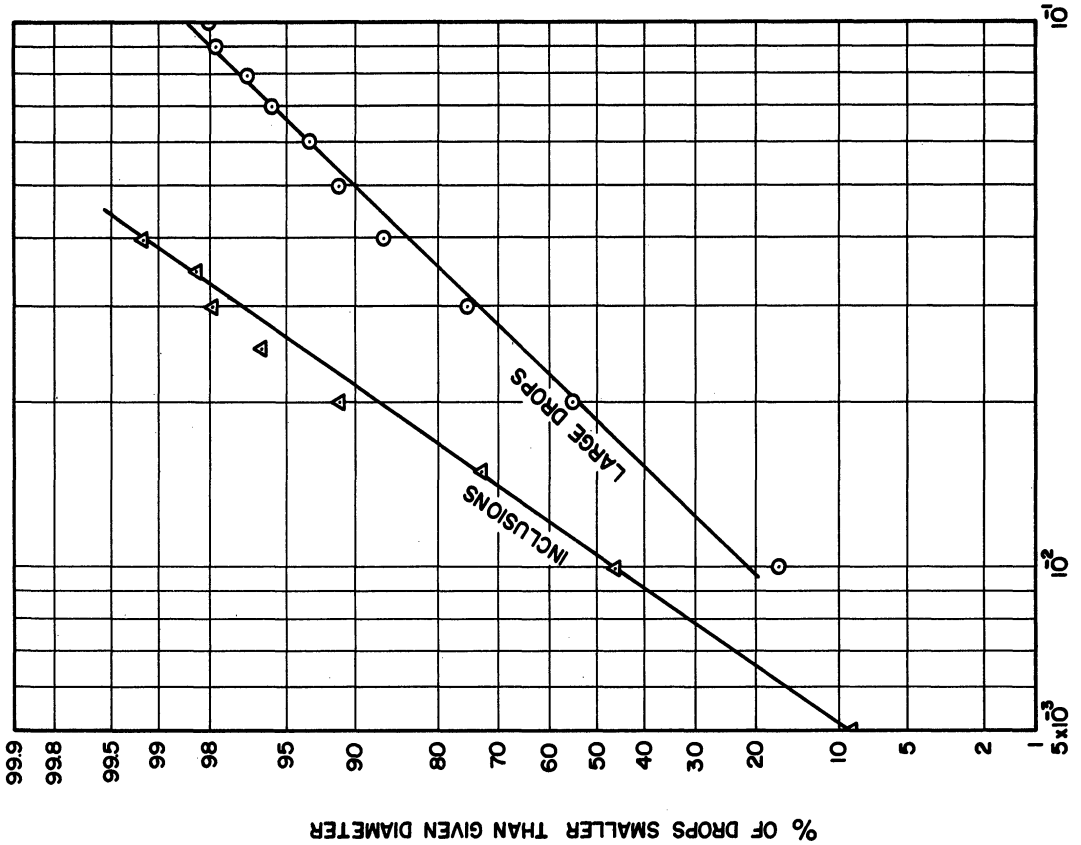

Figure 73. Distribution Plot for Run 15.

TABLE XXXIII

RAW DATA - RUN NUMBER 17

System: Saturated H_2O into saturated CCl_4
Flow Rate: 31 $cm^3/min.$
Nozzle Diameter: .0420 cm.
Interfacial Tension: 32.0 Dynes/cm.
Viscosity of Flowing Phase: 1.0 cps.
Density of Flowing Phase: 1.0 gm/cm^3
Time Delay: 1.51 x 10^{-3} sec.

Large Drop Size Range, cm. x 10^2		0.-1.	1.-2.	2.-3.	3.-4.	4.-5.	5.-6.	6.-7.	7.-8.	8.-9.	9.-10.	10.-11.	11.-12.	12.-13.	13.-14.
No. Large Drops		5	51	37	26	17	7	5	7	5	3	1	1	0	1
Avg. Distance, cm. x 10^2		2.0	2.0	2.0	2.0	2.0	2.0	2.0	2.0	2.0	2.0	2.0	2.0	2.0	2.0
Number of Inclusions by Size Range, cm. x 10^2	0.-.5	0	0	0	0	0	0	0	0	1	1	0	0	0	0
	5.-1.0	0	0	4	1	0	2	1	1	10	3	0	6	0	0
	1.0-1.5	0	0	0	3	0	1	0	0	3	3	0	3	0	0
	1.5-2.0	0	0	0	1	0	0	1	0	1	2	0	0	0	0
	2.0-2.5	0	0	0	0	0	0	0	0	1	2	0	0	0	0
	2.5-3.0	0	0	0	0	0	0	0	1	0	0	0	0	0	0
	3.0-3.5	0	0	0	0	0	0	0	1	1	0	0	1	0	0

TABLE XXXIV

RAW DATA - RUN NUMBER 18

System: Saturated H_2O into saturated CCl_4
Flow Rate: 112 $cm^3/min.$
Nozzle Diameter: .0420 cm.
Interfacial Tension: 32.0 Dynes/cm.
Viscosity of Flowing Phase: 1.0 cps.
Density of Flowing Phase: 1.0 gm/cm^3.
Time Delay: 1.51 x 10^{-3} sec.

Large Drop Size Range, cm. x 10^2		0.-1.	1.-2.	2.-3.	3.-4.	4.-5.	5.-6.	6.-7.	7.-8.	8.-9.	9.-10.
No. Large Drops		67	149	45	25	11	5	10	1	2	1
Avg. Distance, cm. x 10^2		2.0	2.0	2.0	2.0	2.0	2.0	2.0	2.0	2.0	2.0
Number of Inclusions by Size Range, cm. x 10^2	0 -.5	0	0	0	1	2	0	0	0	0	0
	.5-1.0	0	0	1	2	5	0	8	0	1	4
	1.0-1.5	0	0	3	3	2	0	7	0	5	3
	1.5-2.0	0	0	0	1	2	0	2	0	3	2
	2.0-2.5	0	0	0	0	0	0	2	0	0	0
	2.5-3.0	0	0	0	0	0	0	1	0	0	0
	3.0-3.5	0	0	0	0	0	0	1	1	1	0
	3.5-4.0	0	0	0	0	0	0	0	0	1	0

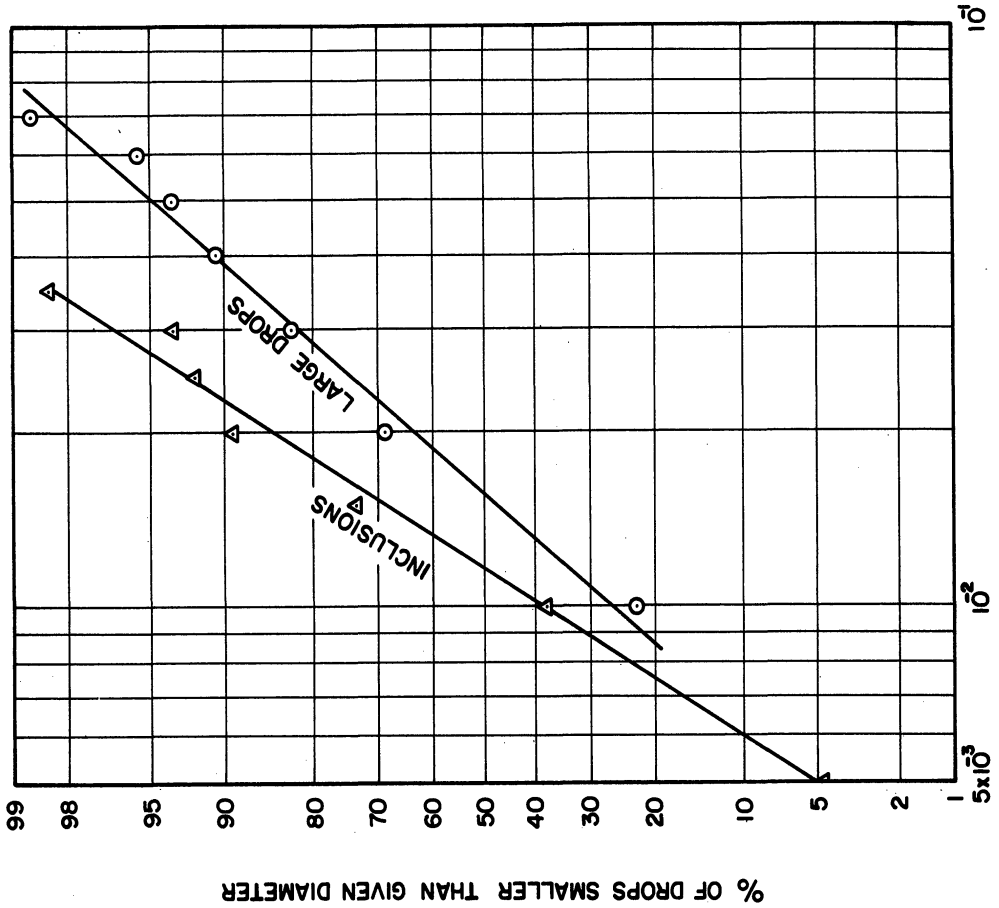

Figure 76. Distribution Plot for Run 18.

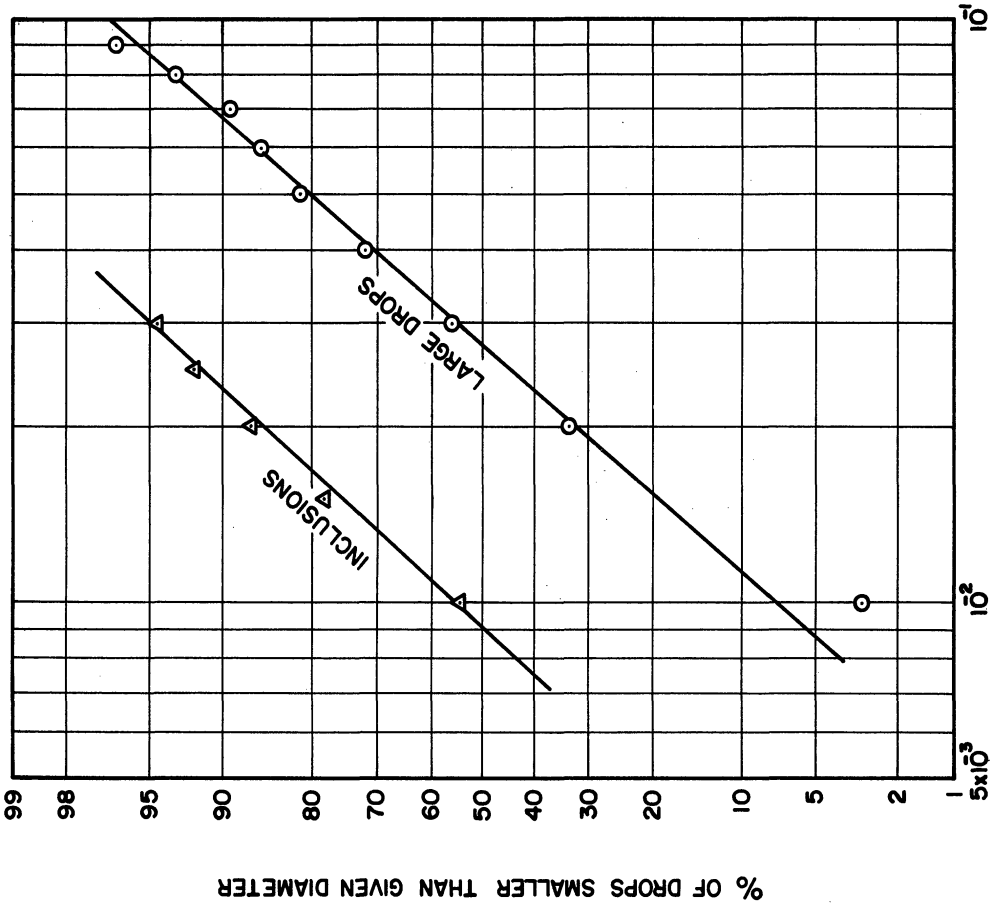

Figure 75. Distribution Plot for Run 17.